Propagation of Hippocampal Ripples to the Neocortex by Way of a Subiculum Retrosplenial Pathway

DISSERTATION

To obtain the academic degree Doctor rerum naturalium (Dr. rer. nat.)

Submitted to the Department of Biology, Chemistry, Pharmacy of Freie Universität Berlin

By Noam Nitzan

January 2020

The experimental work of this thesis was completed from January 2017 to October 2019 under the supervision of Prof. Dr. Dietmar Schmitz at the Neuroscience Research Centre (NWFZ) of the Charité – Universitätsmedizin Berlin, Germany.

1st reviewer: Prof. Dr. Dietmar Schmitz
2nd reviewer: Prof. Dr. Ursula Koch

Date of disputation: 26.08.2020

"I watch the ripples change their size but never leave the stream of warm impermanence…"

David Bowie

Acknowledgements

I would like to start by acknowledging my thesis supervisor, Dietmar Schmitz. From the very beginning of my PhD Dietmar has always been supportive in giving me scientific freedom on one hand and providing me with ideas and insights on the other. His eagerness and sincere joy from scientific collaborations have paved the path that my PhD has finally taken and for this I am greatly indebted.

I am grateful for having the opportunity to collaborate with Sam McKenzie and Gyuri Buzsáki in New York University. Sam introduced me to the world of large-scale electrophysiological recordings and was the ultimate teacher for many complex topics in data analysis. I gained priceless insights from the many discussions we had and from his way of approaching a scientific question. My interaction with Gyuri while working on the paper was perhaps the most intensive part of my PhD but also the most fun and rewarding one. His predictions about the data always proved to be right.

I would like to acknowledge Ursula Koch for agreeing to be my second supervisor and for giving me the opportunity to meet her team and sharing my data with them.

I would also like to thank Richard Kempter for the many insightful discussions we had and for challenging me with so many questions that helped me to better define my own questions.

I am grateful for Nikolaus Maier, John Tukker and Friedrich Johenning, with whom I had many discussions and for sharing their ideas with me. I would further like to thank the outstanding members of the Schmitz lab, in particular Constance Holman and Daniel Parthier, my *in vivo* mates, for the collaborative and open environment. I have learned something from everyone in the lab. I would also like to acknowledge Susanne Rieckmann, Anke Schönherr and Katja Czieselsky for the excellent technical assistant which is unparalleled by any other lab I have ever been to and likely will be in the future.

Finally, and most importantly, I want to express my eternal love and gratitude to my family – my wife Jiyun who has always been there to listen and encourage me and to my parents who unconditionally supported me throughout my academic journey from the very beginning.

Abstract

Sharp wave ripple (SPW-R) events are brief high frequency oscillations observed throughout the hippocampal network during slow-wave sleep and quiet wakefulness. This transient synchronous activity provides the physiological scaffold for the compressed replay of awake sequences, and accumulating data support their crucial role in memory consolidation. The wide range of cortical areas that are strongly depolarized during SPW-Rs, as well as the observed coordinated reactivation of hippocampal and neocortical neural ensembles during slow wave sleep, both support the idea that memory consolidation involves the transfer of processed hippocampal information for long-term storage in distributed cortical networks. However, the majority of these cortical areas do not receive direct hippocampal projections and little is known about the routes taken by neural activity that can support this process. A prominent, yet under-investigated area that may act as a hippocampo-cortical relay is the retrosplenial cortex. Using silicon probe recordings in awake head-fixed mice, we report here the coordinated interplay of retrosplenial and hippocampal activity during SPW-Rs and the existence of SPW-Rs analogues in the retrosplenial cortex. We show that these interactions are topographically organized and layer specific. Using large-coverage high-density recordings, we demonstrate the existence of multiple subclasses of SPW-Rs and show that retrosplenial neurons are tuned to specific constellations of hippocampal output during SPW-Rs. Finally, we show that hippocampal output to the retrosplenial cortex is mediated by a genetically defined subpopulation of subicular bursty neurons. We demonstrate that optogenetically stimulating these vesicular glutamate transporter 2-expressing neurons is sufficient to evoke cortical ripple responses in superficial retrosplenial cortex, while optogenetic inhibition significantly reduces such responses. These results yield a mechanistic understanding of the neural substrate underlying hippocampal-cortical interactions during the awake resting state, and provide insights into how the offline transfer of previously stored information from the hippocampus to the cortex may be coordinated.

Zusammenfassung

Sharp-wave ripple Komplexe (SPW-Rs) sind kurze, hochfrequente oszillatorische Ereignisse, die durch das hippokampale Netzwerk während des Tiefschlafs und im ruhigen Wachzustand beobachtet werden können. Diese transiente, hoch-synchrone Aktivität unterstützt die Reaktivierung von neuronalen Sequenzen, die im Rahmen von vorhergehender Informationsspeicherung beobachtet wurden. Dies und weitere Befunde deutet darauf hin, dass SPW-Rs eine wichtige Rolle in der Gedächtniskonsolidierung spielen. Die Beobachtungen, dass auch eine Vielzahl kortikaler Areale während der hippokampalen SPW-Rs aktiv ist und dass diese Koaktivierung zeitlich koordiniert stattfindet, unterstützen die Idee, dass die Konsolidierung von Gedächtnisinhalten den Transfer von verarbeiteten Informationen aus dem Hippokampus in diverse kortikale Netzwerke involviert. Die Mehrzahl dieser kortikalen Areale erhält allerdings keine direkten hippokampalen Eingänge, so dass die exakten Projektionen für diesen Informationstransfer unbekannt sind. Eine Region, die hippokampale Informationen in den Neokortex vermitteln könnte, ist der retrospleniale Kortex. Mithilfe von *Silicon Probe*-Ableitungen in wachen, kopf-fixierten Mäusen zeigen wir hier eine koordinierte Interaktion von hippokampaler und retrosplenialer Aktivität während SPW-Rs, sowie die Existenz von SPW-R-Äquivalenten im retrosplenialen Kortex. Wir zeigen weiterhin, dass diese Interaktion topografisch organisiert und schichtspezifisch stattfindet. Mithilfe von räumlich hochauflösenden Aufnahmen weisen wir die Existenz mehrerer Klassen von SPW-Rs nach und zeigen, dass unterschiedliche retrospleniale Neurone an spezifische hippokampale Signale gekoppelt sind. Schließlich zeigen wir, dass die Propagation hippokampaler Aktivität in den retrosplenialen Kortex durch eine bestimmte neuronale Subpopulation im Subikulum vermittelt wird, die den vesikulären Glutamat-Transporter 2 exprimiert (sogenannte ‚*burst-firing*' Zellen im Subikulum). Die spezifische optogenetische Aktivierung dieser Zellen kann Ripple-Oszillationen im retrosplenialen Kortex induzieren, während optogenetische Suppression ihrer Aktivität Ripple-Äquivalente im retrosplenialen Kortex stark reduziert. Diese Ergebnisse liefern ein mechanistisches Verständnis für Grundlagen der hippokampal-kortikalen Interaktionen während des ruhigen Wachzustands und des Transfers von transient im Hippokampus gespeicherter Informationen in den Neokortex.

Table of contents

1 INTRODUCTION

Memory systems have evolved to retain information about events or stimuli occurring in the past which may be crucial for the organism's future survival (Nairne et al., 2007). They are ubiquitous throughout the animal kingdom. In fact, even the simplest organisms such as the bacterium E. coli display a primitive form of 'molecular memory', where methylation of receptors allows the cell to compare the current ligand concentration with the past and change its direction of movement accordingly, a process known as chemotaxis (Vladimirov and Sourjik, 2009). Throughout evolution, and with the development of the nervous system, memory systems became increasingly more sophisticated. Vertebrates evolved more than 500 million years ago and developed the telencephalon, including homologues of the hippocampus, which is widely regarded as the magnum opus of memory systems' evolution. This structure allowed animals to process and store information about their surroundings. It allowed them to efficiently assess the biological relevance of chemical, acoustic and visual stimuli and, crucially, it allowed them to make choices about what actions to take and which to withhold. With the evolution of mammals and the appearance of the neocortex another memory system emerged, one that allowed animals to make abstractions and extract statistical regularities about the world. The hippocampal and neocortical memory systems are believed to give rise to two distinct forms of memory – episodic memory for autobiographical events involving place, time and context, as well as semantic memory for facts, rules and concepts which are devoid of any personal involvement (Tulving, 1972). Collectively referred to as the declarative (or explicit) memory system (as opposed to implicit memory for skills and habits), they are believed to support a diverse assortment of other higher cognitive functions and to provide the foundations upon which our language, culture and society have evolved.

With the progress of research, it has become clear that the hippocampal and neocortical memory systems do not exist in isolation. Rather, they are engaged in a perpetual dialogue (Buzsáki, 1996). This communication is mediated by numerous brain oscillations that provide a syntactical structure to neuronal messages (Buzsáki, 2010). This works aims at understanding the physiological details of this memory transformation process.

1.1 The hippocampal formation – anatomy and connectivity

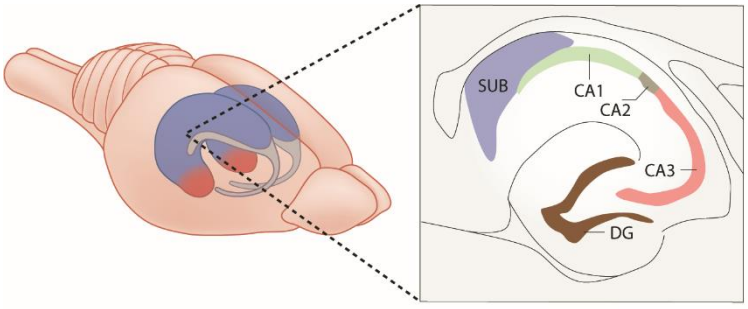

Figure 1.1.1. The rodent hippocampus. Left: The hippocampus extends along the dorso-medial to ventro-lateral axis of the temporal lobe. Dorsal and intermediate segments of the hippocampus (blue) are involved in spatial as well as sensory motor processing, while ventral hippocampus (red) is associated with the processing of emotion, stress and other higher order features. Right: cross-section gross hippocampal anatomy. The hippocampus consists of three major subregions: the dentate gyrus (DG), CA1-3 subfields and the subiculum (SUB). Adapted from Buzsáki and Tingley (2018) and Cembrowski and Spruston (2019).

The hippocampus is a C-shaped elongated brain structure extending from the dorso-medial to ventro-lateral parts of the temporal lobe (Fig. 1.1.1). The striking similarity of the human hippocampus with the seahorse, or *Hippocampus leria* was recognized by the Bolognese anatomist Giulio Cesare Aranzi, who named it (Bir et al., 2015). Together with the olfactory cortex, it is the phylogenetically oldest part of the cortex with only a single layer of principal cells and it is therefore classified as archicortex. The hippocampus consists of three major subregions: the dentate gyrus (DG), the hippocampus proper (CA3, CA2 and CA1) and the subiculum (Fig. 1.1.1) (van Strien et al., 2009). Each of these subdivisions is endowed with unique network characteristics and is believed to support different aspects of declarative memory. The hippocampal subregions are traditionally described as a set of unidirectional, serially connected structures. The main source of inputs to the hippocampus is provided by the entorhinal cortex (EC), which targets all of its subregions via the perforant path. Efferents from EC layer II give rise to the tri-synaptic pathway to the DG and distal CA3. The principal cells of the DG, known as granule cells, project to pyramidal cells in CA3 area via their mossy fibers axons. CA3 cells, in turn, give rise to the Schaffer collaterals, which terminate on the proximal apical dendrites of CA1 cells (stratum radiatum), providing their major input. They also give rise to vast network of associational fibers connecting together neighboring CA3 cells, as well as commissural fibers to the contralateral CA1-3 subfields. In addition, inputs from EC layer III to the distal apical dendrites of CA1 cells (stratum lacunosum-moleculare) and subiculum constitute the direct pathway, also known as the temporoammonic pathway. Additional sources of input to the hippocampus

include the peri- and postrhinal cortices, as well as the anterior cingulate cortex (Rajasethupathy et al., 2015; van Strien et al., 2009). In addition to cortical inputs, the hippocampus also receives subcortical inputs from a vast number of areas including the amygdala, the basal forebrain, the supramammilary nucleus, nucleus reuniens of the thalamus, as well as neuromodulatory inputs from the brainstem (Van Groen and Wyss, 1990) (Fig. 1.1.2).

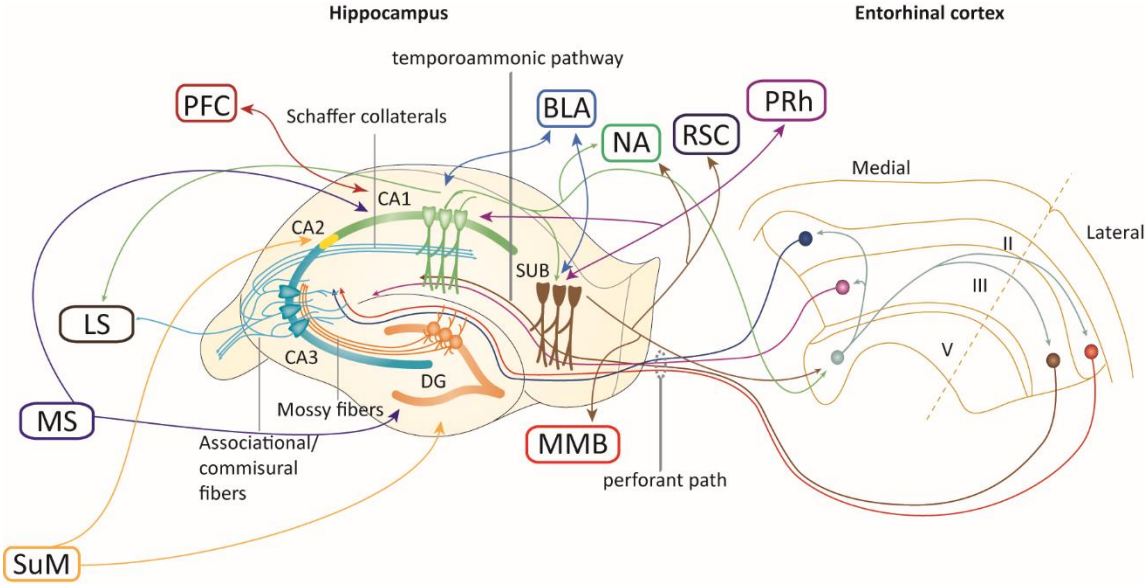

Figure 1.1.2. Hippocampal intrinsic and extrinsic connectivity. The hippocampus (left) receives its major input from superficial layers of the entorhinal cortex (right) which target either the dentate gyrus (DG) and CA3 (via the perforant path) or CA1 and subiculum (via a tract of the perforant path, the temporoammonic pathway). Granule cells in the DG target CA3 pyramidal cells via their mossy fibers. CA3 cells are reciprocally connected with ipsilateral CA3 cells, as well as contralateral CA3 and CA1 cells via associational and commissural fibers, respectively. They also give rise to the Schaffer collaterals that target CA1 area. CA1 area targets both the subiculum (SUB) and layer V EC. The subiculum targets layer V EC, as well as many additional cortical and subcortical areas, providing the majority of extrinsic hippocampal efferents. A non-exhaustive selection of other input and output areas is shown in colored boxes. Arrows indicate the directionality of projection. PFC, prefrontal cortex; BLA, basolateral amygdala; NA, nucleus accumbens; RSC, retrosplenial cortex; PRh, perirhinal cortex; LS, lateral septum; MS, medial septum; SuM, supramammillary nucleus; MMB, medial mammillary bodies. Adapted from Neves, Cooke and Bliss (2008).

Extrinsic projections from the hippocampus are provided by all CA subfields, yet to a very different extent. While the CA3 area gives rise to a rich network of intrinsic efferents, its extra-hippocampal projections are limited to the subcortical lateral septum and diagonal band of Broca (Swanson and Cowan, 1977). CA1 area gives rise to a larger number of extrinsic efferents including cortical areas such as the EC, the medial prefrontal cortex, perirhinal cortex as well as subcortical areas including nucleus accumbens and the amygdala (Aggleton and Christiansen,

2015). Most of CA1 axons, however, target the neighboring subiculum, which conveys the majority of hippocampal output. The subiculum does not only project to the same structures targeted by CA1 area but also to a large number of additional cortical and subcortical targets including the retrosplenial cortex, orbitofrontal cortex anterior thalamic nuclei, septum and mammillary bodies (O'Mara, 2006).

1.2 The hippocampal formation and episodic memory

No brain structure has been implicated in learning and memory as strongly and unequivocally as the hippocampus. The first clear association between hippocampal dysfunction and memory loss dates back to the famous patient H.M. As a treatment for a severe drug resistant epilepsy, H.M. underwent a bilateral surgical removal of his hippocampi and neighboring structures including the amygdala, entorhinal cortex and parahippocampal cortex. This procedure effectively reduced the prevalence of epileptic seizures but left H.M. with a severe anterograde amnesia, preventing him from remembering events experienced after the surgery (Scoville and Milner, 1957). It also resulted in a temporally-graded retrograde amnesia, preventing H.M. from recollecting episodes that took place up to 11 years prior to the surgery, while sparing memories acquired earlier (Sagar et al., 1985). Importantly, other mnemonic domains such as semantic memory, i.e. the knowledge of general facts, ideas and concepts that are not autobiographical as well as motor learning skills were spared by the surgery, suggesting that these mnemonic faculties are largely independent of the hippocampus (Corkin, 1965). The case of patient H.M. and similar human subjects with hippocampal damage have motivated a lesion approach as an animal model of amnesia. This approach yielded numerous studies that indicated deficits of lesioned animals in forming new relational, contextual and spatial associations (Lavenex et al., 2006; Morris et al., 1990; Winocur, 1990; Winocur et al., 2001).

These numerous observations from human and animal studies gave rise to multiple theoretical considerations aiming to model the role of the hippocampus in episodic memory (McClelland et al., 1995; Nadel and Moscovitch, 1997; Squire and Alvarez, 1995; Treves and Rolls, 1994). Most of these models were rooted in earlier ideas dating back to Hebb and Marr (Hebb, 1949; Marr, 1971). The common ground shared by these models is that the hippocampus is a fast

learning memory system that can rapidly store and integrate the representations of correlated inputs from the environment. However, debate between these models remains concerning their predictions about the consolidation of initially labile hippocampal memories. While the 'standard model' (Alvarez and Squire, 1994; McClelland et al., 1995) posits that hippocampal-dependent memories are fully transferred to the neocortex and eventually become independent of the hippocampus, the alternative 'multiple-trace theory' postulates that the hippocampus is involved in the retrieval of all episodic memories, including remote ones (Nadel and Moscovitch, 1997). An alternative view is that the hippocampus acts as an index to distributed neocortical ensembles corresponding to a given memory (Teyler and DiScenna, 1986).

A major development that helped to bridge the results of cognitive studies and physiological correlates of episodic memory was the development of microelectrode recordings, which allowed experimenters to monitor the activity of single neurons in behaving animals. Using this technique, O'Keefe and Dostrovsky (1971), recorded the activity of hippocampal CA1 neurons from rats freely foraging in an open arena. By correlating the animal's location in the environment and the activity of single pyramidal cells, they found that some cells (termed 'place cells') selectively fire when the rat occupies a specific location in the enclosure (termed 'place field') (O'Keefe and Dostrovsky, 1971). Subsequently, place cells have been described in all other hippocampal areas including DG and CA3 (Jung and McNaughton, 1993), CA2 (Mankin et al., 2015) as well as the subiculum (Sharp and Green, 1994). The discovery of place cells has re-inspired Tolman's idea about a cognitive map (Tolman, 1948), and pinpointed the hippocampus as a structure dedicated to forming an internal representation of the environment (O'Keefe and Nadel, 1978). Consistently, hippocampal lesions were shown to severely impair place orientation in rodents (Morris et al., 1982).

The discovery of place cells has motivated further research of spatial navigation and its cellular correlates in rodents, revealing other types of spatially modulated cells in the hippocampus and parahippocampal regions: Head-direction cells, which are modulated by the animal's directional heading were first described in the dorsal presubiculum (Taube et al., 1990) and later identified in numerous other brain areas of the limbic system such as the mammillary bodies, anterior thalamus, medial EC (Taube, 2007) and more recently in the hippocampus

(Acharya et al., 2016). Border cells fire in response to geometrical borders in the environment and were found in the EC (Solstad et al., 2008) and subiculum (Lever et al., 2009). Neurons coding for the animal's speed have been found in the medial EC and hippocampus (Góis and Tort, 2018; Kropff et al., 2015). Finally, grid cells with hexagonal, grid-like firing fields were described in the medial EC and associated structures (Boccara et al., 2010; Hafting et al., 2005). In addition to cells that respond to these single spatial modalities, conjunctive cells, i.e. cells with a multiplexed code that respond to a combination of two or more modalities have also been described (Sargolini et al., 2006).

The seemingly disparate function of the hippocampal formation in episodic memory (from human patients and behavioral studies) and spatial navigation (from single unit recordings in rodents) could be reconciled if one considers the recall of episodic memories as a 'mental travel' (Buzsáki and Moser, 2013; Eichenbaum et al., 1999). According to this view, the evolution of episodic memories is rooted in the sequential activations of neuronal assemblies such as place and grid cells, which are not restricted to the spatial domain. This idea is supported by studies showing that CA1 pyramidal cells that act as place cells during spatial exploration can encode elapsed time when immobile in a task that involves a delay period, thus demonstrating that place cells can also encode discrete moments in time (MacDonald et al., 2011; Pastalkova et al., 2008). This sequential activity during behavior is hypothesized to lay the foundation for the emergence of self-organized patterns such as those observed during network oscillations which I discuss in the following.

1.3 Hippocampal oscillations and their relation to memory functions

Brain oscillations provide a powerful means for neural communication within and between structures (Buzsáki, 2006). Hippocampal oscillations during both sleep and wakefulness have received special focus throughout the years and are a well-established indicator of the animal's brain state, at least in rodents (Kay and Frank, 2019). Hippocampal LFP in rodents can be classified into three major brain states with distinct overt behavioral correlates: 'regular slow activity' during locomotion and rapid eye movement sleep, 'large irregular activity' during low arousal

immobility and slow-wave sleep (SWS) and 'small irregular activity' during intermediate arousal states and cessation of movement (Vanderwolf, 1969).

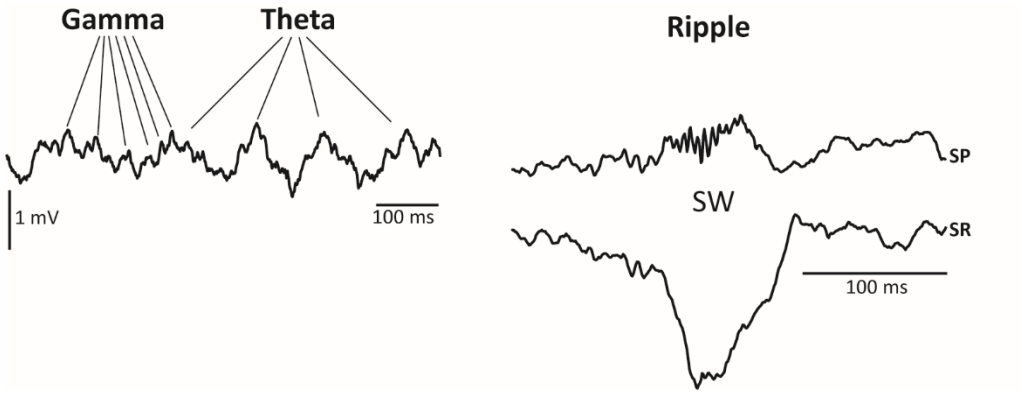

Figure 1.3.1. Hippocampal oscillations. Left, during ambulatory behaviors such as running and exploration the hippocampal network is dominated by the 6-9 Hz theta rhythm. This rhythm is often superimposed with a faster oscillation in the gamma band (30-100 Hz). Right: During consummatory immobile behaviors such as sleeping, eating or grooming, theta is replaced by the irregular occurrence of sharp-wave ripples. These events are composed of the slower sharp-wave component, best observed in apical dendrites layer of CA1 area, stratum radiatum (SR). Sharp waves are often embedded with the short lived ripple oscillation (120-250 Hz), best observed in the pyramidal cell layer, stratum pyramidale (SP).

Regular slow activity is manifested by theta oscillations, a 6-9 Hz rhythm which is of a particular relevance for memory functions (Fig.1.3.1) (Buzsáki, 2002; Green and Arduini, 1954; Robinson et al., 1977; Vanderwolf, 1969). It is believed to reflect the coherent fluctuations of transmembrane currents summed across many hippocampal neurons. Theta oscillations in the hippocampus and surrounding structures are completely abolished by lesions of the medial septum, which is thought to act as the theta pacemaker (Petsche et al., 1962). However, some evidence suggests that other areas such as the supramammilary nucleus and the ventral tegmental area may also contribute to theta generation (Pan and McNaughton, 2002; Vertes et al., 2004). Importantly, reversible abolishment of theta oscillations by septal inactivation was shown to result in a decreased memory performance in both spatial and non-spatial tasks (Mizumori et al., 1990). Moreover, the extent of impairment in a spatial memory task correlated with the amount of reduction in hippocampal theta (Winson, 1978). Theta oscillations are believed to temporally link together neural assemblies during memory encoding, as suggested by the observation that the spiking sequence of individual place cells within a given theta cycle can predict the past, present and future locations of the animal (Buzsáki and Tingley, 2018). As

the animal moves throughout the environment, new place cells representing upcoming locations join the assembly while neurons whose place field the animal has already passed disappear. The activity of every given place cell exhibits a unique temporal relationship with the local theta rhythm, where spikes emitted by the place cell progressively shift to earlier phases of the local theta oscillation as the animal traverses the place field. This phenomenon is known as theta phase precession or theta sequences (Skaggs et al., 1996). Two recent studies have demonstrated that obliterating hippocampal theta by inactivation of the medial septum left place cell coding intact (Brandon et al., 2014), while disrupting the emergence of organized neural assemblies and their sequential activation, resulting in a decreased task performance (Wang et al., 2015). Together, these data suggest that theta sequences, rather than place cells per se, contribute to memory function.

Theta oscillations are often nested with the faster gamma rhythm, a 30-100 Hz oscillation in the local field potential that is believed to reflect the competition between excitatory and inhibitory neurons (Fig.1.3.1) (Buzsáki and Wang, 2012). Gamma oscillations are not confined to the hippocampus and are commonly observed in other cortical and subcortical areas as well. Similar to hippocampal gamma, which is modulated by the slower theta rhythm, cortical gamma is often coupled to and modulated by the phase of lower frequency oscillations such as slow waves or sleep spindles (Takeuchi et al., 2016), a phenomenon known as phase-amplitude coupling. Gamma oscillations are the most variable rhythm, both in frequency and amplitude, which complicates studying their underlying mechanisms and function. However, recent experiments have led to the growing consensus that, at least in the case of the CA1 subfield, different gamma sub-bands are driven by distinct inputs, with low gamma driven by the CA3 area whereby mid-high gamma is entrained by EC inputs (Belluscio et al., 2012; Colgin et al., 2009; Fernández-Ruiz et al., 2017). Accordingly, low gamma activity is prevalent in stratum radiatum, where CA3 axons terminate, whereas mid-high gamma dominates in stratum lacunosum-moleculare, which is targeted by EC inputs. Importantly, CA3 and EC inputs to CA1 are associated with memory recall and memory encoding, respectively (Colgin, 2016; Treves and Rolls, 1994), suggesting that different gamma sub-bands carry out different mnemonic functions. Given the high variability in gamma frequency and the fact that gamma oscillations can be observed during

virtually all brain states, it is likely to support multiple cognitive functions (Fries, 2015). One idea that has gained strong experimental support is the functional cell assembly hypothesis (Buzsáki, 2010; Harris, 2005; Harris et al., 2003), which is rooted in earlier ideas from Hebb (Hebb, 1949), and postulates that gamma oscillations dynamically organize the firing of individual members of a neural assembly. This idea is supported by the fact that the duration of a single gamma cycle overlaps with several other important physiological factors such as the average membrane time constant of pyramidal neurons (Spruston and Johnston, 1992), the duration of α-amino-3-hydroxy-5-methyl-4-isoxazolepropionic acid (AMPA) receptor mediated excitatory post synaptic potentials (EPSPs) and gamma aminobutyric ($GABA_A$) receptor mediated inhibitory post synaptic potentials (IPSPs) (Johnston and Wu, 1995), as well as the time window for synaptic plasticity (Magee and Johnston, 1997; Markram et al., 1997). Altogether, these observations suggest that gamma oscillations offer a time window for maximized cooperativity between neurons.

Another hippocampal rhythm instrumental for memory is the sharp-wave ripple complex (SPW-R), an irregular LFP pattern which is most prominently observed during "off-line" states such as awake immobility, consummatory behaviors and SWS (Fig.1.3.1) (Buzsáki, 2015; Buzsáki et al., 1992; Korte and Schmitz, 2016). SPW-Rs comprise a slower sharp-wave (SW) component which reflects the depolarization of CA1 pyramidal cells' apical dendrites in stratum radiatum by synchronous population discharges of CA3 pyramidal cells via the Schaffer collaterals. They are often embedded with a faster oscillatory component (120-250 Hz) termed 'ripple', which reflects the local interplay between excitation and inhibition of pyramidal cells in the pyramidal cell layer, where it is best

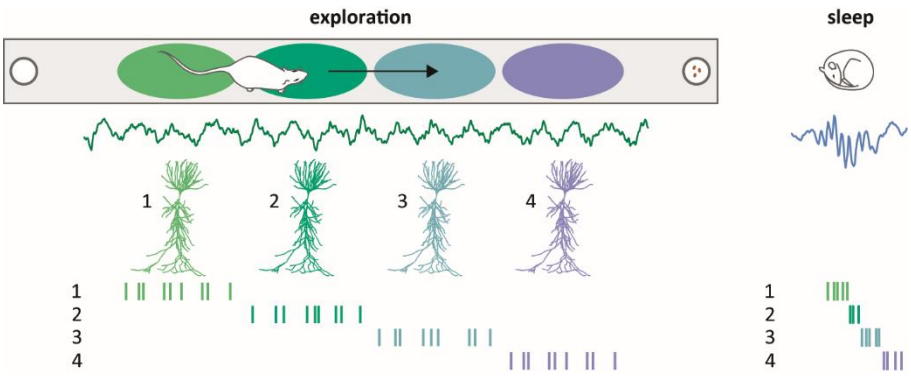

Figure 1.3.2. Replay of awake sequences. Left: During exploration of a linear track the hippocampal network is dominated by the theta rhythm (middle green trace). A sequence of place cells (here 1→4, bottom panel) are consecutively activated as the rat enters their respective place fields (top ellipses). Right: During the subsequent sleep session, the same place cells that were active on the track are reactivated in the same order, this time coupled to the faster ripple. From Girardeau and Zugaro (2011).

observed (Buzsáki, 2015; Ylinen et al., 1995).

Despite the extensive experimental attention that ripple oscillations have received in recent decades, the mechanisms underlying their induction and rhythmogenesis are still a matter of debate. Several hypotheses were proposed to explain how excitatory barrages could result in such an organized oscillatory event. The main candidates have been (1) gap junctions between pyramidal cells (Draguhn et al., 1998; Schmitz et al., 2001; Traub and Bibbig, 2000); (2) reciprocal inhibition between GABAergic interneurons interconnected either electrically (Holzbecher and Kempter, 2018; Pais et al., 2003) or chemically (Schlingloff et al., 2014; Taxidis et al., 2012; Ylinen et al., 1995); (3) balance between excitation and inhibition (Brunel and Wang, 2003; English et al., 2014; Memmesheimer, 2010); and (4) feedback loops between pyramidal neurons and reciprocally connected interneurons (Stark et al., 2014).

SPW-Rs have been strongly implicated in systems consolidation and memory retrieval, as well as other cognitive processes such as planning, decision-making and imagination (Buzsáki, 2015; Joo and Frank, 2018). This view is supported by the observation that ripple oscillations are often embedded with forward or reverse sequences of place cell firing observed during preceding experience, temporally compressed ~10-20 fold, a phenomenon known as 'replay' or 'reactivation' (Fig. 1.3.2) (Diba and Buzsáki, 2007; Lee and Wilson, 2002). A causal role for SPW-Rs in systems consolidation is supported by the finding that disrupting SPW-Rs, either electrically or optogenetically, impairs memory performance (Ego-Stengel and Wilson, 2010; Girardeau et al., 2009; Jadhav et al., 2012; Roux et al., 2017). Consistently, blockade of CA3 output in transgenic animals was shown to alter CA1 ripple properties and to interfere with consolidation of contextual fear memory (Nakashiba et al., 2009).

The observed phenomenon of replay implies that SPW-Rs can bring together the firing of cells which were well separated in time during behavior into timescales relevant for synaptic plasticity. Consistent with this notion, SPW-Rs have also been hypothesized to contribute to synaptic consolidation by enhancing the synaptic efficacy between CA3 pyramidal cells and their target CA1 cells resulting in long-term synaptic potentiation (LTP) (Buzsáki, 1989). This view has gained recent support from two independent findings: an *in vitro* study demonstrated that reactivated place cell firing patterns can induce LTP between CA3 -> CA1 synapses, but only if

accompanied by a SPW-R (Sadowski et al., 2016). Subsequently, a second study discovered that SPW-Rs promote the N-methyl-D-aspartate (NMDA) receptor dependent long-term depression (LTD) at CA3-CA1 synapses (Norimoto et al., 2018). The authors proposed that SPW-Rs serve to 'reset' unnecessary synapses reflecting uncorrelated pre- and postsynaptic activity and help avoiding memory saturation, consistent with the proposed role of SWS (De Vivo et al., 2017). These findings, which at first may seem contradictory, highlight the potential dual role of SPW-Rs in erasing older memory traces by downscaling irrelevant synapses while strengthening a minority of memory relevant synapses reflecting newer memory engrams.

Multiple theories have been put forth to explain the contribution of brain oscillations to episodic memory (Hanslmayr et al., 2016; Hasselmo, 2007; Nyhus and Curran, 2010; Teyler and DiScenna, 1986). Perhaps most influential and widely accepted is the two-stage model (Buzsáki, 1989; Diekelmann and Born, 2010; Frankland and Bontempi, 2005; Kumaran et al., 2016; Marshall and Born, 2007). This model postulates that during exploratory behaviors associated with theta rhythm (i.e. memory encoding) neocortical information is transmitted to the hippocampus via the EC, reaching the granule cells of the DG. The activity of granule cells, in turn, can transiently induce a weak heterosynaptic potentiation of CA3 cells. Upon the termination of the exploratory behavior or during sleep (i.e. memory consolidation), the weakly potentiated CA3 cells will initiate a population burst (a sharp wave) that will in turn induce a ripple event in CA1 and strengthen the connections between CA3 neurons and their target CA1 cells (Buzsáki, 1989). This is consistent with the observation that CA3 and CA1 cells reach maximal discharge synchrony during SWS (Buzsáki, 1989). The excitatory outflow from CA1 area is expected to reverberate back to the EC, and be further conveyed to different associational areas of the neocortex for long-term storage of the memory trace, a process that is assumed to repeat many times during a single sleep session.

1.4 Coupling between hippocampal and neocortical rhythms

Similar to hippocampal rhythms, neocortical activity patterns perpetually change with brain state changes. Neocortical oscillations have been heavily studied during sleep, and are a useful indicator for sleep stage (Diekelmann and Born, 2010). Neocortical LFP during SWS is

characterized by highly regular slow oscillations in the delta range (0.5 – 4 Hz) reflecting the fluctuations between membrane hyperpolarization and neural silence (DOWN-state) and depolarization and associated spiking (UP-state) of a large number of cortical neurons (Steriade et al., 1993). Although the phase of slow oscillations can be influenced by thalamic activity (Steriade et al., 1993), the fact that they persist even after large thalamic lesions (Steriade et al., 1993) and can be observed in isolated cortical slices (Sanchez-Vives and McCormick, 2000) suggests that they are locally generated in the neocortex. Slow oscillations have been hypothesized to underlie sleep homeostasis by facilitating local synaptic changes, a process which is believed to convey the beneficial effects of sleep on memory (Tononi and Cirelli, 2003). In support of this view, slow oscillation power was shown to undergo a specific increase in the motor cortex of human subjects following a motor learning task (Huber et al., 2004). Moreover, triggering slow waves using transcranial magnetic stimulation in humans was shown to improve memory performance (Marshall et al., 2006), further establishing a role of this cortical rhythm in memory processing. Another prominent cortical rhythm observed during SWS are spindles, bouts of 7-14 Hz oscillatory activity lasting for ~1 second (Steriade et al., 1993). Spindle oscillations are generated in the thalamus as the result of synaptic interactions between inhibitory interneurons in the reticular nucleus and thalamocortical cells in various dorsal thalamic nuclei (Steriade et al., 1993). Sleep spindles have also been implicated in memory processing, as suggested by their increased density following learning (Antony et al., 2019), yet their exact involvement is poorly understood.

Numerous electrophysiological studies employing simultaneous recordings from the hippocampus and various cortical structures reported a strong coupling between cortical and hippocampal rhythms (Fig. 1.4.1). These interactions were shown to heavily depend on brain state changes, with enhanced cross-structural communication during SWS as compared to REM sleep (Wierzynski et al., 2009). Hippocampal ripples show a bimodal coupling to slow oscillations with an increased ripple probability around the transitions from a DOWN to an UP state and vice versa but very low probability during DOWN states (Battaglia et al., 2004; Sirota et al., 2003). Sleep spindles, in turn, tend to follow slow waves by few hundreds of milliseconds and are often coupled with ripples themselves (Siapas and Wilson, 1998; Sirota et al., 2003). This transient

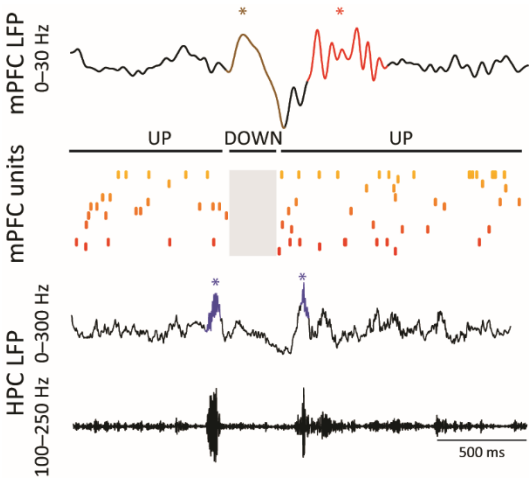

Figure 1.4.1. Coupling of hippocampal and neocortical oscillations. During slow wave sleep, the neocortical local field potential is dominated by slow waves (top panel brown trace and asterisk) and alternating periods of neural firing and global silence known as UP and DOWN states (middle panel). Slow waves are often followed by thalamo-cortical sleep spindles (top red trace and asterisk). Hippocampal SPW-Rs (bottom blue trace and asterisk and ripple-band filtered trace below) are often coupled to the transitions between UP and DOWN states as well as to sleep spindles. Modified from Maingret et al (2016).

oscillatory coupling has been hypothesized to facilitate the transfer of information between the hippocampus and neocortex by providing a temporal window of increased excitability and synaptic plasticity in both structures (Diekelmann and Born, 2010). Consistent with this idea, more recent studies have found that, during those brief periods of cross-structural oscillatory coupling, neocortical and hippocampal neuronal ensembles display a coordinated reactivation of awake sequences (Ji and Wilson, 2007; Peyrache et al., 2009; Rothschild et al., 2017). Finally, evidence for a causal role of the hippocampal-cortical dialogue in memory consolidation was provided by two recent studies. The first study found that electrical stimulation of the neocortex during SWS could induce a slow-wave which was often followed by a sleep-spindle. By triggering the electrical stimulation upon hippocampal SPW-R detection in a closed-loop manner the experimenters were able to artificially boost the coupling between hippocampal SPW-Rs, cortical slow-oscillations and sleep spindles (Maingret et al., 2016). This manipulation, when employed in the sleep session following the acquisition of a spatial memory task, was capable of enhancing memory performance in the following test session, but only if the stimulation was applied within 250 ms after SPW-R detection. A second study found that a closed-loop optogenetic stimulation of the thalamus that was contingent upon slow-wave detection could boost the coupling between slow-waves, spindles and hippocampal SPW-Rs and improve memory performance in a contextual memory task. Conversely, closed-loop optogenetic suppression of the thalamus reduced the incidence of sleep spindles and impaired memory performance on the same task (Latchoumane et al., 2017).

Together these data highlight the importance of hippocampal-cortical coupling during SWS and provide a physiological substrate for the 'two-stage' model of memory consolidation.

In contrast to the wealth of data on neocortical activity patterns during sleep, variations in neural activity in the awake brain are comparably subtle and their underlying mechanisms are poorly understood (Harris and Thiele, 2011). Unlike the hippocampus, which exhibits regular theta oscillations during overt behaviors, neocortical patterns in the awake active brain lack a robust theta and have been traditionally classified as 'desynchronized' (Vanderwolf, 1971). This view has been recently challenged by a series of breakthroughs in cortical physiology in awake rodents which pointed the existence of an additional prominent population pattern characterized by ~6-10 Hz LFP oscillations that occasionally alternates with desynchronized LFP during waking behavior (Crochet and Petersen, 2006; Luczak et al., 2013; McGinley et al., 2015a; Petersen et al., 2003). This strongly synchronous neocortical pattern was hypothesized to correspond to the evolutionary precursor of alpha oscillations in primates (Nicolelis et al., 1995; Senzai et al., 2019). At the neuronal level the synchronized pattern is characterized by alternating population firing and silent periods reminiscent of the DOWN state of SWS, previously referred to as 'activity packets' (Luczak et al., 2009, 2013). However, despite those meaningful insights, it remains unclear whether hippocampal-cortical communication in the awake resting state undergoes brain-state dependent modulation similar to that observed during sleep (Wierzynski et al., 2009).

1.5 Cell-type diversity in the hippocampus

The brain's ability to perform complex cognitive functions such as memory processing requires its constituents to execute a diverse assortment of operations. This quality is realized by maintaining a high degree of heterogeneity, even within a given cell-type. The high degree of heterogeneity within hippocampal pyramidal cells has been first recognized by Lorente de Nó, who, using Golgi staining, identified strong differences in the dendritic and axonal morphology of CA3 pyramidal cells, leading to its division in 'a', 'b' and 'c' subregions (de Nó, 1934). More recent advances in molecular biology and electrophysiology have motivated the further subdivision of neurons based on differential gene expression, electrophysiological properties as

well as functional properties such as projection pattern and participation in network events. A particularly well studied heterogeneity in the hippocampus is that of GABAergic interneurons. Despite the fact that they represent only ~15% of the overall neuronal population in the hippocampus, inhibitory interneurons show a tremendous diversity, giving rise to more than 15 different subclasses with distinct anatomical distribution, morphology, connectivity, embryogenesis, gene expression patterns and participation in network events (Freund and Buzsáki, 1996; Pelkey et al., 2017; Somogyi and Klausberger, 2005). Nevertheless, principal cells of the hippocampus also display high diversity, which is perhaps best studied in the CA1 region where it is observed across each axis under examination. Proximal and distal subdivisions of CA1 are preferentially targeted by the medial and lateral entorhinal cortices, respectively (Ito and Schuman, 2012; Steward, 1976). This distinctive input pattern is manifested by a decreasing gradient in spatial information along the proximo-distal axis, consistent with the stronger engagement of the medial EC in spatial processing (Hargreaves et al., 2005). Perhaps even more striking is the heterogeneity of CA1 neurons observed along its dorso-ventral axis. Pyramidal cells in these opposing hippocampal poles differ with respect to their downstream targets where dorsal CA1 neurons preferentially target areas involved in spatial navigation while areas innervated by ventral neurons are associated with motivated behavior, emotions and stress. Dorsal and ventral CA1 pyramidal cells also differ with respect to other properties such as place field size, which shows a gradual increase from dorsal to ventral recordings sites, intrinsic excitability, which is greater in ventral CA1 pyramids (Malik et al., 2016), as well as gene expression patterns (Cembrowski and Spruston, 2019; Cembrowski et al., 2016; Fanselow and Dong, 2010). Finally, heterogeneity of CA1 neurons has also been described along the deep-superficial axis. Deep, calbindin-immunonegative pyramidal CA1 neurons are burstier, fire at higher rates, prone to place tuning, preferentially suppressed during SPW-Rs and are selectively contacted by CA2 cells. In contrast, superficial, calbindin-expressing, pyramidal cells tend to be recruited by SPW-R events and carry more stable spatial representations (Danielson et al., 2016; Kohara et al., 2014; Mizuseki et al., 2011; Valero et al., 2015).

Another example of hippocampal cell-type diversity which is of particular relevance for this study is the subiculum. The subiculum acts as the primary output of the hippocampus, with

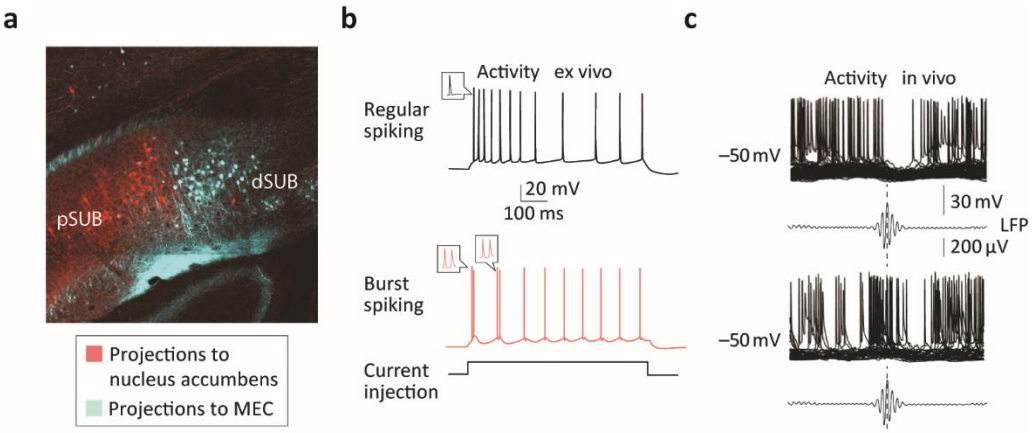

Figure 1.5.1. Cell-type diversity in the subiculum. a) Injections of retrograde viruses in nucleus accumbens and medial EC result in labeling of cells in proximal (pSUB, red) and distal (dSUB, cyan) subiculum, respectively. b) Subicular pyramidal cells can be distinguished based on their firing pattern following suprathreshold current injecting *in vitro* which can be either regular (top, black) or bursty (bottom, red). c) Bursting and non-bursting subicular cells are differentially recruited during SPW-R events *in vivo*. While non-bursting cells tend to be silenced during SPW-Rs (top) the activity of bursting cells is up-regulated. Average LFP centered around ripple peak is shown below each case. Modified from Cembrowski and Spruston (2019).

extensive efferents to a vast number of cortical and subcortical downstream targets. Despite its relatively small size, the subiculum shows a high degree of heterogeneity that is most strongly manifested along its proximo-distal axes (Fig. 1.5.1). The proximal subiculum projects to nucleus accumbens, lateral septum, lateral EC, perirhinal cortex and prelimbic cortex, areas which have been traditionally associated with the processing of context related non-spatial information (Naber and Witter, 1998). In addition, a subset of subicular cells in proximal subiculum sends back-projections to CA1 cells (Sun et al., 2014, 2019; Xu et al., 2016). The distal subiculum, on the other hand, projects to presubiculum, retrosplenial cortex (RSC), medial EC and the medial mammillary bodies, brain regions which are involved with spatial processing and belong to the theta system (Fig. 1.5.1a) (Aggleton and Brown, 1999; Naber and Witter, 1998). Subicular pyramidal cells also differ with respect to their firing pattern with regular firing cells located mainly in proximal subiculum and intrinsically bursting cells in distal subiculum (Fig. 1.5.1b) (Behr et al., 2009). Earlier studies revealed that the burst propensity of distal subicular neurons does not depend upon the magnitude of synaptic inputs, but rather on the activation of voltage-gated Ca^{2+} channels. The resulting Ca^{2+} tail currents lead to an afterdepolarization, which in turn drives a burst of two or more action potentials (Jung et al., 2001; Staff et al., 2000). Distal subicular cells were also shown to exhibit higher spatial information and stronger theta modulation compared

to their proximal peers (Kim et al., 2012). Intriguingly, the bursting activity of distal subicular cells can be upregulated by the synergetic activation of group I, subtype 1 metabotropic glutamate receptors and muscarinic acetylcholine receptors, suggesting that the output of these cells dominates during theta and spatial exploration associated with cholinergic inputs from the medial septum (Moore et al., 2009). Moreover, proximal and distal subicular cells express different forms of LTP with CA1 cells, suggesting different involvement in memory functions (Wozny et al., 2008). Other differences along those axes, such as pharmacological responsiveness, dendritic morphology and gene expression have also been documented, further establishing the distinction between those subdivisions (Cembrowski et al., 2018a, 2018b; Graves et al., 2012; Kim and Spruston, 2012). Importantly, regularly firing cells in proximal subiculum and bursty cells in distal subiculum are also differentially embedded in network oscillations, with bursty cells predominantly excited and regularly firing cells inhibited by SPW-Rs (Fig. 1.5.1c) (Böhm et al., 2015).

1.6 Aims of study

Ripple oscillations are believed to fulfill their ascribed role in memory consolidation by facilitating the transfer of hippocampal representations to distributed cortical networks (Buzsáki, 1989; Frankland and Bontempi, 2005; Kumaran et al., 2016; McClelland et al., 1995). This view is supported by multiple experimental findings indicating a strong increase in activity in a plethora of cortical areas during SPW-R events (Logothetis et al., 2012; Peyrache et al., 2009; Sirota et al., 2003; Wang and Ikemoto, 2016; Wilber et al., 2017). Yet, paradoxically, the majority of these cortical areas do not receive direct hippocampal output. Consequently, the paths as well as mechanisms by which the hippocampus broadcasts the ripple content to the rest of the neocortex remain largely unexplored. Previous work examining the propagation of SPW-R activity from the hippocampus to the neocortex has focused primarily on the medial EC and related para-hippocampal structures (Chrobak and Buzsáki, 1996), while other hippocampal-cortical pathways remain unexplored.

One candidate area capable of mediating processed hippocampal output which remains relatively unexplored is the retrosplenial cortex (RSC). The RSC is situated at the septal interface

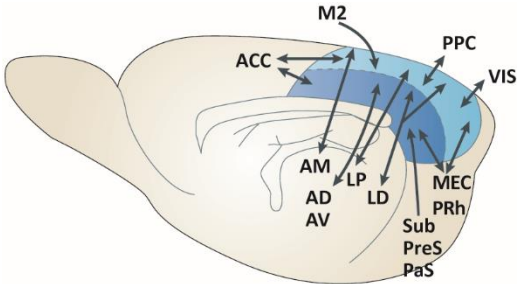

Figure 1.6.1. Connections of the retrosplenial cortex. a) Main connections of the rodent RSC. Dysgranular RSC (area 30) is indicated in cyan, granular RSC (area 29) in blue. M2, secondary motor cortex; PPC, posterior parietal cortex; VIS, visual cortex; AM, AD, AV, medial, dorsal and ventral anterior thalamic nuclei, respectively; LP, lateroposterior thalamus; LD, laterodorsal thalamus; PreS, presubiculum; PaS, parasubiculum; PRh, perirhinal cortex. Modified from Vann et al (2009).

between the dorsal hippocampus and the neocortex and is one of the largest cortical areas in the rodent brain (Vann et al., 2009). Anatomically, the RSC is divided into two subdivisions: the granular RSC (gRSC, area 29), a 4-layered parahippocampal-cortical transition zone as well as the dysgranular RSC (dRSC, area 30), a fully neocortical structure. It is strongly interconnected with a variety of sensory and associational areas including the medial EC, prefrontal cortex, posterior parietal cortex, visual cortex, as well as with subcortical structures such as the anterior dorsal thalamic nuclei and the claustrum (Fig. 1.6.1) (Sugar et al., 2011). Furthermore, the RSC has been heavily implicated in spatial navigation and in the integration of multiple spatial frames of reference. Several studies pointed the existent of different types of spatially modulated cells in the RSC including classical head-direction cells (Chen et al., 1994) and bidirectional head-direction cells (Jacob et al., 2017), place-by-direction cells (Alexander and Nitz, 2015; Cho and Sharp, 2001) and classical place cells (Mao et al., 2017). In addition, several lines of evidence indicate that the RSC is involved in the processing, storage and retrieval of contextual memories. For example, the RSC exhibits a robust increase in immediate early gene activity following spatial learning task or contextual fear conditioning (Czajkowski et al., 2014; Keene and Bucci, 2008; Milczarek et al., 2018). Furthermore, inactivation of the RSC can impair learning, while activation of RSC engram cells is sufficient to induce memory recall in a contextual fear-conditioning task independently of the hippocampus (Cowansage et al., 2014). In-line with its role in spatial navigation and episodic memory, lesions to the RSC in humans result in deficits in orientation and memory retrieval. Consistently, it is also among the first areas to show signs of Alzheimer's disease pathology (Vann et al., 2009).

Earlier tracing studies indicated that the gRSC receives topographically organized inputs from the subiculum (Van Groen and Wyss, 2003; Wyss and Van Groen, 1992). Subsequently,

retrograde tracing studies have shown that these inputs stem from bursting cells in distal subiculum (Kim and Spruston, 2012). However, the functional relevance of these inputs, the information they carry and their exact postsynaptic targets were unknown in the absence of genetic access to the bursting subicular cells. Moreover, whether and how this pathway contributes to the propagation of hippocampal network activity to the neocortex remained largely unexplored.

The aims of this study were to address these questions using a bottom-up approach:

1. In order to examine whether the gRSC could mediate SPW-R-associated activity, we first sought to thoroughly characterize how RSC activity, including LFP and single units, is modulated by hippocampal SPW-Rs in naïve animals.
2. As discussed above, subicular projections to the gRSC were shown to arise from bursting cells in distal subiculum. We therefore sought to identify a genetic marker for bursting subicular cells and test its validity *in vitro* by using a Cre recombinase marker line.
3. Once a Cre line has been validated, we sought to employ it to map the connectivity between subicular bursting cells and the gRSC using channel rhodopsin 2 (ChR2) – assisted circuit mapping in order to uncover the targets of these subicular efferents.
4. Finally, using intervention experiments, we sought to establish a causal link between subicular bursting cells and retrosplenial responses and to identify the exact contribution of the hippocampus to ripple associated responses in the gRSC in awake animals.

2 METHODS

2.1 Animal Research

All experiments were conducted in accordance with European guidelines and with permission from local regulatory authorities (Berlin Landesamt für Gesundheit und Soziales, permits G0092/15 and G0150/17 and the Institutional Animal Care and Use Committee of New York University Medical Center). Total numbers of animals used for this study were as follows: 8 wild type C57BL/6 mice (JAX: 005304), 24 transgenic VGlut2-Cre mice (JAX: 016963) and 3 transgenic CaMKII-Cre::Ai32 mice (JAX 005359 with JAX 012569).

2.2 Stereotaxic surgery and viral injections

Mice were anesthetized under isoflurane (1.5% vol/vol in oxygen) and body temperature was maintained at 37°C. The coordinates for targeting the subiculum and the RSC were as follows (from Bregma, in mm): -3.0 AP, ± 1.6 ML, -1.6 DV and -2.7 AP, ± 0.75 ML, -1.0 DV, respectively. A NanoFil syringe with a 34-gauge needle (with UMP3 microinjection system and Micro4 controller; all from WPI Inc. Sarasota, USA) was used to inject 100 nL of AAV virus with various constructs (Charité viral core facility; titer $1.3x10^{11}$-$1.6x10^{12}$ VG/mL) at a rate of 20 nL/minute, waiting 5 minutes after each injection before slowly retracting the needle. Animals were allowed to recover for at least 4 weeks before the experiment to allow for a proper expression of the construct at the axon terminals. For *in-vivo* head plate implantation, the craniotomy site (AP: -2.5-3.0, ML: 0.5-2.5) was marked, and a stainless steel ground screw was placed in the contralateral frontal bone, or, in the transgenic CaMKII-Cre::Ai32 mice, a stainless steel wire was implanted intra-cranially above the cerebellum. A custom-made metal lightweight head holder was attached to the skull using adhesive cement (Paladur; Heraues, Germany). After surgery, mice were returned to their home cage and allowed to recover for a minimum of 2 days before habituation started. Habituation in the recording setup was repeated for up to one week in increasing increments of fixation time until the animal sat quietly for at least 1 h. On the first day of an experiment, mice were anesthetized and a craniotomy was made above the left granular

portion of the RSC (gRSC) and dorsal CA1 or subiculum and covered with silicon sealant (Kwik Cast, MicroProbes). Mice were allowed to recover for at least 3 h before the experiment. Before the recording started, Kwik-Cast sealant was removed and the brain was washed with saline. An acute silicon probe (A4x8-5mm-100-400-703-A32; Isomura32; ISO-3x-tet-lin; A8x32-Poly2-5mm-20s-lin-160; Neuronexus, Ann-Arbor, MI, USA), in many cases covered with a fluorescent dye to enable post-hoc track identification (DiI, DiR or DiO, Thermo Fisher Scientific, MI, USA), was lowered slowly into the brain at a 30° angle (coronal orientation) until ripples were clearly visually detectable on the hippocampal shanks (~1.5-1.7 mm DV). Recordings started 15-20 min after the probe reached final depth and lasted approximately 60 min. After the end of the recording, the probe was slowly retracted, the brain washed with saline and covered again with Kwik-Cast sealant.

2.3 Acute slice electrophysiology

Animals (n = 12 VGlut2-Cre mice; 11 males, 1 female; age: 2-3 months) were deeply anesthetized with isoflurane, decapitated and the brains removed. Tissue blocks containing the RSC or subiculum were then mounted on a vibratome (VT1200S, Leica Biosystems, Wetzlar, Germany), and slices were cut coronally at 300 µm nominal thickness. The slices were moved to an interface chamber where they were stored for 1-5 h before being transferred to the recording chamber where they were perfused at a rate of 3-4 ml/minute. The recording chamber was mounted on an upright microscope equipped for IR-DIC microscopy. Whole-cell recordings were performed using a Multiclamp 700A (Axon Instruments, CA, USA) using glass microelectrodes filled with 120 mM K-gluconate, 10 mM Hepes, 3 mM Mg-ATP, 10 mM KCl, 5 mM EGTA, 2 mM $MgSO_4$, 0.3 mM Na-GTP, 14 mM phosphocreatine and 2mg/mL biocytin. The resistances of the electrodes ranged between 3 and 5 MΩ. Access resistance (< 20 MΩ) was continuously monitored during the recording and was not allowed to fluctuate by more than 20%. Data were analyzed online using Igor Pro and offline using Matlab (Matworks) and were not corrected for liquid junction potential. Light-evoked responses were detected if the peak of the postsynaptic potential averaged over >10 repetitions crossed ± 0.4 mV.

2.4 Histological processing

At the end of the *in vivo* experiments, animals were deeply anesthetized using urethane (2.5 g kg^{-1} body weight) and transcardially perfused with phosphate-buffered saline (PBS), followed by 4% paraformaldehyde (PFA) in PBS. Following an overnight fixation in PFA, brains were carefully washed in PBS before they were mounted on a vibratome (Leica VT1000S, Leica Biosystems, Wetzlar, Germany) and cut into 100 µm slices. Sections were mounted in either Vectashield (Vector laboratories) or DAPI-containing Fluoroshield (Sigma-Aldrich). For *in-vitro* experiments, slices were transferred to a PFA solution and fixated overnight. Immunoreactions for GAD-67 were carried out using primary mouse antibody (diluted 1:500, MAB5406, Millipore) and secondary Alexa 555 (1:500, A-21424, Invitrogen). Streptavidin was conjugated to Alexa 647 (1:500, S32357, Invitrogen) for visualizing the biocytin. Sections were then mounted in Fluoroshield and imaged using a Leica TCS SP5 confocal microscope (Leica Biosystems, Wetzlar, Germany). Images were analyzed using the free software ImageJ. The location of individual cortical recording sites was assigned to either deep or superficial layers based probe tracks and recording depth

2.5 Extracellular data preprocessing

Signals were acquired using an RHD2000 system (Intan Technologies, LA, USA) at 20 kHz and resampled at 1.0 or 1.25 kHz using a low-pass sinc filter with a 450 Hz cut-off band to extract the LFP data. Spike clusters were extracted from the high-passed filtered and channel whitened signal using Kilosort (Pachitariu et al., 2016); a manual curating step, where units were merged based on common refractoriness and waveform similarity was performed using Klusters (http://neurosuite.sourceforge.net/) (Hazan et al., 2006).

2.6 *In vivo* data analysis

Ripple detection: Ripples were detected by selecting the channel with the largest ripple amplitude using visual inspection and filtering the LFP signal at 100 – 280 Hz in forward and reverse direction using a 2nd order Butterworth filter. The signal was then rectified, and smoothed using a Savitzky-

Golay filter. Ripple events were defined as events where the smoothed rectified signal was more than 2 SDs and the filtered signal more than 4 SDs above the respective mean for at least 20 ms. In the case of two events separated by less than 40 ms (peak to peak), the event with the smaller amplitude was discarded. Detections were visually inspected using Neuroscope (http://neurosuite.sourceforge.net/).

SPW-R and stimulation modulation: Only sessions with > 100 ripple events selected for analysis. Peri-event time histograms (PETHs) and cross-correlograms were constructed using SPW-Rs separated from each other by at least 500 ms to avoid contribution from ripple bursts (Davidson et al., 2009). Significance of SPW-R and stimulation PETHs was calculated using an adapted convolution method (Stark and Abeles, 2009).

Spectral analysis: Spectrograms and phase coherograms were constructed using a complex Morlet wavelet convolution with logarithmically spaced number of cycles (Cohen, 2014) and are either plotted on a logarithmic scale or z-score normalized relative to a baseline period at least 100 ms prior to SPW-R/ stimulation onset. Power coherograms were constructed using the Matlab function 'wcoherence'. Spike – LFP coherence was computed using a multi-taper based analysis (Chronux, Bokil et al., 2010) with 5 tapers and a time-bandwidth product of 3. Phase was extracted using the filter Hilbert method. Only units significantly modulated by SPW-Rs (with a significant phase preference, defined as $p < 0.05$ and ITPC > 0.1) on Rayleigh's test of circular non-uniformity were selected for analysis. Inter-trial phase clustering (ITPC) was computed as: $ITPC_{tf} = \left| n^{-1} \sum_{r=1}^{n} e^{ik_{tfr}} \right|$, where n is the overall number of ripples and k is phase angle (in radians) at ripple number r and time frequency point *tf,* which was set to be the trough of the ripple (Cohen, 2014).

Identification of negative waves: Negative waves were identified in a superficial channel chosen by visual inspection using a template matching algorithm defined based on visual selection of identified events in Clamp fit 10.4 (Molecular Devices, CA, USA) and thresholded at 1 RMS.

CSD analysis: CSD was estimated using the inverse method (Pettersen et al., 2006). Analysis was performed on an average of > 150 evoked potentials from one shank in 8 or 15 cortical depths after subtraction of the shank average.

Phase-amplitude coupling: the coupling between high frequency amplitude and lower frequency phase was estimated using a modulation index (Tort et al., 2008). Phase was calculated at 39 frequencies from 2-40 Hz and power was calculated at 91 frequencies from 50-500 Hz using wavelet convolution. Phase time series were binned into 50 intervals and the mean wavelet amplitude at each bin was computed. The modulation index was extracted by measuring the divergence of the observed power distribution from the uniform distribution. Significance of MI values was deemed by creating 200 randomly shifted surrogates for each power frequency and computing a P_z value. Non-significant values ($p<0.05$) were set to zero.

Independent component analysis (ICA): ICA-based separation of voltage signals was performed using the function 'jader' from the EEGLAB toolbox (https://sccn.ucsd.edu/eeglab/index.php).

Cross-correlograms and autocorrelograms: cross-correlation histograms (cross-correlograms) were computed by counting and binning the lags of spikes from neuron A referenced to each spike of neuron B. Autocorrelograms (ACGs) were computed by counting the lags of spikes taken from a given spike within a window of ±250 ms with regard to a reference spike from the same spike train. This procedure was repeated for every spike.

Cross-covariance estimation: The cross-covariance was calculated as previously described (Siapas et al., 2005). In short, the cross-covariance estimate was first computed as $CCE = \frac{CCH}{b * T} - R1 * R2$ with CCH as the cross-correlation histogram, b the bin size, T the period of observation and R1 and R2 as the firing rate of a hippocampal and a retrosplenial unit, respectively. The standardized cross-covariance was then computed as $CCE * \sqrt{\frac{b*T}{R1*R2}}$.

Packet detection and state-index definition: activity packets were defined as local maxima in the smoothed MUA population vector (Gaussian SD: 30 ms) that exceeded the local average (in a 10s window) for at least 25 ms by at least 60% and were surrounded by local minima (<20% of the local average) for at least 25 ms. Events with inter-packet interval below 15 ms were merged together. Packets were only identified in sessions with >15 units. Accurate detection was visually inspected using Neuroscope. The state-index (SI) was computed by shifting a moving window

(0.5s) along the smoothed MUA firing rate (step size: 1 ms) and counting the proportion of nonzero time bins (Luczak et al., 2013).

Electromyogram (EMG) signal was extracted as previously described (Schomburg et al., 2014; Watson et al., 2016). In short, the LFP from multiple recording sites was filtered between 300-600 Hz and the zero time lag correlation coefficient between them was computed over a sliding window of 0.5 s.

Unit separation: Units were separated into putative pyramids and interneurons based on the spike width, waveform asymmetry and firing-rate using k-means (English et al., 2017) (Fig. 2.5.1). Units with firing rate < 0.5 Hz or ISI violation > 0.01 were discarded.

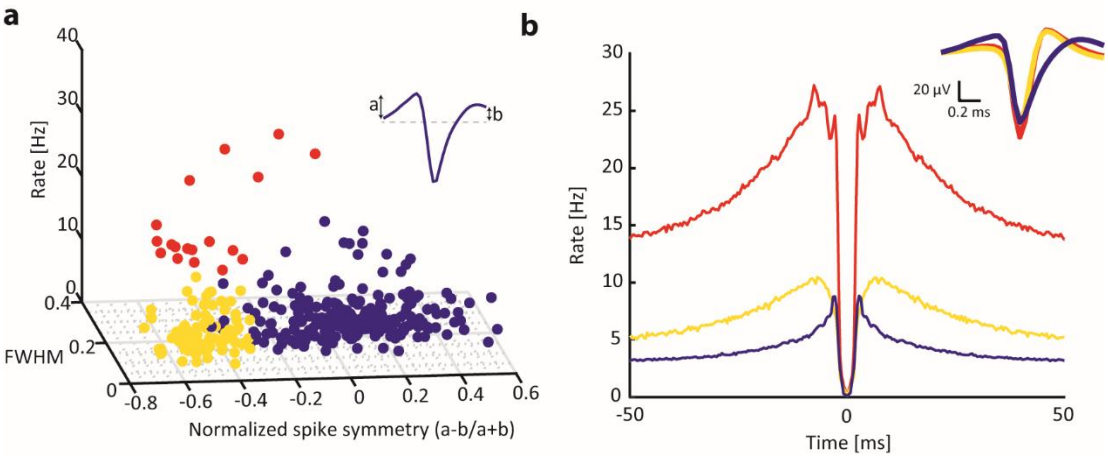

Figure 2.5.1. Example of unit separation. a) Units were separated into putative fast-spiking interneurons (red), low-spiking interneurons (yellow) and pyramids (blue) based on firing rate, waveform width (FWHM) and waveform asymmetry (inset). Low and fast spiking interneurons were re-grouped. b) Average autocorrelograms for the three groups (inset, average waveforms), based on n = 335 units recorded from all gRSC layers from n = 8 mice.

Clustering of hippocampal SPW-Rs: SPW-Rs were detected as described above and the normalized firing rate of dorsal hippocampal neurons was calculated for a single 100 ms time window after ripple onset. Fast-spiking interneurons were excluded from these firing rate vectors. K-means clustering (k = 10) was then used to categorize CA1 ripples according to each 10-dimensional vector representation.

RSC discrimination of hippocampal SPW-R type: Peri-event time histograms (10 ms bins) of RSC activity was constructed around CA1 ripples. Ripple type discrimination was assessed using an

ANCOVA, where the groups were CA1 ripple cluster ID, and the continuous covariate was the mean population firing rate in CA1, used to control for the fact that more RSC neurons fire after larger CA1 population bursts. A group main effect of $p < 0.01$ was used as threshold for ripple type discrimination. In addition, the labels of the ripple clusters were shuffled and the observed F-ratio from the ANCOVA test was compared to the one derived from the shuffle distribution.

RSC LFP discrimination of hippocampal SPW-R type: Spectrograms were computed using wavelet convolution of the down-sampled LFP using a modified Morlet kernel with 80 logarithmically spaced frequency bands from 5-300 Hz. Frequency amplitudes were z-score normalized relative to the entire ±500 ms observation window. Using a similar model as that used for RSC units, an ANCOVA was used to determine whether energy at a specific frequency band at a specific time around ripple onset distinguished ripple type, while regressing out the effect of CA1 population firing rate. The p-values describing the main effect of ripple cluster ID were combined across subjects (n = 3 mice) using Fisher's method $-2 * \sum_{i=1}^{n} \log p_i \approx \chi^2(2 * n)$, where the global p-value was taken from the χ^2 distribution with 2*n d.f.

2.7 t-SNE analysis of hippocampal ripple clusters

For each session, each ripple was defined by two population firing rate vectors: one for the hippocampus and one for gRSC. The hippocampal population vector was defined as above, while the firing rates for the gRSC were taken over the 200ms after hippocampal ripple onset. t-distributed stochastic neighbor embedding (t-SNE) (van der Maaten and Hinton, 2008) was calculated separately for each region using perplexity = 30. To quantify the clustering of gRSC ripple activity in this lower dimensional space, the t-SNE coordinates were binned (bin size = 1 arbitrary unit) and smoothed (2D Gaussian, σ = 4 AU) and normalized by the number of ripples within each cluster. The observed density was compared against a shuffle distribution (n = 1000) in which the labels were randomized.

2.8 Optogenetic manipulations *in vivo*

For optogenetic manipulations in CamKII-Cre::Ai32 animals, (F1 generation of breeding JAX 005359 with JAX 012569; 3 adult females), we used either a 256 channel A8x32-Poly2-5mm-20s-lin-160 Neuronexus probe with optic fibers (50 µm core diameter) mounted on each shank and coupled to a laser diode (Thor Labs, NJ, USA) or a 32-site silicon probe with integrated µLEDs (Neurolight, MI, USA). For optogenetic manipulations in VGlut2-Cre animals (JAX: 016963, 2-3 month old, 8 males and 3 females), we used 32 channel ISO-3x-tet-lin probe (Neuronexus, MI, USA) mounted with an optic fiber (50 µm core diameter) coupled to a LED light delivery system (Plexon Inc., TX, USA). Photostimulation consisted of 5-10 ms (for tagging experiments) or 100 ms (for iHFOs) 473 nm and 5 s 532 nm light pulses. Measured light power at the probe tip ranged between 350-750 µW for 473 nm and 150 µW for 532 nm. Closed loop stimulation was accomplished by filtering a manually selected hippocampal channel in the ripple band, on which light stimulation was triggered by crossing of a manually set threshold (Power 1401, Cambridge Electronic Design Limited, UK).

2.9 Data and code availability

The majority of the code used for this study was adapted from the buzcode repository (https://github.com/buzsakilab/buzcode) and the FMAT toolbox and is available under http://fmatoolbox.sourceforge.net/. Data can be made available upon request.

3 RESULTS

3.1 Transient ripple oscillations in the gRSC

To investigate the flow of information from the hippocampus to the gRSC, we performed silicon probe recordings in the dorsal CA1 and subiculum and different layers of the gRSC in awake, head-fixed mice (n = 8 C57Bl/6N). Mice were habituated for 5 to 7 days until they remained quiet for approximately 1 h (Methods).

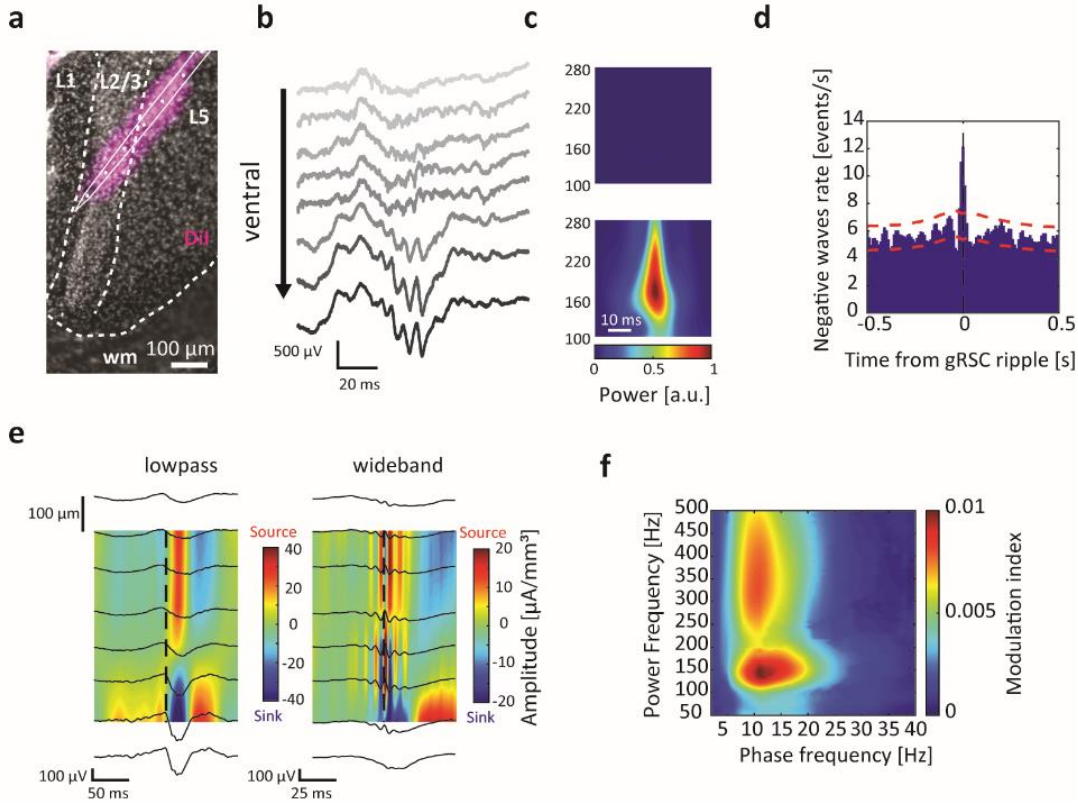

Figure 3.1.1. Ripple oscillations in the gRSC. a) Example histological verification of probe location. wm, white matter. b) Laminar profile from eight channels ranging from dorsal (top) to ventral (bottom), showing a stronger expression of ripple activity in superficial layers. c) Ripple power is increased in superficial (bottom), compared to deep layers (top). Wavelet spectrograms centred around ripple peak averaged across 312 events from one example recording. d) Cross-correlogram between cortical ripple events and negative waves in superficial gRSC (n =8 sessions from 4 animals; 1,914 ripples, 72,422 negative waves). Red lines, 95% confidence intervals. e) CSD analysis from two example sessions showing low-passed filtered (left) and broadband (right) versions centred around gRSC ripple peak (dashed line; 496 and 288 events, respectively). f) Averaged phase-amplitude comodulogram for superficial gRSC LFP showing cross-frequency coupling between gRSC ripples and negative waves occurring at around 10 Hz (n = 10 sessions from 6 mice).

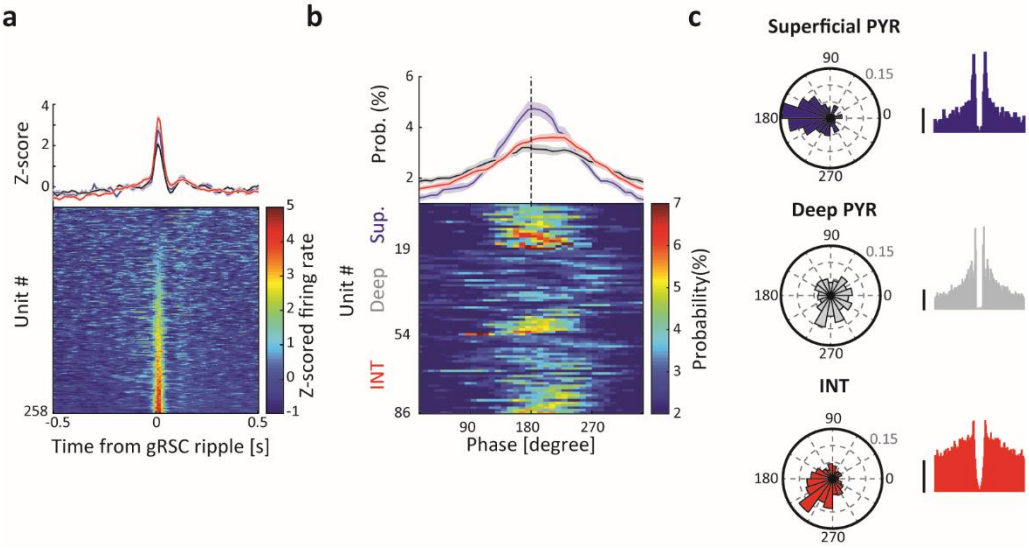

Figure 3.1.2. Modulation of gRSC units by local ripple oscillations. a) Z-score normalized PETH showing the average (mean ± s.e.m; top) and individual (bottom) responses of 258 gRSC units to cortical ripples sorted into superficial pyramids (blue), deep pyramids (black) and interneurons (red). b) Average (top; mean ± s.e.m) and color-coded histograms (bottom) of preferred gRSC ripple phase of putative superficial pyramids (blue, top rows), deep pyramids (grey, middle rows) and interneurons (red, bottom rows) that are significantly phase-modulated based on circular Rayleigh test (superficial pyramids 19/51 = 37%,; deep pyramids 35/174 = 19%; INTs 32/110= 29%). c) Example polar plots of phase-locking to gRSC ripples (left) and the corresponding autocorrelogram (ACG, right) of putative superficial pyramids (top panel blue), deep pyramids (middle panel grey) and INT (bottom panel red). Radial axis: probability. ACGs range ±25 ms, scale bar 5 Hz.

Laminar recordings from the gRSC with silicon probes (Fig. 3.1.1a) during immobility revealed that LFP activity in superficial layers of gRSC is dominated by large negative polarity waves (mean amplitude: -91.42 ± 0.21 µV; mean frequency 5.38 ± 1.36 Hz), likely reflecting synaptic inputs to neurons in layers 2 and 3 (L2/3) and, possibly, to the apical dendrites of layer 5 (L5) neurons. These large transients were occasionally embedded with short, fast oscillatory pattern in the frequency range of 140–200 Hz, termed here as 'gRSC ripple' (Fig. 3.1.1b). gRSC ripple triggered spectrograms showed that the largest amplitude gRSC ripple was localized to more ventral recording sites, which were histologically confirmed to correspond to superficial layers (Fig. 3.1.1c). Cross-correlation between gRSC ripples and negative polarity waves identified using a template matching algorithm (Methods) confirmed a significant coupling between those events (Fig. 3.1.1d). Low frequency negative waves had their largest amplitude in superficial layers and their polarity reversed in deeper layers. This phase reversal resulted in a corresponding sink-source dipole in the current source density (CSD) map (Fig. 3.1.1e). Phase-amplitude

coupling analysis confirmed a significant coupling between ripple band power and lower frequencies phase with a peak at 11 Hz (Fig. 3.1.1f).

Next, we quantified the relationship between neuronal spiking and LFP in the gRSC. We isolated single units, which were classified as putative pyramidal neurons or interneurons (Methods) (English et al., 2017). Pyramidal cells were further divided into deep and superficial layer neurons based on post-hoc reconstruction of probe tracks. Neuronal firing in gRSC was strongly time-locked to gRSC ripple events, as indicated by peri-event time histograms (PETHs; Fig. 3.1.2a). Examination of phase relationship between spikes and LFP ripple waves indicated that a larger proportion of superficial units were significantly phase-locked to the ripple events (37%, 19/51) than neurons in deep layers (19%, 35/180). The spiking of putative interneurons lagged behind that of the ripple trough-locked pyramidal neurons by 20-30^{o} (Buzsáki et al., 1992) (Fig. 3.1.2b-c; $p<0.05$; rank sum test). Motivated by previous studies showing that hippocampal, entorhinal and neocortical ripples often co-occur (Chrobak and Buzsáki, 1996; Khodagholy et al., 2017), we next examined whether hippocampal SPW-Rs propagate to gRSC.

3.2 Propagation of hippocampal ripples into the gRSC

A comparison of gRSC ripples with ripple events recorded in CA1 area revealed that, although both events did not differ with respect to their spectral maxima (maximal power gRSC ripples: 137.65 ± 1.50, CA1 ripples: 137.05 ± 1.92 n.s.), gRSC ripples were shorter (gRSC ripples: 26.10 ±

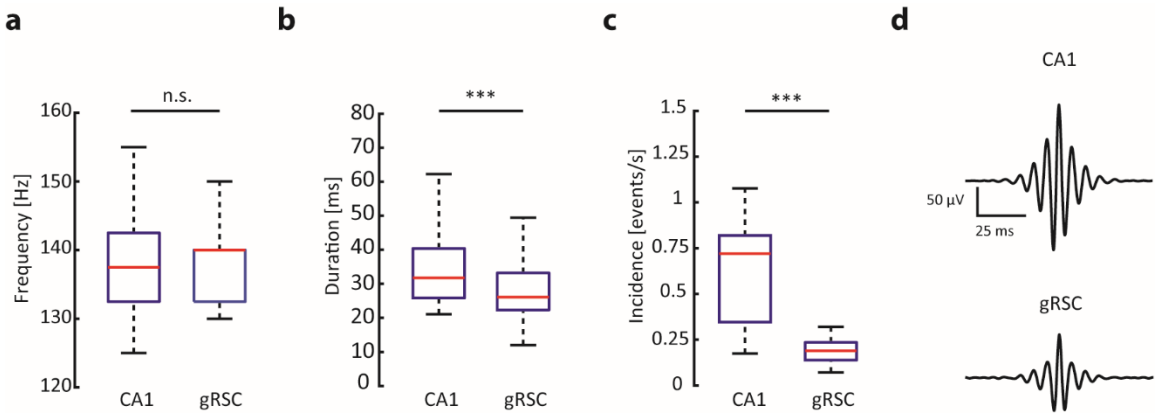

Figure 3.2.1. Comparison of gRSC and CA1 ripples a) CA1 (left) and gRSC (right) ripple frequency. Red lines, median; blue lines, quartiles. n.s., not significant. b) CA1 and gRSC ripple duration. $p<0.001$, rank sum test. c) CA1 and gRSC ripple incidence. d) Average waveforms of CA1 (top) and gRSC (bottom) ripples (n = 19 sessions from 6 animals; 22,694 CA1 ripples, 8,501 gRSC ripples).

0.14 ms; CA1 ripples: 34.47 ± 0.08 ;median ± s.e.m), consisted of fewer cycles (gRSC ripples: 5.02 ± 0.02 cycles, CA1 ripples: 7.16 ± 0.01) and occurred at a lower incidence (gRSC ripples: 0.23 ± 0.03 Hz, CA1 ripples: 0.68 ± 0.11 Hz; n = 19 sessions from 6 animals; 8,501 gRSC ripples) (Fig. 3.2.1). Cross-correlation analysis between negative polarity waves in the gRSC and CA1 SPW-Rs indicated that some, but not all, of these waves coincided with SPW-Rs recorded in CA1 pyramidal cell layer or in the subiculum, suggesting that they could reflect hippocampal inputs (Fig. 3.2.2a-c). However, as the incidence of hippocampal SPW-Rs was lower than that of the large amplitude

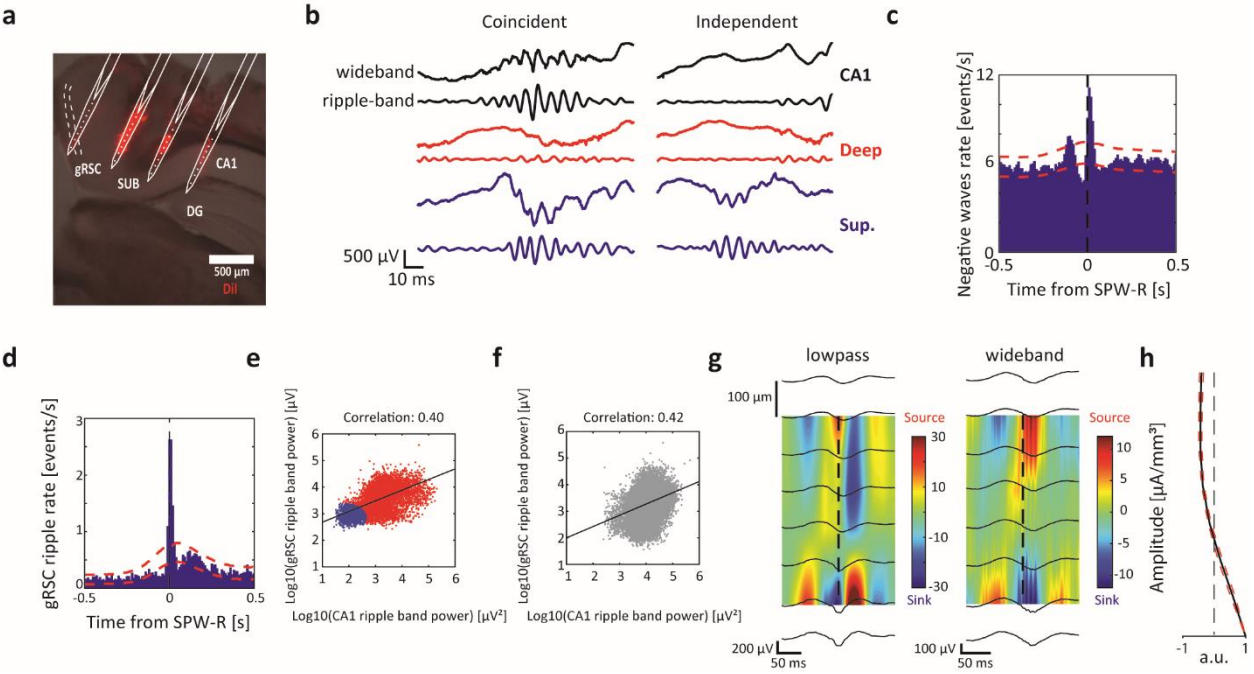

Figure 3.2.2. gRSC activity is temporally coupled to hippocampal SPW-Rs. a) Example histological verification of probe location. Relevant areas are labelled; L2/3 is marked by dashed lines. b) Two examples of gRSC ripples showing traces of wide-band (top trace) and ripple band (bottom trace) filtered activity from CA1 area (top, black), deep layers gRSC (middle, red) and superficial layers gRSC (bottom, blue). c) Cross-correlogram between SPW-R events and negative waves in superficial gRSC (n = 8 sessions from 4 animals; 3,409 SPW-Rs, 72,422 negative waves). Red lines, 95% confidence intervals. d) Cross-correlogram between CA1 (reference) and gRSC ripples (n = 18 sessions from 6 animals; 22,694 CA1 SPW-Rs, 8,501 gRSC ripples). e) The majority of gRSC ripple events (red, 75%) are associated with an increased ripple-band power in CA1 whereas only a minority are not (blue, 25%). gRSC ripple events were clustered into two groups using Gaussian mixture models (n = 8,501 gRSC ripples from 6 animals). f) CA1 ripples were also associated with an increased gRSC ripple band power (n = 22,694 CA1 ripples). g) CSD analysis from two example sessions showing low-passed filtered (left) and broad-band (right) versions centred around CA1 SPW-R peak (dashed line; 821 and 430 events, respectively). h) ICA (mean ± s.e.m) decomposition of voltage traces from the gRSC centred around CA1 SPW-R showing an increase in voltage loadings in superficial layers (8 sessions from 7 animals).

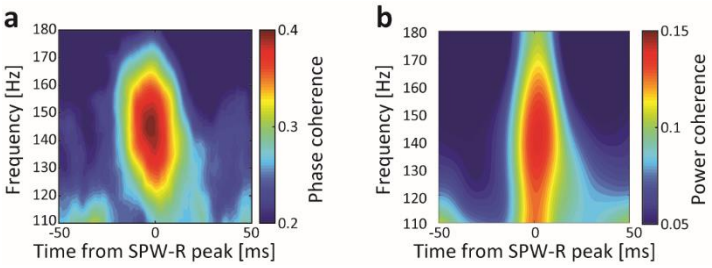

Figure 3.2.3. gRSC activity is spectrally coupled to hippocampal SPW-Rs. a) Wavelet phase coherogram between CA1 and superficial gRSC LFP centred around CA1 SPW-R detection (7,150 events from 7 animals). b) Same, but for power coherence.

waves in the superficial layers of gRSC, only a fraction of the cortical waves would be expected to be related to CA1 SPW-Rs. Hippocampal SPW-R – gRSC negative wave correlation was often preceded by an additional smaller peak by approximately 100 ms (Fig.3.2.2c), implying that co-occurrences of these cross-regional events were embedded in other cortical rhythms (Battaglia et al., 2004; Sirota et al., 2003). Temporal analysis of the correlation between CA1 and gRSC ripple events indicated that 19.37 ± 1.87% of identified gRSC ripples followed the CA1 ripple within a 25 ms time window, whereas only 9.20 ± 0.92 % preceded it within the same interval (Fig.3.2.2d). The majority of gRSC ripple events were associated with an increased ripple-band power in CA1 and vice versa, indicating a strong comodulation of ripple events across these regions (Fig.3.2.2e-f). CA1 ripple event-triggered CSD analysis demonstrated the presence of a superficial sink in gRSC (Fig. 3.2.2g), suggesting the existence of lamina-specific depolarization. When individual waves of CA1 ripples were used as a reference, both LFP ripples and ripple-related CSD sinks in superficial gRSC traces (Fig. 3.2.2g, right) were smaller compared to when local gRSC ripples waves were used as the reference (cf. Fig. 3.1.1e), indicating that local, rather than remote, currents contribute to their generation. CSD analysis assumes vertical conductivity, which was violated in this study due to the angle of probe placement (Fig. 3.2.2a). To complement the CSD analysis, the sink-source profile was validated using independent component analysis (ICA) for blind source separation, which identified an increase in voltage load in superficial layers (Fig. 3.2.2h; n = 8 sessions from 7 animals; p = 0.0002, rank sum test between first IC loads of top and bottom channels). To quantify the relation between CA1 SPW-Rs and gRSC ripples, we calculated their wavelet phase- and power coherence. Both measures showed a peak in the ripple frequency band (Fig. 3.2.3), suggesting a fine-time scale coupling between these high frequency oscillations. In a subset of experiments (n = 4 sessions from 2 mice) where CA1, subiculum and superficial gRSC layers were all successfully targeted, ripple peaks in each

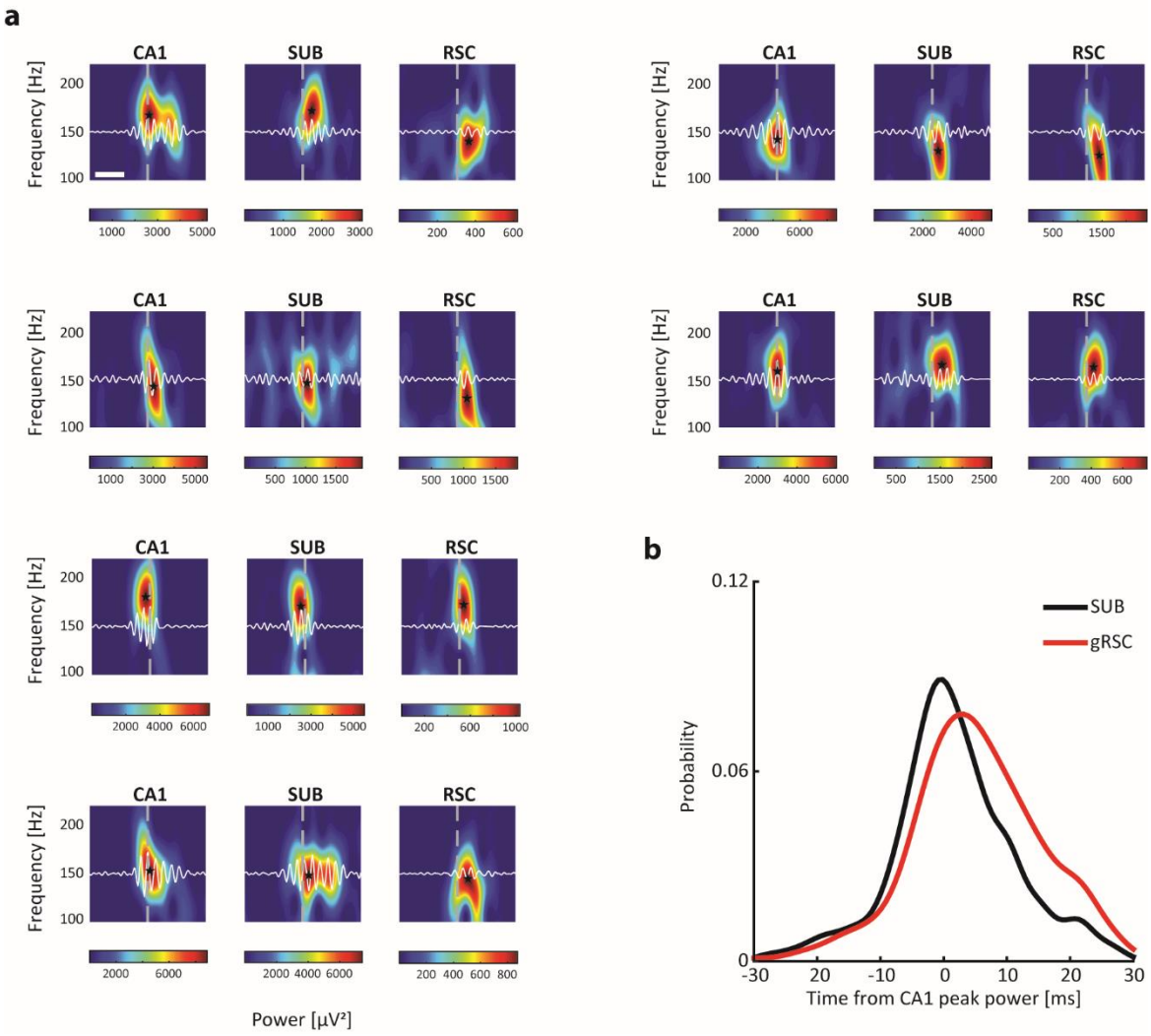

Figure 3.2.4. Propagation of ripple activity along the hippocampal output axes. a) Individual examples of simultaneously detected CA1, subiculum and gRSC ripples. Ripple band filtered traces are overlaid in white. Dashed grey line denotes maximal amplitude ripple wave detected in CA1. Black star denotes ripple peak power. Scale bar, 25 ms. b) Kernel-smoothed histograms showing the distributions of subicular and gRSC ripple peak power lags, relative to CA1 ripple peak power (mean lag subiculum: 1.70 ± 0.32 ms; mean lag gRSC: 5.18 ± 0.34 ms; $p = 1.52 \times 10^{-17}$, signed rank sum test; n = 4 sessions from 2 mice where simultaneous targeting of CA1, subiculum and superficial gRSC was histologically confirmed).

area were identified and the time lags relative to CA1 ripple peak power were computed. Consistent with the anatomical connectivity, subicular ripple probability peaked after that of CA1 (1.70 ± 0.32 ms), while gRSC ripples exhibited an even longer delay (5.18 ± 0.34 ms; $p < 0.001$, signed rank sum test) from CA1 ripples (Fig. 3.2.4).

Unit firing in gRSC was also time-locked to hippocampal SPW-R events, with responses of individual units showing either a single peak or drop in firing rate, or more complex SPW-R-

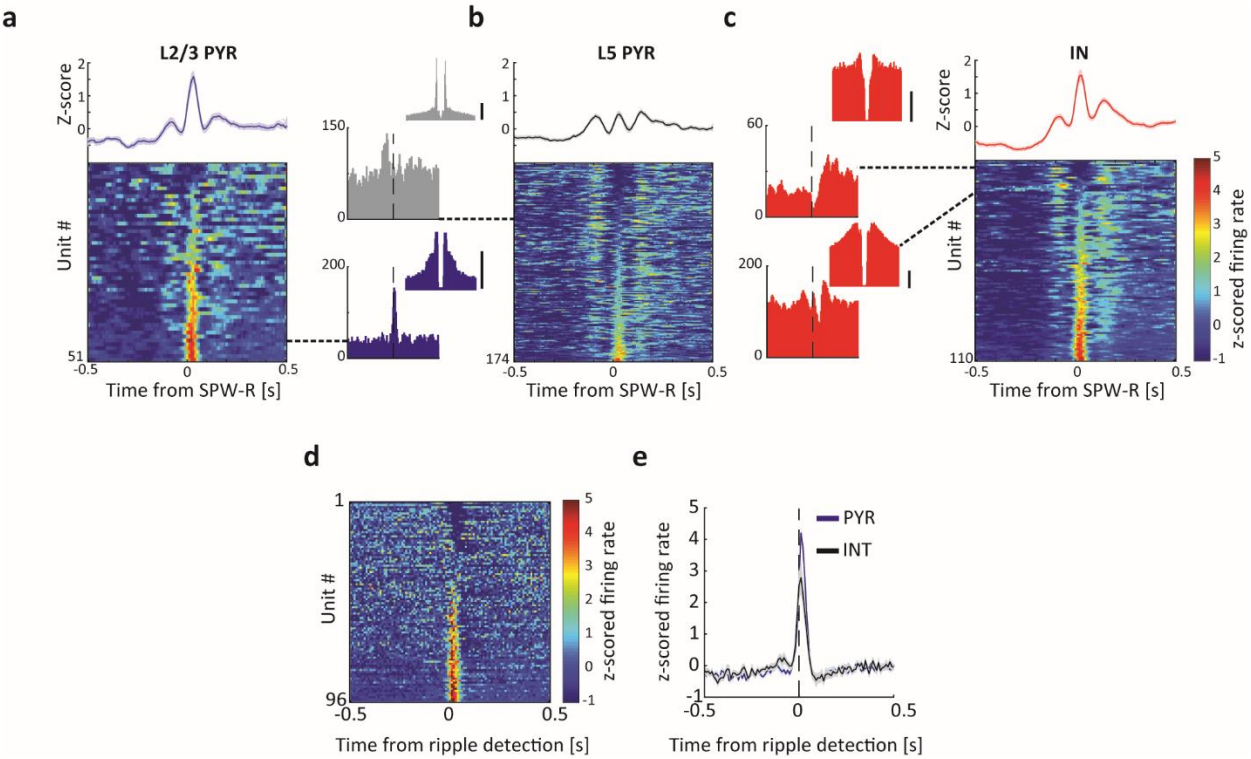

Figure 3.2.5. Unit activity in the gRSC is modulated by CA1 ripples. a-c) Z-score normalized PETHs showing the average (mean ± s.e.m; top) and individual (bottom) responses of superficial (a) and deep (b) pyramidal neurons, as well as interneurons (c) sorted based on ripple modulation. Middle panels show example PETHs and the corresponding ACG (± 25 ms). Scale bars, 10 Hz; Y-axis: spike count. d) Z-score normalized PETH of CA1 pyramidal cells centred ripple detection. e) Average z-score normalized responses of CA1 pyramidal cells (blue) and interneurons (grey).

related discharge patterns (Fig. 3.2.5a-c). At the population level, SPW-R-associated responses were characterized by a peak locked to SPW-R onset time, and were often both preceded and followed by secondary peaks at approximately 100 ms from SPW-R onset. These secondary peaks were absent from the PETHs of CA1 units (Fig. 3.2.5d-e), suggesting that this gRSC activity was unlikely to have been driven by the hippocampus. Compared to deep gRSC units, superficial neurons responded earlier after SPW-R (mean latency to peak of superficial neurons: 23 ± 2 ms; deep: 32 ± 3 ms, Fig. 3.2.5a-b) and showed stronger SPW-R event modulation (37/51 of superficial neurons, 72% were significantly modulated compared to 51/174, 29%, deep neurons). A large fraction of putative gRSC interneurons were also affected (Fig. 3.2.5c; 78/110 of interneurons, 71% were significantly modulated). Interneurons exhibited heterogeneous responses suggesting a cell type-specific modulation by SPW-Rs similar to hippocampal interneurons (Klausberger et al., 2003). When individual cycles of hippocampal SPW-Rs were

used as a reference, significant phase locking was observed in a considerable fraction of superficial pyramids and interneurons, but not deep pyramids (Fig. 3.2.6a-b; superficial 15/51, 29%; deep 14/174, 8%; interneurons 21/110, 19%). These results were supported by a spike-LFP coherence analysis, which also indicated an increase in ripple band coherence in superficial, but not in deep layers (Fig. 3.2.6c).

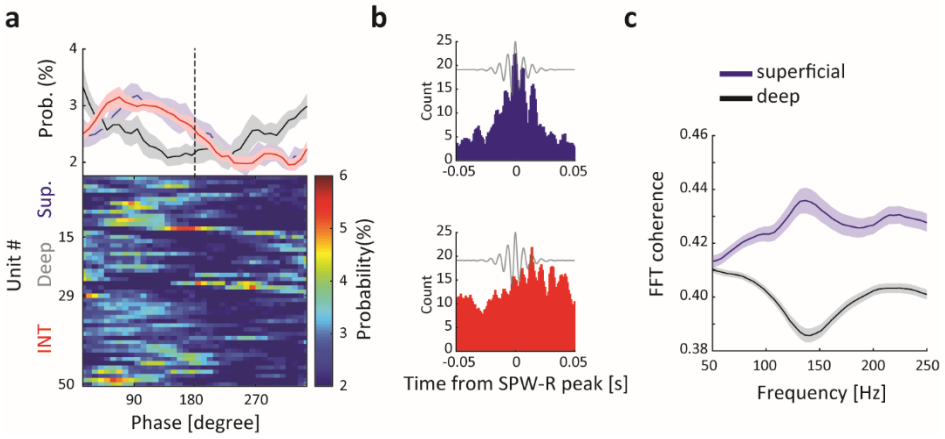

Figure 3.2.6. gRSC units display layer specific phase locking to CA1 ripples. a) Average (top; mean ± s.e.m) and color-coded histograms (bottom) of preferred CA1 ripple phase of superficial pyramids (blue, top rows), deep pyramids (grey, middle rows) and interneurons (red, bottom rows) that are significantly phase-modulated based on circular Rayleigh test (superficial pyramids 15/51 = 29%; deep pyramids 14/174 = 8%; interneurons 21/110 = 19%). b) High resolution CA1 SPW-R triggered PETH of an example superficial unit (top, blue) and an interneuron (bottom, red) significantly modulated by individual ripple waves. c) Average (mean ± s.e.m) spike-LFP coherence between superficial (blue) and deep (black) units and CA1 LFP (± 100 ms around SPW-R peak) showing a strong tuning of superficial, but not deep, cells to the ripple band (n = 27 sessions from 8 animals).

To further test the influence of SPW-R activity on hippocampal – gRSC communication, we examined the co-modulation of CA1 and superficial and deep gRSC unit pairs during and outside of SPW-R epochs. We used the standardized cross-covariance measure, which provides an estimate for the strength of interactions between pairs of simultaneously recorded neurons, normalized by their firing rates and by the period of observation (Siapas et al., 2005). Peak cross-covariance was higher within SPW-R epochs (250 ms before and after ripples with CA1 units as reference) compared to periods outside SPW-Rs for both superficial and deep units, and peaked at positive values, suggesting an increase of excitatory drive from the CA1 to the gRSC at times of SPW-Rs. In line with the SPW-R-induced responses (Fig. 3.2.5), CA1 spiking co-varied stronger with superficial gRSC unit activity than with activity in deep gRSC. Superficial gRSC also exhibited a shorter latency to peak covariance (8.5 ms ± 0.4 ms), compared to spiking activity of units in deeper layers (12 ± 0.3 ms; Fig. 3.2.7; p's < 0.001, Bonferroni-corrected rank sum tests). In

summary, these data suggest that modulation of gRSC neurons by hippocampal SPW-Rs is layer-specific and that a substantial amount of information is transferred between these structures during SPW-Rs.

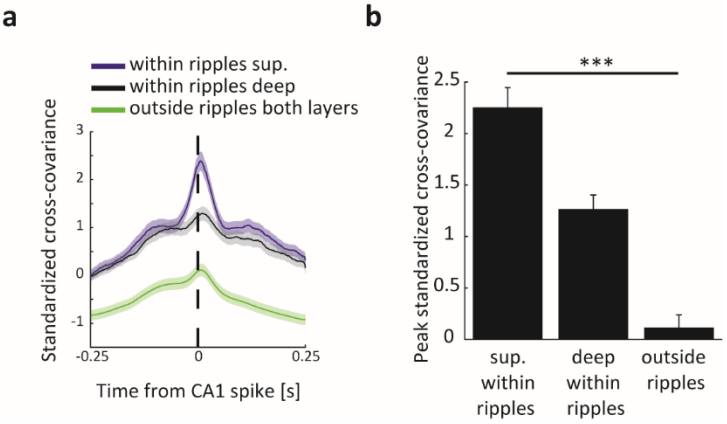

Figure 3.2.7. Layer dependent enhancement of coupling between gRSC and CA1 units during ripples. a) Standardized cross-covariance during SPW-Rs averaged over pairs of superficial (black) and deep (red) gRSC units firing within and outside of SPW-Rs epochs (green, averaged across both layers) (n = 27 sessions from 8 animals; 209 CA1 – superficial gRSC pairs, 351 CA1 – deep gRSC pairs and 560 CA1 – gRSC units outside ripples). b) Peak standardized cross-covariance (mean ± s.e.m) of superficial and deep gRSC units within ripple epochs and of units from all layers outside of ripple epochs. All groups are significantly different from each other ($p<0.001$ Bonferroni- corrected rank sum tests).

3.3 Mapping of functional topology between the dorsal hippocampus and gRSC

We next explored the route taken by CA1 SPW-R to reach gRSC targets. To this end, we performed parallel recordings using 8-shank 256-site silicon probes positioned along the anterior-posterior axis of the gRSC and either 8-shank 256-site (mounted with optic fibers) or 4-shank 32-site (with integrated µLEDs; see Methods) silicon probes positioned along the subiculo-fimbrial axis of the dorsal hippocampus in awake head-fixed CaMKII-Cre::Ai32 mice (n = 3). We induced artificial local oscillations optogenetically at specific anatomical locations in dorsal CA1 and subiculum (Fig. 3.3.1a). Optogenetic activation (100 ms square pulse) of CA1 evoked strong oscillatory activity (Fig. 3.3.1b), termed as induced high-frequency oscillations (iHFOs; Stark et al., 2014). For these mapping experiments, we used relatively strong light intensity that induced large amplitude but relatively low frequency oscillation (possibly due to cycle skipping and ChR2 deactivation). iHFOs could be induced at any given location along the subiculo-fimbrial axis of the CA1 str. pyramidale with a similar magnitude. Stimulation in the subiculum or at the subicular end of CA1 (CA1a) reliably evoked a series of concatenated large-amplitude negative waves in gRSC, which

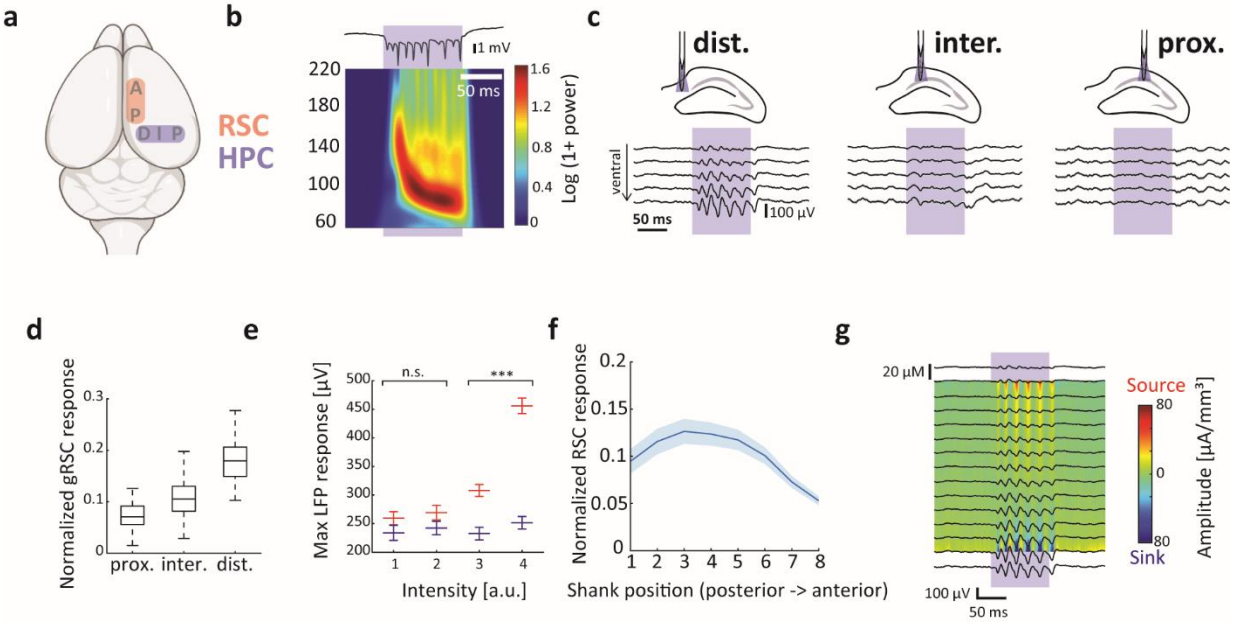

Figure 3.3.1. Mapping of functional topology between the dorsal hippocampus and gRSC. a) Schematic depiction of probe placement. Two 8-shank probes were used to cover 1050 µm of dorsal CA1 and subiculum medial-lateral axis and the gRSC anterior-posterior axis. b) Exemplary voltage trace (top) and wavelet spectrogram averaged over 100 events (bottom) of iHFOs induced and recorded in the pyramidal cell layer of CA1. In all panels, the time of light stimulation is depicted by a blue shaded area. c) Voltage traces (mean ± s.e.m) from five channels ranging from dorsal (top trace) to ventral (bottom trace) showing gRSC LFP responses to distal (left), intermediate (middle) and proximal (right) CA1 stimulation averaged over >300 events from one animal. d) The ratio between the magnitude of local responses in CA1 and subiculum to stimulation and the evoked responses in the gRSC plotted as a function of the location of stimulation along the proximal-distal axis of the dorsal hippocampus. Middle line, median; box, quartiles. e) Maximal gRSC LFP response to light stimulation plotted against different stimulation intensities of proximal (blue) and distal (red) sites in dorsal CA1. Distal stimulation sites often included or bordered subiculum. Asterisks denote $p<0.001$. f) Normalized gRSC LFP responses to >300 CA1 stimulations as a function of shank position along AP axis (mean ± s.e.m). g) CSD analysis of responses to distal CA1 stimulation and the corresponding voltage traces averaged over >300 events from one animal.

increased in amplitude with increasing stimulation intensity (Fig. 3.3.1c, e). In contrast, stimulation of more proximal sites of CA1 induced smaller or no discernible gRSC responses (Fig. 3.3.1c, e). Hippocampal LFP responses recorded on shanks away from the site of stimulation decayed to baseline levels within ~400 µm, ruling out the possibility of directly activating the gRSC (data not shown). To quantify the magnitude of evoked responses for each stimulation site, evoked gRSC potentials were normalized with respect to the locally induced CA1 responses, which indicated a gradual proximal-distal increase in response magnitude (Fig. 3.3.1d). The magnitude of evoked responses in the gRSC depended not only on the site of CA1 stimulation but

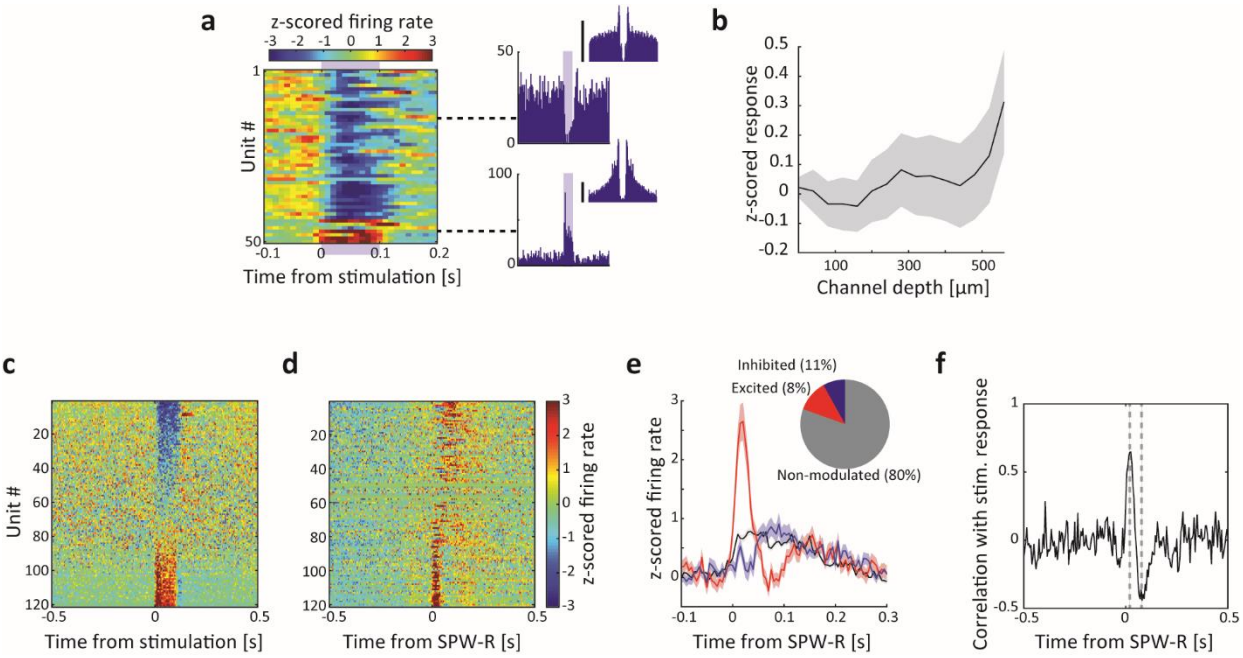

Figure 3.3.2. Mapping of functional topology between the dorsal hippocampus and gRSC. a) Left: Normalized raster plot of gRSC unit firing in response to distal CA1 stimulation from one shank, sorted based on the location of maximal waveform amplitude. Right: individual examples of a deep inhibited pyramid (top) and a superficial excited pyramid (bottom). Y-axis, spike count; scale bar, 5 Hz. b) Summary of z-scored firing responses to distal CA1 stimulation as a function of maximal waveform depth (mean ± s.e.m., n = 3 sessions from 3 animals). c) Z-score normalized responses of gRSC units significantly modulated by CA1 stimulation sorted based on response magnitude. d) Z-score normalized responses of gRSC units to CA1 SPW-Rs sorted as in (c). e) Averaged z-scored firing rate in response to stimulation of gRSC units which are positively (red), negatively (blue) or not modulated (black, not shown in c and d) by hippocampal stimulation (mean ± s.e.m). Inset, proportions of each group. f) Firing time from SPW-R onset is correlated with response magnitude. Dashed grey lines mark maximal and minimal correlation, respectively.

also on the distance from the stimulation site, with more anterior portions of the gRSC (bordering the anterior cingulate cortex, ACC) exhibiting weaker responses (Fig. 3.3.1f). Similar to the responses to spontaneous SPW-Rs, induced responses were also more prominent in superficial layers, as indicated by the strong sinks in the CSD map (Fig. 3.3.1g). We recorded 619 gRSC units during optogenetic hippocampal stimulation. The majority of excited units were located at superficial recording sites, whereas firing rates of many deep layer units were suppressed (Fig. 3.3.2a-b). Stimulation-excited units (n = 50/619, 8%) were recruited earlier after SPW-R onset compared to inhibited units (n = 71/619, 11%; Fig. 3.3.2c-e). As a result, early firing after SPW-Rs was correlated with the stimulation-induced firing, while the late firing was correlated with the stimulus-induced inhibition (Fig. 3.3.2f). These results indicate a functional topography between

CA1, the subiculum and gRSC. They also suggest that, while gRSC responses to hippocampal activity are governed by direct excitation in superficial layers, feed-forward inhibition dominates in deep layers, which together influence the sequential response of gRSC neurons to SPW-Rs.

3.4 A fraction of gRSC neurons are preferentially recruited by unique hippocampal activity patterns

A key question is whether gRSC neurons respond specifically to unique combinations of hippocampal activity during SPW-Rs, or whether SPW-Rs provide the necessary level of excitation needed for the induction of local ripples that, in turn, self-organizes neuronal content (Girardeau et al., 2017; O'Neill et al., 2017; Ólafsdóttir et al., 2016; Ramirez-Villegas et al., 2015). To address this question, we used a k-means (k = 10; Fig. 3.4.1a-b) clustering algorithm to classify CA1 SPW-

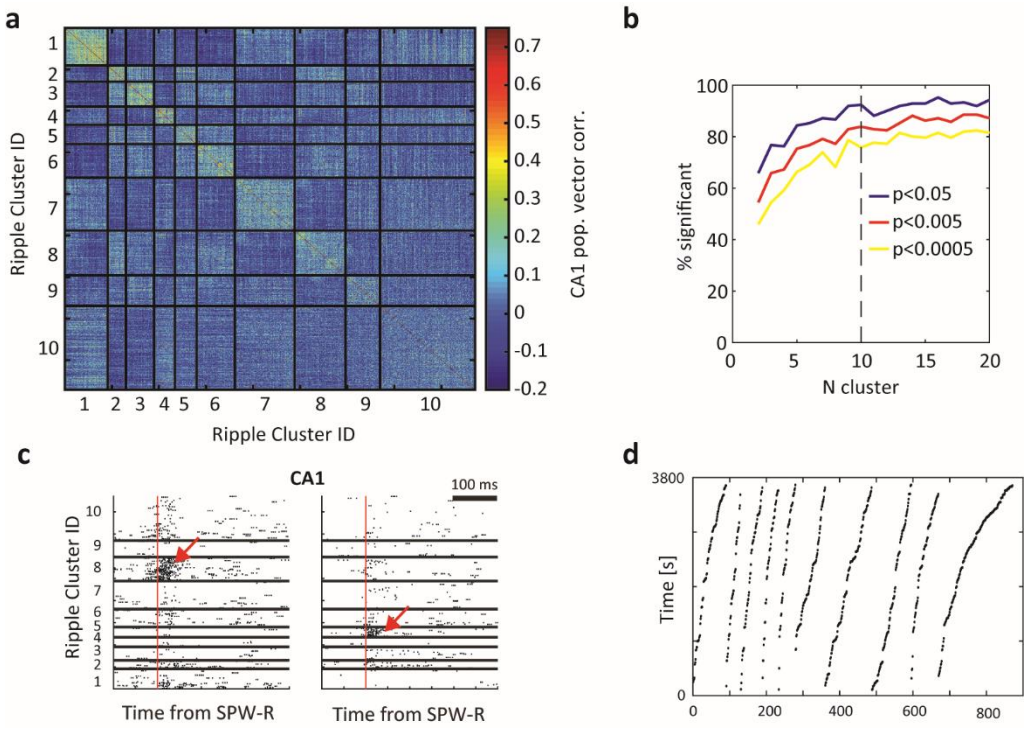

Figure 3.4.1. Hippocampal SPW-Rs form separate clusters. a) Example similarity matrix showing the correlation of population firing rate vectors of CA1 ensembles during ripples. Matrix sorted by ripple cluster labels (N = 871 ripples). b) The percentage of CA1 neurons whose firing was significantly modulated by cluster ID (regressing out mean population firing rate), as a function of the number of clusters in the k-means analysis. Dashed line is set at k = 10, the number of ripple types used throughout. c) Two example CA1 neuron responses to different ripple types (red arrows). Red line, ripple onset. d) The distribution of SPW-R in time from one subject, sorted by SPW-R cluster, showing that a SPW-R of a given type can occur at any point in time during the recording session.

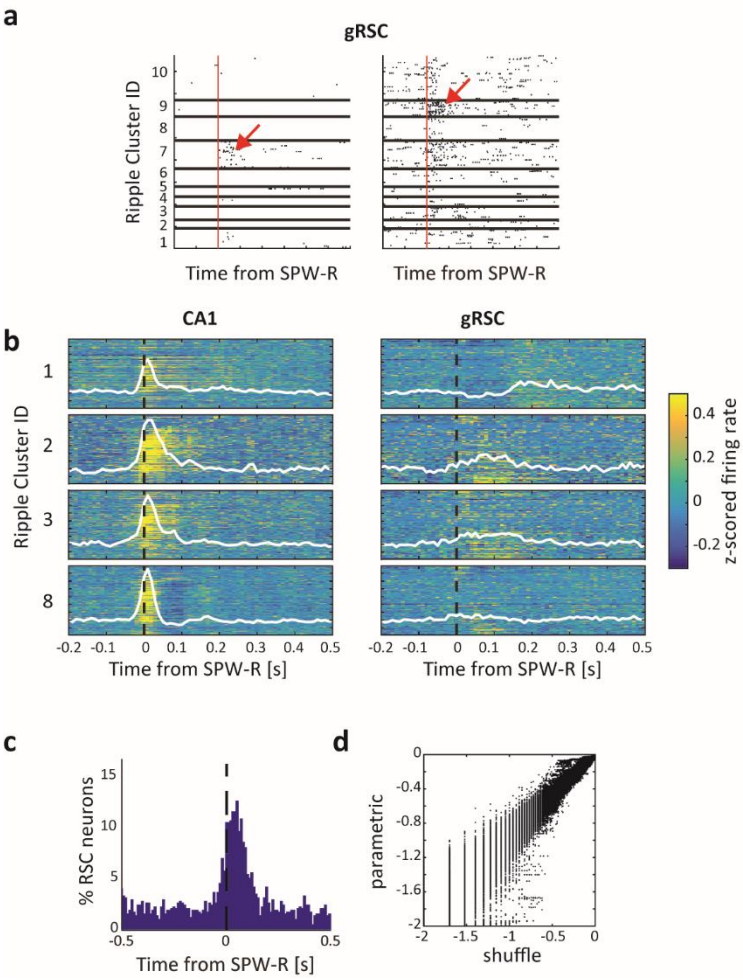

Figure 3.4.2. Retrosplenial activity distinguishes CA1 ripple firing patterns. a) Example responses of two gRSC neurons to different CA1 ripple types (red arrows). Red line, ripple onset. b) Population responses to four classes of ripple. Each row of each panel shows the normalized firing rate of an individual neuron around ripple onset, averaged across all ripples of the same type. White line, population average. c) Percentage of retrosplenial neurons that discriminate ripple types at each time lag around ripple onset. d) The correlation between the p-values obtained using a parametric ANCOVA test and after shuffling the labels of the ripple clusters and comparing the observed F-ratio from the ANCOVA test to the ones derived from the shuffle distribution.

Rs in our high-density recordings (n = 3 sessions from 3 mice, 5,442 ripples) based on the population vector of firing rates of CA1 neurons during the SPW-R. The resulting similarity matrix (Fig. 3.4.1a) indicated varying degrees of differences of the clustered SPW-R categories, likely reflecting different subsets as well as different weightings of active neurons. SPW-Rs of a given cluster were distributed throughout the entire recording session in all animals (Fig. 3.4.1d). By definition, the activity of CA1 neurons strongly discriminated different SPW-R subtypes, responding to only one or few ripple clusters (Fig. 3.4.1c). Importantly, we found that the activity of gRSC neurons (n = 619 units) also discriminated CA1 SPW-R types. Individual neurons responded maximally to specific SPW-Rs types or the combination of their subsets (Fig. 3.4.2a). As a result, each SPW-R type was associated with specific population firing patterns of gRSC neurons, with some gRSC neurons showing opposing activity patterns with respect to different clusters of SPW-Rs (Fig. 3.4.2b). Overall, 46.8% of gRSC neurons discriminated SPW-R type at some point within the 100 ms after ripple onset (Fig. 3.4.2c; $p < .01$; ANCOVA with 10 ripples groups and CA1 population firing rate

as a continuous nuisance regressor), with the majority of neurons discriminating SPW-R type within 60 ms after SPW-R onset. These findings were validated using non-parametric shuffling analysis (Fig. 3.4.2d). Those differences were also preserved in the low-dimensional representation of the different ripple clusters and their associated gRSC responses (Fig. 3.4.3).

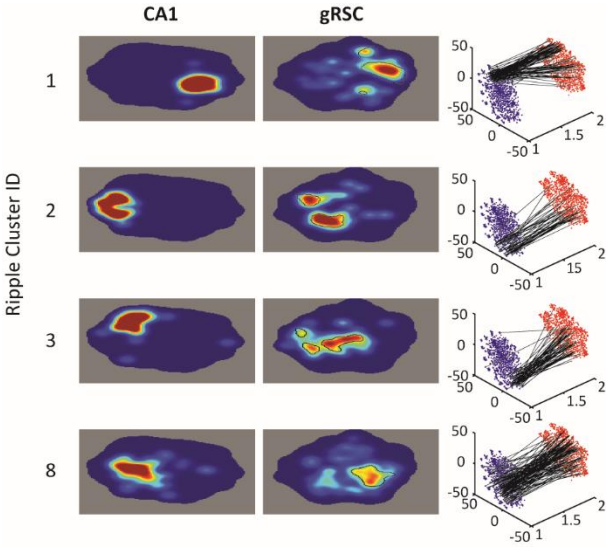

Figure 3.4.3. Dimensionality reduction of different SPW-R clusters using t-SNE. Two-dimensional histograms of the t-SNE representation for each of the four ripple cluster types shown in Fig. 3.4.2b for CA1 (left), gRSC (middle), and their event-by-event correspondence (right, black lines; red – CA1, blue - gRSC). Black contours in the gRSC denote the region of t-SNE space with higher density than expected by chance ($p < 0.01$).

3.5 Hippocampal – gRSC communication is state dependent

Previous studies have established that the probability of occurrence of hippocampal SPW-Rs is biased by ongoing brain activity, such as UP and DOWN states of slow oscillations of sleep (Steriade et al., 1993; Timofeev et al., 2001) and sleep spindles (Battaglia et al., 2004; Isomura et al., 2006; Mölle et al., 2006; Peyrache et al., 2009; Sirota et al., 2003). However, the influence of brain state changes on neurotransmission in the awake immobile animal is less clear (McGinley et al., 2015b).

In accordance with previous recordings in sensory neocortex of awake restrained rodents (Luczak et al., 2013), gRSC population activity fluctuated between synchronized epochs marked by 3-10 Hz activity packets and a desynchronized state associated with either high or low electromyographic activity (segregated using cut-offs at the minimum of the bimodal distribution (Watson et al., 2016) (Methods). We defined activity packets as events where bursts of population activity were surrounded by near silence and reached at least 60% of its long-term average for more than 40 ms (Methods). These fluctuations were quantified using the state-index

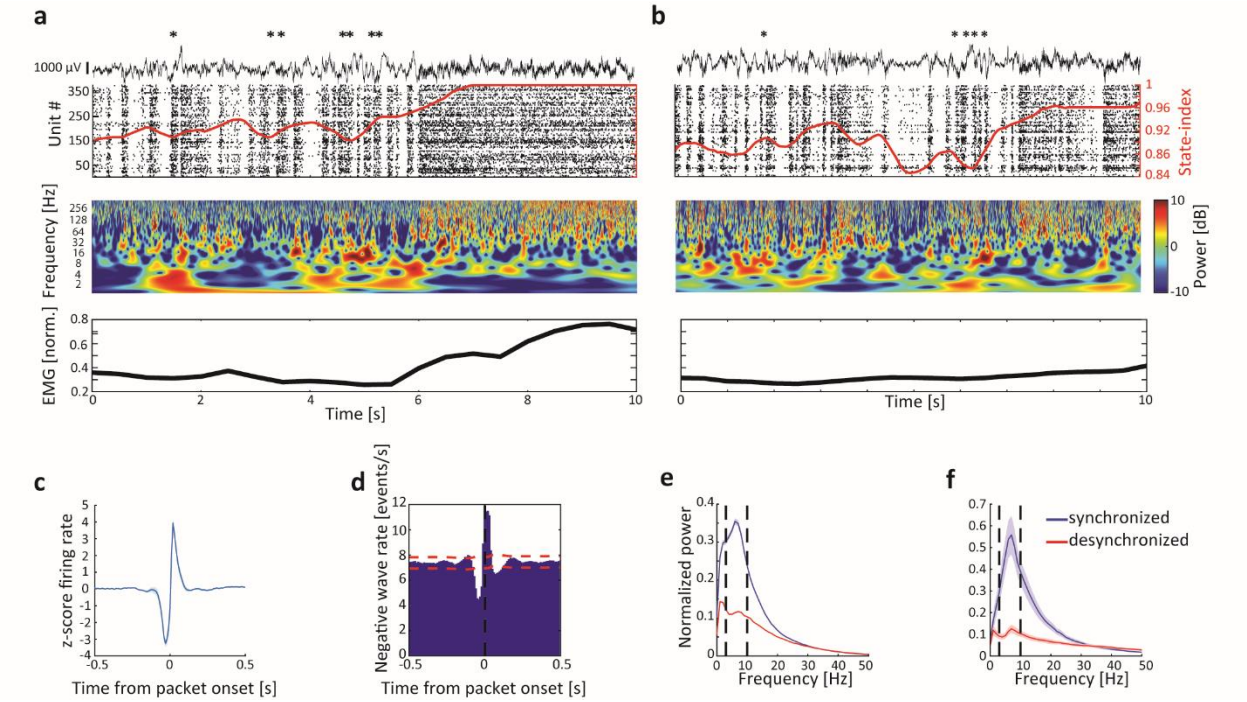

Figure 3.5.1. gRSC activity alternates between a synchronized and a desynchronized state. a) Top panel: example of 10s gRSC LFP (top), spiking activity (bottom) and the corresponding state-index (red) showing a state transition from a synchronized to a desynchronized state. Asterisks, SPW-Rs detected in CA1. Middle panel: Wavelet spectrogram of the LFP trace shown above. Note the absence of low frequency activity in the desynchronized state and the alternating high frequency activity in the synchronized state reflecting population bursts. Bottom panel: corresponding EMG activity. b) Same, but for a transition to a desynchronized state without a prominent EMG increase. c) z-score normalized gRSC MUA rate relative to packet onsets (n = 12 sessions from 4 animals, 58,987 packets). d) The rate of negative waves detected in superficial layers of the gRSC relative to packet onset (n = 9 sessions from 4 animals 156,210 negative waves and 22,365 packets). e) Normalized power spectrum of MUA activity from concatenated epochs classified using the state index as either synchronized or desynchronized (8 sessions from 4 animals). f) Same, but for LFP activity.

measure (Luczak et al., 2013) (Fig. 3.5.1.a top panel; Methods). Synchronized epochs were associated with low frequency activity reflecting negative waves, as well as bursts of gamma-band and high frequency activity, reflecting population bursts (Fig. 3.5.1).

We next asked how ongoing cortical activity affects the efficacy of hippocampal-cortical coupling during SPW-Rs. CA1-gRSC population cross-covariance was larger during synchronized states (Fig. 3.5.2a), compared to both desynchronized epochs with or without increase in electromyographic activity ($p < 0.001$; Bonferroni corrected rank sum test), despite similar overall firing rates in each state in both structures (Fig. 3.5.2b). SPW-Rs were virtually absent during

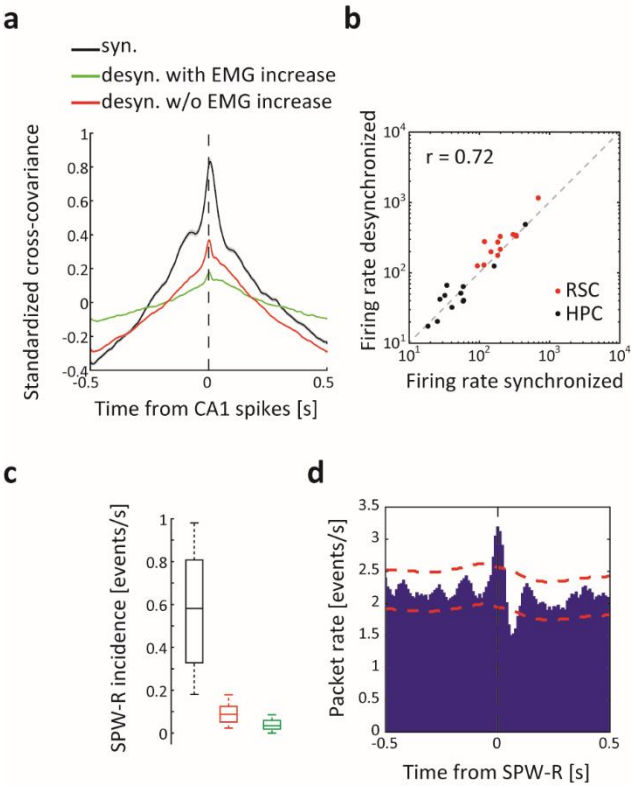

Figure 3.5.2. Hippocampal-gRSC coupling is state dependent. a) Standardized cross-covariance between dorsal CA1 and subiculum and gRSC unit pairs taken from synchronized (black) and desynchronized regimes either with (green) or without (red) increase in EMG activity (n = 12 sessions from 5 animals 19,064 pairs). b) A scatter plot showing the mean MUA rates in gRSC (red) and CA1 (black) across synchronized and desynchronized states defined using the state-index. Least-square slope = 0.72 (n = 12 sessions from 5 animals). Dashed diagonal represents perfect correlation. Global MUA rates across synchronized and desynchronized states are unchanged in both structures (p's > 0.05, signed rank sum tests). c) SPW-R rate is reduced during desynchronized compared to synchronized regimes. Middle line, median; box, quartiles (n = 10 sessions from 4 animals). Same color coding as in (a). d) Cross-correlogram between hippocampal SPW-Rs and gRSC activity packets (n = 8 sessions from 5 animals, 6,303 SPW-Rs and 9,625 packets).

desynchronized state associated with increased EMG and theta oscillation (Fig. 3.5.2c) (Buzsáki et al., 1992). Analogous to the coupling of SPW-Rs to SWS UP and DOWN states (Battaglia et al., 2004; Isomura et al., 2006; Peyrache et al., 2009), hippocampal SPW-Rs were significantly coupled to cortical packets in the waking state (Fig. 3.5.2d; n = 8 sessions from 3 CaMKII::Ai32 and 2 VGlut2-Cre [see below] animals; $p < 0.05$).

Previous work has demonstrated that, even within individual brain-states, rapid changes in arousal levels can dictate subthreshold dynamics and network activity (Hulse et al., 2017). To examine whether fluctuations within the synchronized cortical state contribute to the differential readout of SPW-Rs by gRSC neurons, we tested whether spectral properties at each time point surrounding hippocampal SPW-R onset differed based on SPW-R type (Fig. 3.5.3), while regressing out the effect of CA1 population firing rate (Methods). After SPW-R onset, divergent spectral LFP patterns were observed according to SPW-R subtype (n = 3 mice, one session per mouse), with significant differences in low frequency bands, reflecting the occurrence of a cortical negative wave (compare Fig. 3.5.3a and b) and in higher bands reflecting gamma band power and spiking. In contrast to the unit discrimination of ripple type, which proceeded ripple

onset (Fig. 3.4.2c), LFP magnitude in the 6-10 Hz frequency range prior to SPW-R onset significantly differed according to SPW-R subtype (Fig. 3.5.3c). These results suggest that the cortical state at the time of SPW-R is predictive of the currently active hippocampal ensemble, which in turn affects which gRSC neurons fire in response to hippocampal drive.

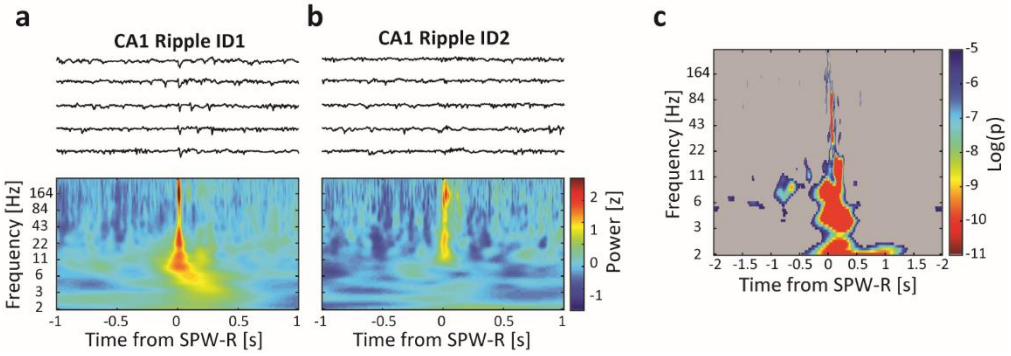

Figure 3.5.3. Different SPW-R clusters are associated with distinct spectral features. a) Top: Example LFP traces from most superficial and posterior gRSC electrode time locked to the onset of CA1 ripple cluster ID1. Bottom: Mean spectrogram for cluster ID1. b) Same as Panel E for ripple cluster ID2. c) The degree to which the power of each frequency band at each lag around ripple onset distinguishes ripple cluster ID. Non-significant areas are shown in grey. Corrected for multiple comparisons at each time $p < 0.0004$.

3.6 VGlut2 functions a marker for subicular bursting cells *in vitro*

Earlier tracing studies indicated that hippocampal projections to the gRSC arise mainly from the subiculum (Van Groen and Wyss, 2003; Honda and Ishizuka, 2015; Wyss and Van Groen, 1992). More recently it has been demonstrated that this pathway involves bursting pyramidal cells in distal subiculum (Kim and Spruston, 2012). However, a detailed dissection of this pathway was hampered by the lack of specific genetic markers allowing to target this subpopulation. Since bursting subicular cells are found mainly in distal subiculum (Greene and Totterdell, 1997), we used the publicly available Allen Brain Atlas repository to screen for genes with strong expression in distal, but not proximal subiculum or other nearby areas. This procedure pointed the vesicular glutamate transporter 2 (VGlut2) gene as a promising candidate (Fig. 3.6.1a; Allen Brain Atlas, experiment #73818754). To test the validity of the VGlut2 gene as a marker for bursting cells *in vitro* VGlut2-Cre animals were virally injected with an AAV9-SwitchON-mRubyNLS-ChR2(H134R)-EYFP construct in the dorsal subiculum (3.6.1b). This 'switch' construct allows for the expression of mRuby in Cre-negative cells, while the ChR2-EYFP coding sequence is reversely oriented. In

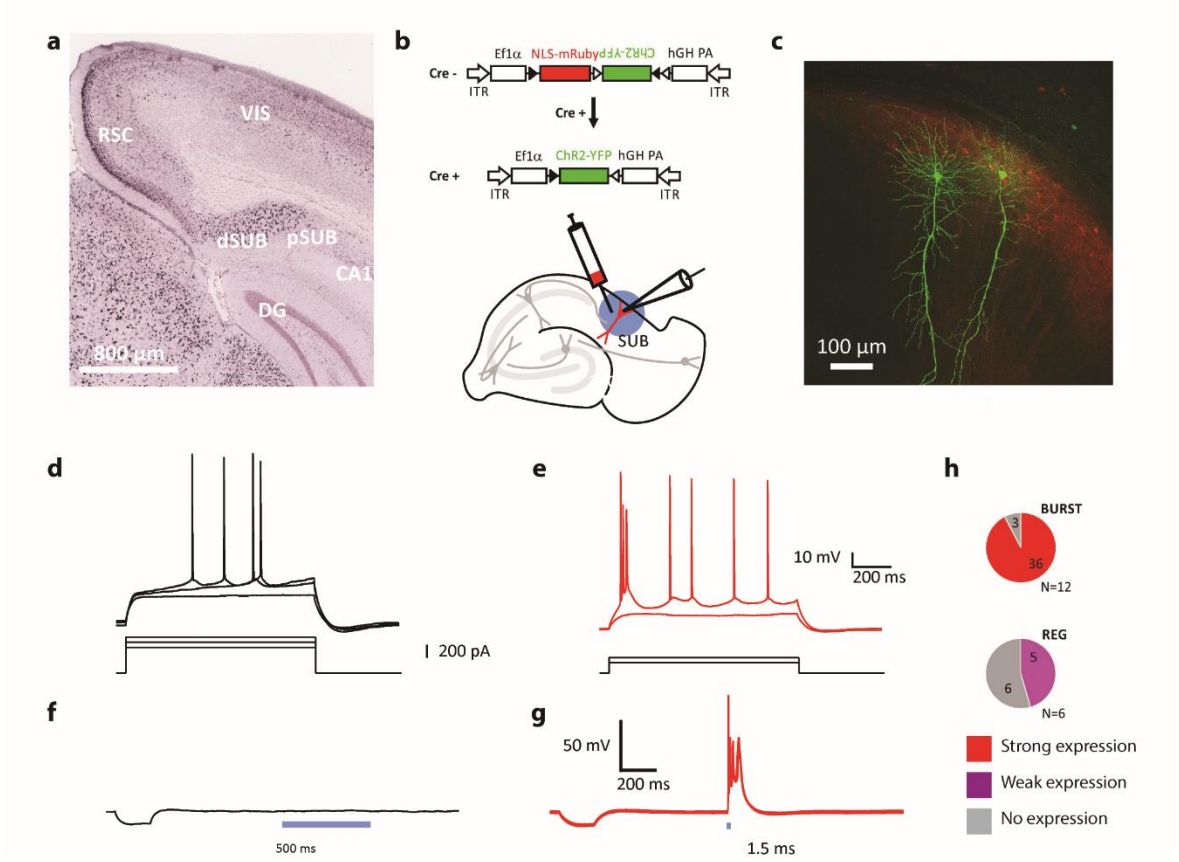

Figure 3.6.1. VGlut2 acts as a marker for bursting subicular cells. a) *In situ* hybridization indicates that VGlut2 is expressed in distal (dSUB), but not proximal subiculum (pSUB). RSC, retrosplenial cortex; VIS, visual cortex, DG, dentate gyrus. From Allen Brain Atlas. b) Top: A switch construct allows for the expression of mRuby fused to a nuclear localization signal (NLS) under the control of EF1α in Cre-negative cells, ChR2-EYFP sequence is reversed and cannot be expressed. In Cre-positive cells NLS-mRuby sequence is excised by Cre recombinase and ChR2-EYFP is inserted in correct orientation. Bottom: acute slices were prepared from animals virally injected in the dorsal subiculum. c) Maximal z-stack projection of two biocytin filled cells and mRuby-expressing cells in subiculum. d) Firing pattern of a subicular regular firing cell. e) Same, but for a subicular bursting cell. Same scaling as (d). f) Exemplary response of a regularly firing cell to 500 ms blue light pulse. g) Exemplary response of a bursting cell to 1.5 ms blue light pulse. h) Summary of responses to blue light stimulation from all cells, classified into bursting (top) or regular firing cells. From Wozny et al (2018).

Cre-positive cells, in contrast, Cre recombinase removes the NLS-mRuby coding sequence and facilitates the insertion of the ChR2-EYFP in correct orientation (3.6.1b top). We performed whole-cell patch clamp recordings from cells across the subiculum (3.6.1b bottom, c), whereby cells were first characterized for their electrophysiological firing pattern before they were stimulated with short blue light pulses to test for expression of ChR2 (Fig. 3.6.1d-g). We found that 92% (36/39 cells from 12 animals) of the bursting cells fired action potential in response to light, suggesting a strong ChR2 expression. In contrast, the majority of regularly firing subicular

cells (6/11 cells, 54% from 6 animals) were not responsive to light while the remaining 46% displayed small light-evoked potentials, suggesting weak expression (Fig. 3.6.1f-h). In summary, these results establish the VGlut2 gene as a reliable marker for bursting cells in the subiculum *in vitro* (Wozny et al., 2018).

3.7 Subicular bursting neurons target superficial layers of the gRSC

Having established the VGlut2 gene as a marker for bursting subicular cells *in vitro*, we next sought test the involvement of bursting subicular cells in the hippocampus-gRSC route. We first employed a ChR2-assisted circuit mapping strategy, by injecting the same switch vector in the dorsal subiculum of VGlut2-Cre mice (Fig. 3.7.1a). The design of this switch vector was useful in

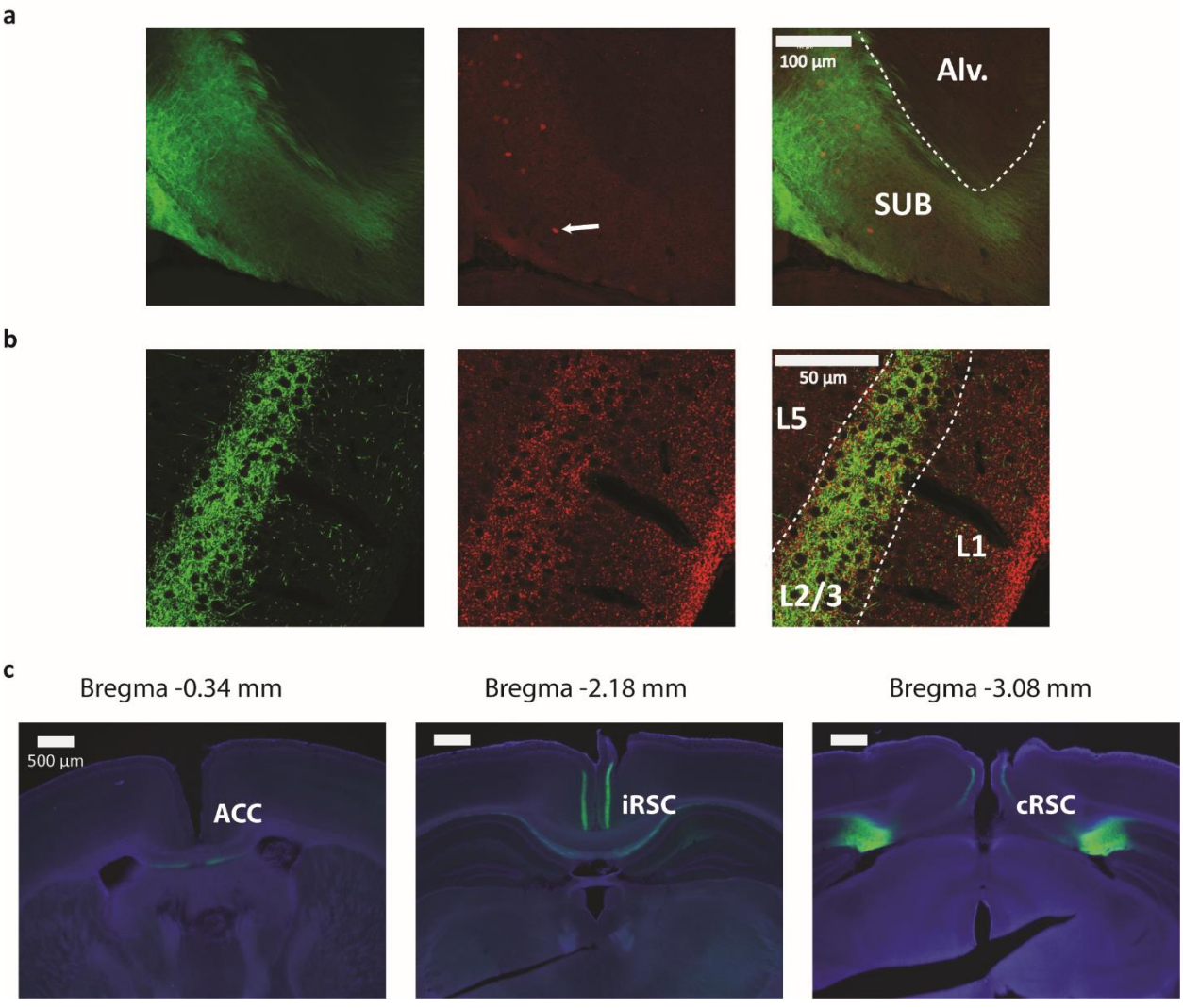

(Legend on next page)

Figure 3.7.1. Histology of subicular VGlut2$^+$ projections to the gRSC. a) A Cre-switch leading to the expression of ChR2-eYFP (green) in Cre-positive cells and mRuby (red) in Cre-negative cells was used to assess the amount of virus spread from the area of injection and to exclude potential spread into the gRSC. White arrow depicts the most distal mRuby expressing cell detected in this section (magnification: 20x). Alv.: Alveus. b) VGlut2 immunostaining of brain slices from VGlut2-Cre animals injected with AAV9-SwitchON-mRubyNLS-ChR2(H134R)-EYFP shows colocalization (right, merged) of subicular terminals (left, green) and VGlut2 antibodies (middle, red) in the superficial layers of the RSC (magnification: 60x). c) Subicular – gRSC projections follow an anterior-posterior gradient showing strong axonal labeling (green) in caudal and intermediate sections (cRSC and iRSC, respectively) which gradually weakens in rostral sections and terminates at the border with the ACC (magnification: 2.5x). Blue: DAPI.

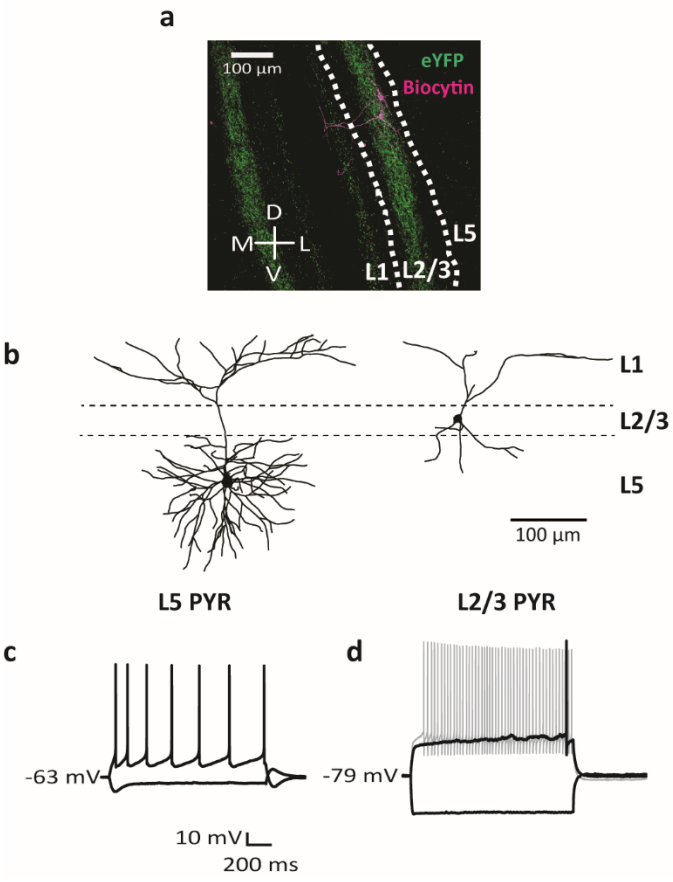

Figure 3.7.2. Biophysical properties of superficial and deep gRSC cells). a) Magnified image showing the (bilateral) restriction of subicular VGlut2$^+$ terminals to L2/3 (green), as well as two biocytin-labelled L2/3 pyramids (magenta). White lines, L2/3. b) Reconstructed representative examples of deep (left) and superficial (right) gRSC pyramids. Superficial cell is the one shown in (a). c) Membrane potential responses of a deep gRSC pyramid to injection of ±80 pA d) Responses of a superficial cell to current injection of ±80 pA (black) and 160 pA (grey).

ruling out viral spread to the gRSC, where VGlut2 is also sparsely expressed (Allen Brain Atlas, experiment #73818754) (Fig. 3.6.1a). In all mice used for this experiment (n = 8), viral expression was limited to the dorsal subiculum and showed dense axonal termination in L2/3 gRSC and strongly co-localized with VGlut2-reactive fibers (Fig. 3.7.1b). VGlut2$^+$ axons extended across the entire anterior-posterior axis of the gRSC but exhibited a gradient in intensity, reaching their maximum above the splenium and decreasing toward more rostral parts at the border with the anterior cingulate cortex, explaining the gradually weakening responses along this axis to hippocampal stimulation (section 3.3). VGlut2$^+$ fibers sharply terminated at the border with the anterior cingulate cortex and at the border between the granular and dysgranular RSC (Fig. 3.7.1c).

In cortical slices *in vitro*, we recorded from 73 cells intracellularly, which were subdivided into L2/3 pyramids (n = 44), L5 pyramids (n = 22) and fast spiking interneurons (n = 7, 5 in L2/3 and 2 in L5) based on morphology, firing pattern and, in a subset of the experiments, GAD-67 immunostaining. L2/3 pyramids were smaller than L5 pyramids, and exhibited a late-spiking phenotype, a strongly hyperpolarized resting membrane potential, and no sag potentials (Fig. 3.7.2 and Table 3.1) (Kurotani et al., 2013). Brief, 10 ms pulses of blue light evoked excitatory EPSPs in 68% (30/44) of L2/3 cells (Fig. 3.7.3a, c), with a mean latency of 2.66 ± 0.15 ms (Fig. 3.7.3d). In a subset of the experiments, we blocked action potential evoked neurotransmission by tetrodotoxin to confirm that these connections were monosynaptic. After all light-evoked responses were abolished, we added the K^+ channel blocker 4-AP to the extracellular medium to rescue monosynaptic transmission (Fig. 3.7.3a). Monosynaptic coupling between subicular $VGlut2^+$ fiber and gRSC was confirmed for all tested L2/3 pyramidal neurons (n = 6/6). Likewise, light stimulation of subicular fibers in superficial layers reliably evoked EPSPs in all tested interneurons (n = 5/5, Fig. 3.7.4). In stark contrast to superficial layers, and in contrast to a previous report (Yamawaki et al., 2019a) (likely arising from the minimal injection volume and the ability to assess viral spread using the Switch vector in our study) YFP-labelled subicular fibers in deep layers were extremely sparse and light pulses delivered either to somatic or apical regions failed to evoke measurable responses in deep pyramidal cells (Fig. 3.7.3b-c). In contrast to deep

	Rm (MΩ)	Vrest (mV)	Cm (pF)	AP threshold (mV)	Rheobase (pA)	AP height (mV)	AP FWHM (ms)	AHP (mV)	Sag (mV)	Tau (ms)
L2/3 PYR	238.25 ± 9.91	-79.26 ± 0.78	68.53 ± 6.22	-35.36 ± 0.69	94.17 ± 4.66	66.54 ± 1.45	0.52 ± 0.01	20.52 ± 0.54	-1.02 ± 0.09	15.41 ± 1.13
L5 PYR	140.10 ± 13.25	-64.45 ± 1.05	272.10 ± 27.24	-37.52 ± 1.07	115.00 ± 9.26	77.50 ± 2.64	0.60 ± 0.02	13.42 ± 0.87	-11.85 ± 1.02	37.64 ± 3.28
FS INTs	95.47 ± 13.98	-73.40 ± 1.33	100.89 ± 18.97	-37.27 ± 2.05	451.42 ± 105.27	65.28 ± 3.38	0.25 ± 0.01	24.62 ± 1.41	-2.43 ± 0.64	8.13 ± 0.79

Table 3.7.1. Biophysical properties of RSC neurons. Summary of biophysical properties (mean ± s.e.m.) of superficial pyramids (n = 44 cells), deep pyramids (n = 22 cells) and fast-spiking interneurons (FS INTs; n = 7 cells, 5 from superficial and 2 from deep layers). Rm: membrane-resistance, Vrest: resting membrane potential Cm: capacitance, AP: action potential, AHP: after hyperpolarization, FWHM: full-width at half maximum.

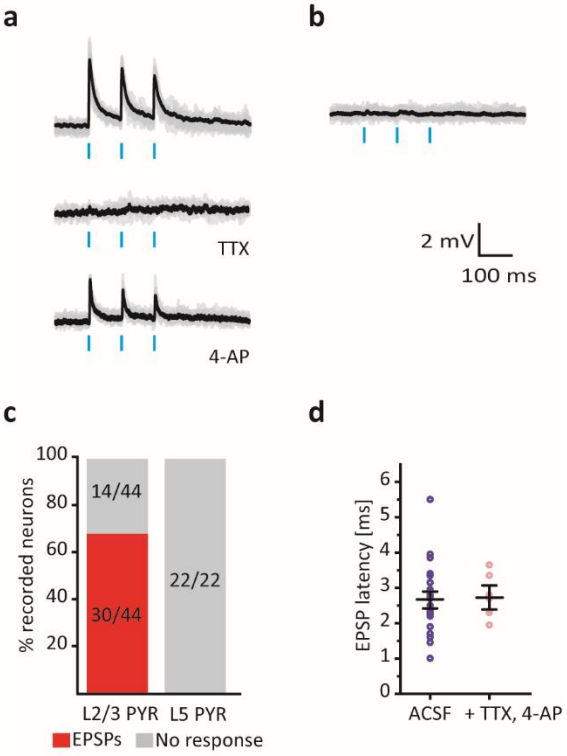

Figure 3.7.3. Laminar specific responses of gRSC pyramidal cells to subicular fiber stimulation. a) Example responses of a L2/3 gRSC pyramidal cell in ASCF (top), after adding 10 µM TTX (middle) and after the addition of 4-AP (bottom). b) Example traces of responses to light stimulation of a deep gRSC pyramid in ACSF. c) Summary of responses of gRSC pyramids to subicular VGlut2^{+} fiber stimulation. d) EPSP latencies of all responsive superficial cells (n = 30) and a subset where TTX and 4-AP were applied (n = 6), indicating monosynaptic connections. Black lines, mean ± s.e.m.

layer pyramids, we did observe light-evoked responses in deep layer interneurons (n = 2/2; Fig. 3.7.4b-c).

To validate that subicular neurons that project to gRSC are indeed mainly bursting cells (Cembrowski et al., 2018a; Kim and Spruston, 2012), we injected a non Cre-dependent rAAV2-retro-tdTomato virus (Tervo et al., 2016), a recently developed retrograde monosynaptic tracer, into the gRSC of a VGlut2-Cre mouse. Labelled neurons were restricted to the dorsal subiculum and showed a bursting phenotype (n = 8 cells from one animal; Fig. 3.7.5).

Reciprocally, we tested whether VGlut2-negative, putative non-bursting cells give rise to similar projection pattern and downstream responses in the gRSC. We injected Cre-Off ChR2-EYFP in the dorsal subiculum of VGlut2-Cre mice (n = 3; Fig. 3.7.6a) and measured light-evoked synaptic responses in superficial and deep gRSC

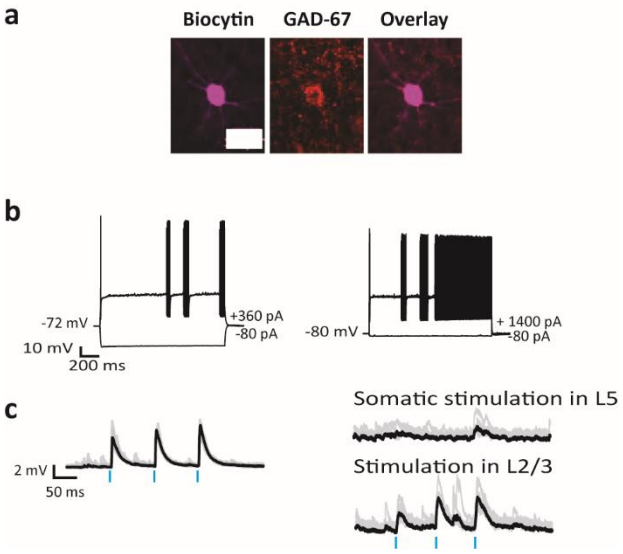

Figure 3.7.4. Interneurons across all gRSC layers receive subicular inputs. a) Example of a patched INT in superficial layers of the RSC, identified using GAD-67 immunostaining (left, magenta: biocytin, red: anti-GAD67 antibody). Scale bar, 20 µm. b) Electrophysiological characterization of INTs in superficial (left) and deep (right) gRSC layers. c) Responses of the cells shown in (b) to light stimulation. Note the stronger responses of the deep layer INT when stimulated in L2/3.

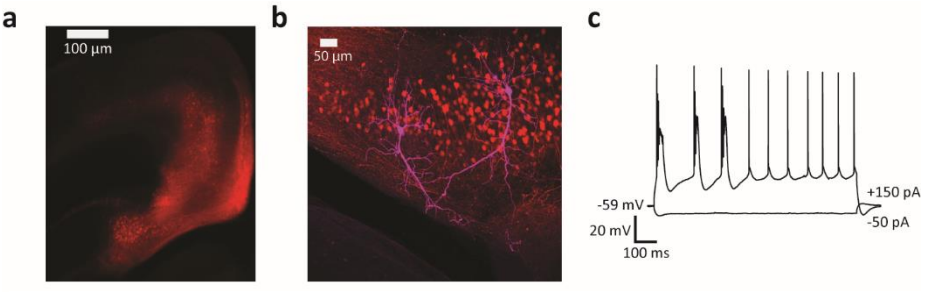

Figure 3.7.5. Retrograde viral injection in gRSC labels subicular bursting cells. a) rAAV2-retro-mRuby injected in the gRSC retrogradely labeled cells in distal subiculum. b) Magnified (20x) image showing two labelled cells that were patched (magenta). c) Example characterization of a retrogradely labelled cell. All recorded cells exhibited a bursty firing pattern (right, n = 8 cells from one animal).

cells. When holding cells at a more depolarized membrane potential (-50 mV), we found that light stimulation evoked mostly inhibitory responses in both superficial (15/24, 62%) and deep cells (7/11, 63%). In contrast, EPSPs were evoked in only a small subset of superficial (4/24, 16%) and deep (2/11, 18%) cells, with the remaining neurons showing no light-evoked responses (Fig. 3.7.6b-c). Furthermore, subicular terminals labelled by the Cre-off vector (i.e. stemming from non-VGlut2$^+$ cells) resided mostly in L1 and deep layers and were less prominent in L2/3 (Fig. 3.7.6a). These results are in contrast to the pattern observed by switch vector injections and by VGlut2 immunostaining (Fig. 3.7.1), but consistent with the mutually exclusive distribution of VGlut1 and VGlut2 terminals in superficial and deep layers of the gRSC and the paucity of VGlut1-positive terminals in superficial layers (Varoqui et al., 2002). To verify that these projections emerged from non-bursting cells, we recorded from subicular neurons in the presence of synaptic blockers to identify presynaptic neurons expressing ChR2-EYFP. Of the 23 subicular cells tested, 4/6 putative regular firing cells and 8/8 putative interneurons fired action potentials in response to light stimulation, but only 1/9 identified bursting cells responded to light (Fig. 3.7.6d-f). Overall, these experiments suggest a division of labor in the subiculum, whereby bursting VGlut2$^+$ pyramidal cells excite superficial gRSC and the VGlut2-negative cells drive predominantly inhibition in both superficial and deep gRSC cells. The source of the inhibitory drive is likely feedforward activation of inhibitory interneurons in gRSC, possibly complemented by direct long-range GABAergic projections (Jinno et al., 2007; Miyashita and Rockland, 2007; Yamawaki et al., 2019b).

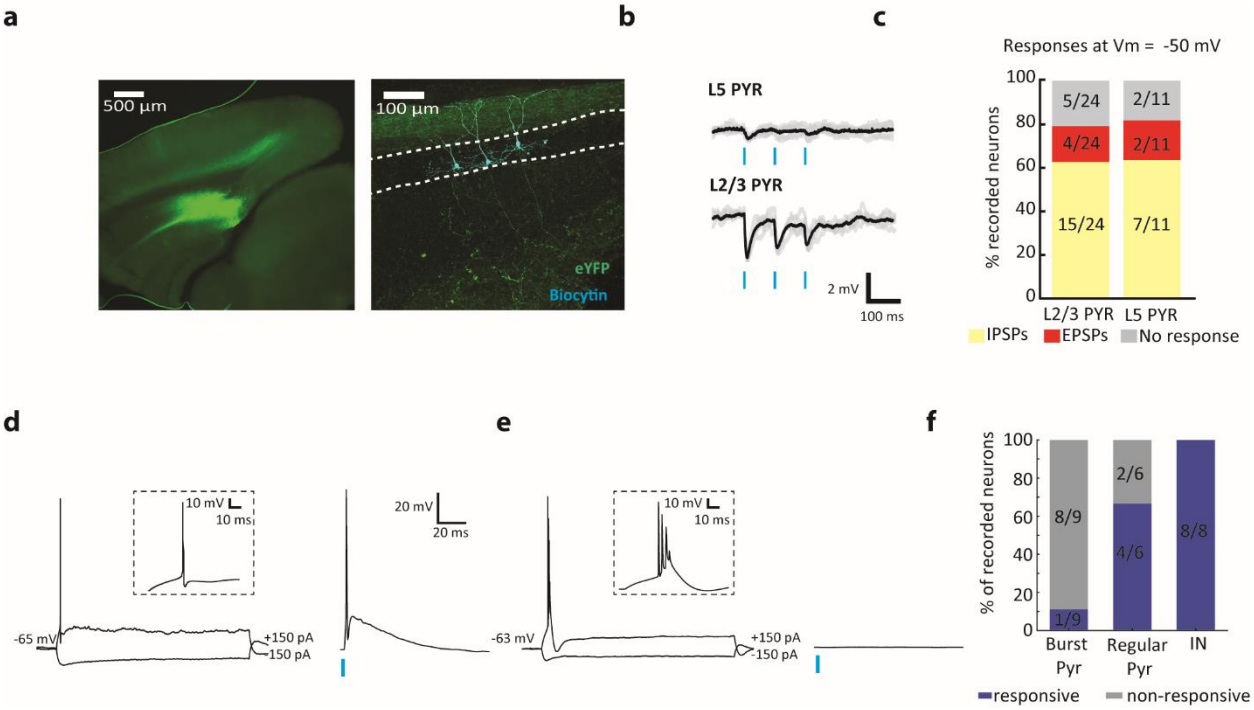

Figure 3.7.6. Cre-negative subicular cells promote inhibitory responses in gRSC. a) Left: a Cre-Off AAV-ChR2-YFP virus was injected into the dorsal subiculum to label VGlut2-negative cells. Right: subicular infection of VGlut2-Cre animals with Cre-off virus shows fiber labeling (green) predominantly in L1 and deeper layers, but to a lesser extent in L2. Three patched biocytin-filled pyramids are labeled in cyan. b) Examples of light-evoked responses from a deep (top) and a superficial (bottom) cell held at -50mV, revealing inhibitory inputs. c) Summary of light evoked responses from superficial and deep layers in VGlut2-Cre animals (n = 3 mice) injected with a Cre-Off AAV-ChR2-YFP virus. d) Electrophysiological firing pattern (left) and light-evoked responses (right) of an example subicular pyramidal cell infected by the Cre-Off AAV-ChR2-YFP virus, showing a regular firing pattern. Inset, zoomed-in action potential. e) Same, but for a subicular bursting cell. Note the absence of light-evoked responses. Same scale bars as in d. f) Summary of light-evoked responses in subicular cells (n = 23 cells from 3 animals).

3.8 Identification of subicular bursting cells *in vivo*

Subicular bursting cells are strongly activated during SPW-R events (Böhm et al., 2015). The relation between burst propensity of neurons *in vivo* and SPW-R modulation was previously quantified in intracellular recordings based on the unambiguous bursting pattern following rheobase current injection (Böhm et al., 2015). However, this relation is less clear in extracellular recordings, where spike autocorrelograms (ACGs) are used to quantify the extent of complex spike bursts. Our aims here were twofold: first, to test whether the findings of Böhm et al. (2015) using intracellular recordings *in vivo* and *in vitro,* can be extended to extracellular unit recordings

and the emission of complex spikes, and second, to test the validity of the VGlut2-Cre line as a reliable marker for bursting cells *in vivo*. We recorded from 196 subicular units in VGlut2-Cre mice (n = 3) injected with ChR2-EYFP (Fig. 3.8.1a) and used brief light pulses (10 ms) at random intervals throughout the recording session to identify VGlut2-positive neurons. Light stimulation

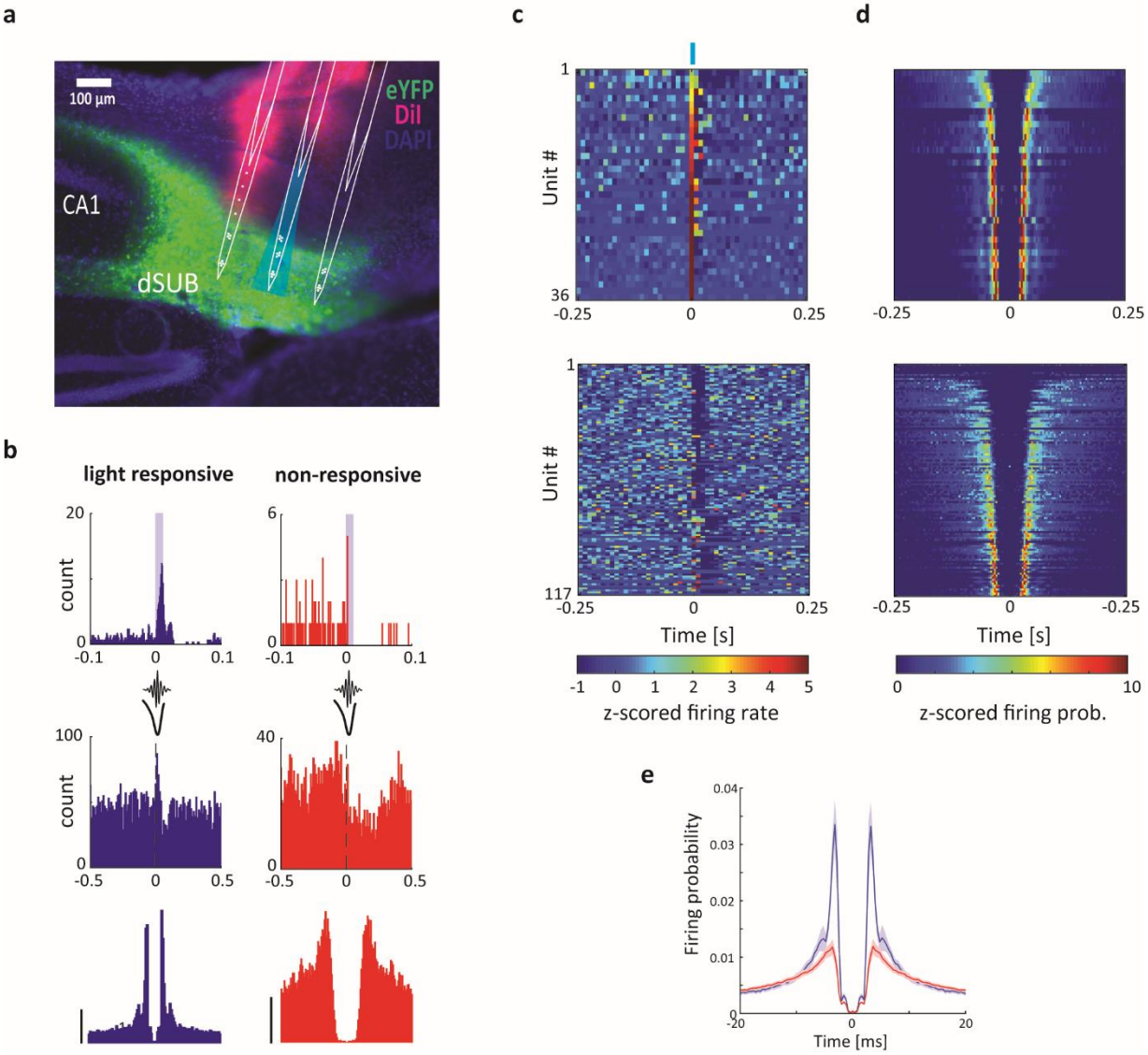

Figure 3.8.1. Identification of subicular bursting cells *in vivo*. a) Subicular bursting cells were labelled with ChR2-eYFP (green) using the VGlut2-Cre mouse line. Probes were coated with a dye (DiI, magenta) to confirm subicular targeting. b) Examples of a light responsive (blue, top left) and a non-responsive (red, top right) subicular units, their responses to SPW-Rs (middle) and their ACGs (bottom). ACG range ± 25 ms; scale bar, 10 Hz. c) Z-score normalized PETHs showing the responses of all units, which are positively (top) modulated or not positively modulated (bottom) within the 10 ms blue light stimulation (blue bar at 0 s, n = 6 sessions from 3 mice). d) Color-coded z-scored ACGs of the cells in (c). e) Average ACGs of light responsive (blue) and non-positively responsive (red) units.

increased unit activity in the subiculum, but not in CA1, confirming a specific localization of the construct to the subiculum (data not shown). Putative pyramidal cells were separated into light responsive and non-responsive groups (Fig. 3.8.1b top row and 3.8.1c). Only units that displayed a significant increase in firing rate within the 10-ms long light pulse were considered directly light activated. Inspection of individual and average ACGs of light responsive and non-responsive units suggested striking differences in burstiness (Fig. 3.8.1d-e). To quantify those differences, we applied a double exponential fit model to several key features of the ACG which were indicative for burst firing (Fig. 3.8.3). Fit parameters of responsive pyramids significantly differed from non-responsive cells in both rising slope, peak height and decay slope (p's < 0.001, rank sum test, Fig.3.8.3c), but not in baseline firing probability (p = 0.093). Thus, light-responsive cells had a stronger tendency to be bursty, consistent with previous *in vitro* results showing that VGlut2 is a specific marker for bursting cells in the subiculum (Wozny et al., 2018).

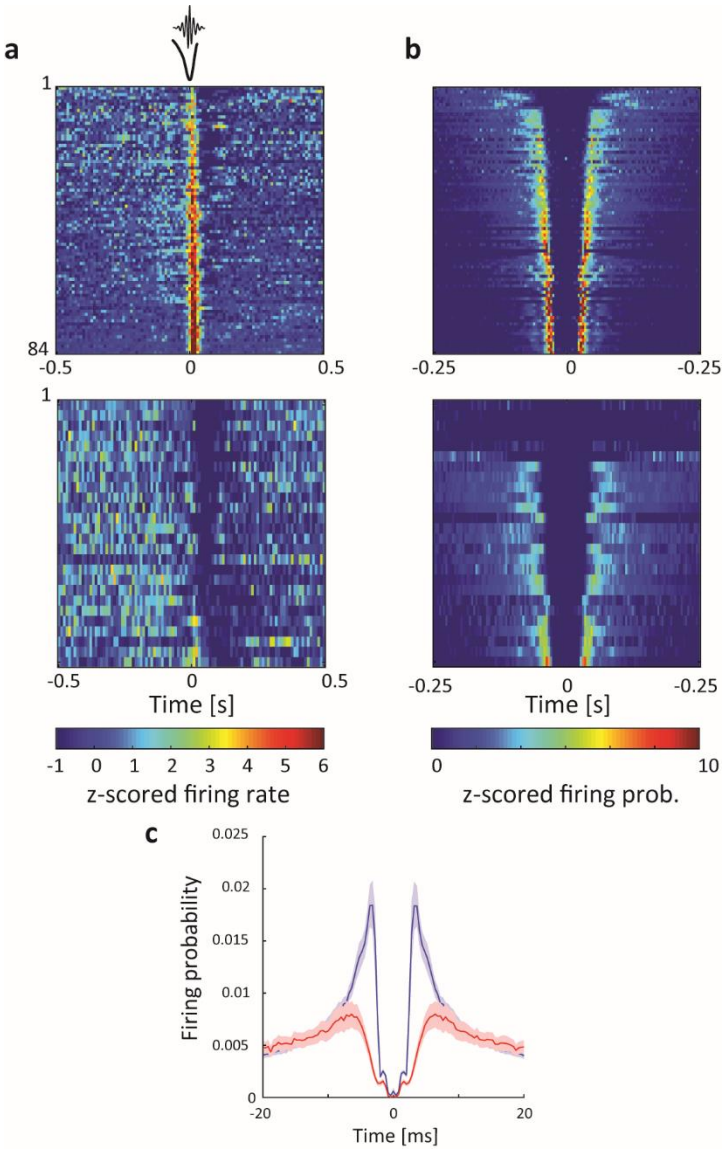

Figure 3.8.2. Modulation of subicular cells activity by SPW-R. a) Z-score normalized PETHs showing the responses of all positively (top) or negatively (bottom) SPW-Rs modulated units (n = 6 sessions from 3 mice). b). Color-coded z-scored ACGs of the cells in (a). c) Average ACGs of SPW-R positively (blue) and negatively (red) modulated units.

Next, we classified neurons according to their modulation by local SPW-Rs (Fig. 3.8.2). To avoid ambiguities, units that did not show significant up- or down-modulation of their firing rates

by SPW-Rs were excluded from the analysis (n = 43). Ripple-excited units (n = 84) displayed more bursty ACGs than ripple-suppressed units (Fig. 3.8.1b bottom row, Fig. 3.8.2 and Fig. 3.8.3d) (n = 26; p's < 0.05, Wilcoxon rank sum tests). The majority (72%, 26/36) of light-responsive neurons belonged to the SPW-R – excited group (Fig. 3.8.3a). It is noteworthy that these opto-tagged cells likely underestimate the VGlut2^{+} population due to multiple factors such as transfection efficiency and reduced activation of cells on sites distal to the light source. In summary, these results validate the VGlut-2 gene as a marker for bursting subicular cells and show that these neurons are excited by SPW-Rs.

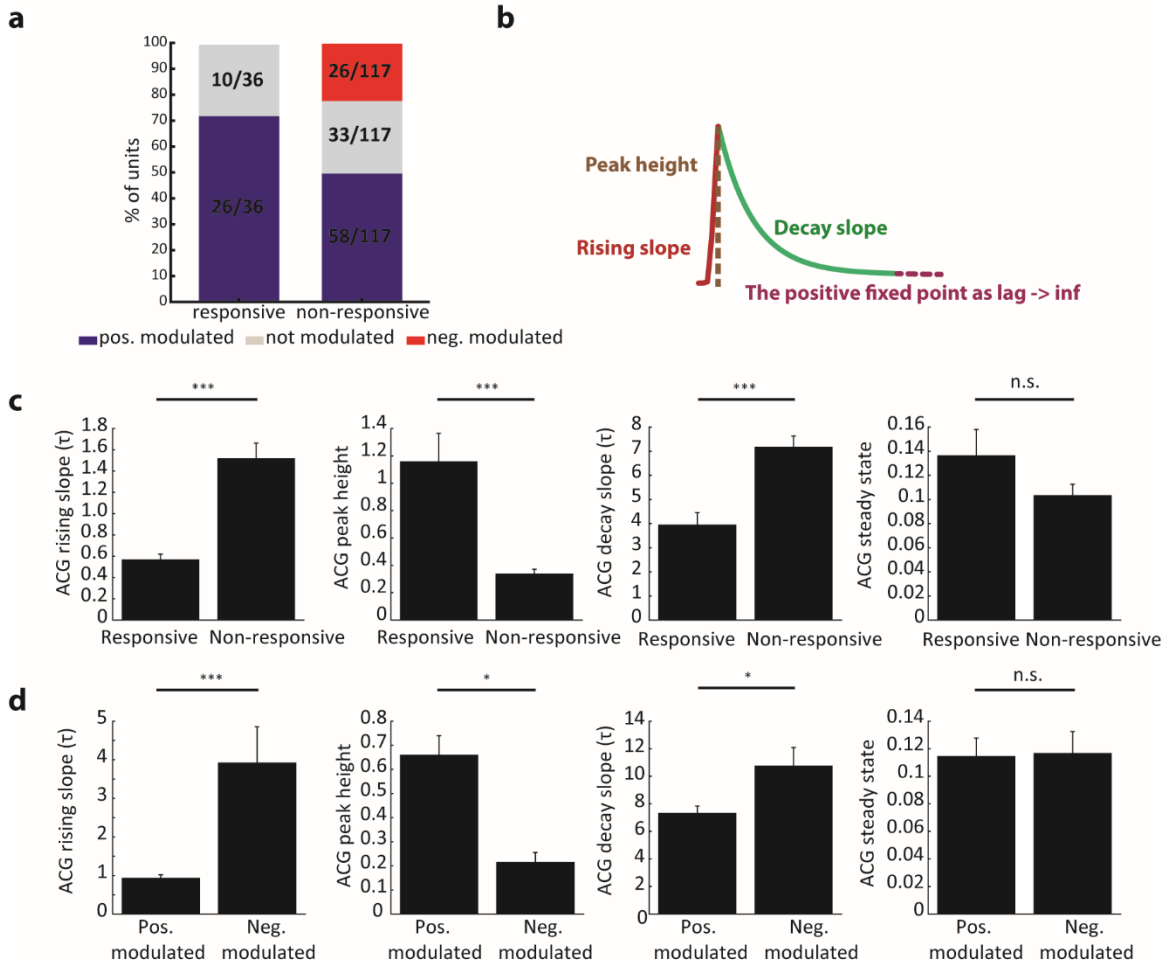

Figure 3.8.3. Quantitative assessment of burstiness based on light and SPW-R modulation. a) Summary of SPW-R modulation as a function of light responsiveness (n = 6 sessions from 3 animals; 36 light responsive units and 120 non-responsive units). b) A double exponential fit model of the ACG was used to determine significant differences in burstiness based on rising slope, peak height and decay slope. The positive lag reflects baseline firing probability. c) Summary of fit model parameters for light responsive and non-responsive units. d) Summary of fit model parameters for SPW-R positively and negatively modulated units (*p<0.05 ***p<0.001; rank sum tests).

3.9 Subicular bursting neurons mediate SPW-R – related hippocampal output

We next investigated whether the ripple coupling observed between the hippocampus and the gRSC can be mediated by VGlut2$^+$ subicular bursting cells. We simultaneously monitored dorsal subiculum and gRSC activity in VGlut2-Cre mice injected with ChR2 in dorsal subiculum, while optogenetically inducing high-frequency oscillations (100 ms sinusoidal or square pulses) in the subiculum (n = 10 sessions from 4 mice) (Stark et al., 2014). Optogenetic stimulation of bursting subicular VGlut2$^+$ cells was sufficient to induce local ripple-like high-frequency oscillations in the subiculum (iHFO; Fig. 3.9.1). The activity of light-responsive subicular pyramidal units was up modulated around spontaneous gRSC ripple events and ramped prior to that of gRSC units (Fig. 3.9.2). Similar to the gRSC responses to spontaneous SPW-Rs, iHFOs were associated with a negative wave and increased ripple band power in superficial, but not deep layers of the gRSC (Fig. 3.9.3). In many gRSC neurons, optical stimulation initially induced spike suppression, followed by rebound

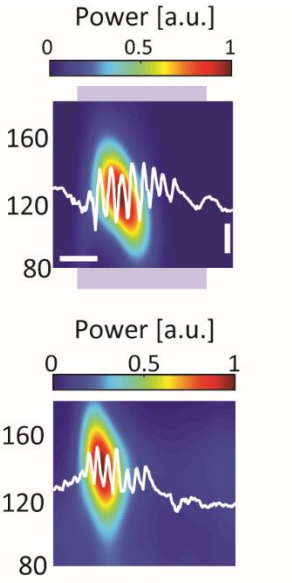

Figure 3.9.1. Optogenetic induction of ripples in the subiculum. Example wavelet spectrograms of iHFOs (top, shaded blue area) and spontaneous ripples (bottom, averages of 155 iHFOs and 742 spontaneous ripples from one session). Example traces are overlaid in white. Y-axis, frequency; Horizontal scale bar, 25 ms; Vertical scale bar, 200 µV.

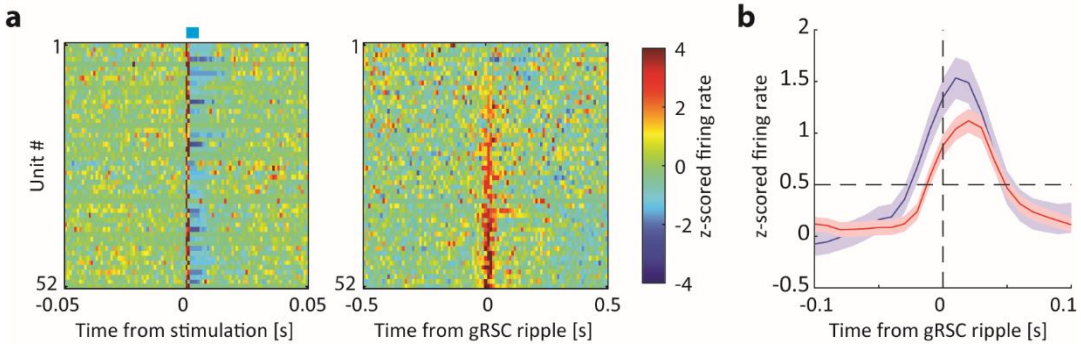

Figure 3.9.2. Activation of bursting subicular cells precedes gRSC cells during gRSC ripples. a) Left: z-score normalized PETHs of putative pyramidal subicular cells which are significantly up-modulated by 5 ms blue light pulses (n = 7 sessions from 2 animals). Right: z-score normalized PETHs of the same cells in response to gRSC ripples (sorted as in the left panel). b) Average z-score normalized responses of the subicular cells shown in left and middle panels (blue) as well as of gRSC units (red, n = 175 units). Time to reach a z-score of 0.5 (dashed horizontal line) is significantly earlier for subicular cells (subicular cells: 26 ± 2 ms before gRSC ripple, gRSC cells: 15 ± 1 ms before gRSC ripple; p = 0.0009, rank-sum test).

spiking approximately 100 ms after the stimulation onset (Fig. 3.9.4a-b). A similar temporal relationship was detected between subicular stimulation and cortical packets (Fig. 3.9.4c; n = 13 sessions from 4 mice).

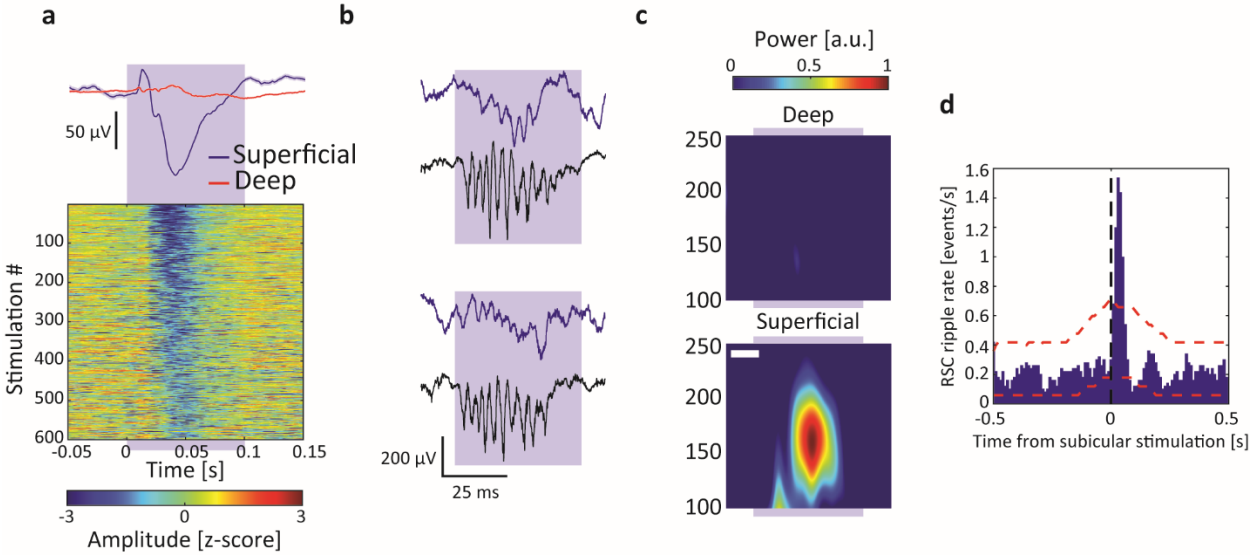

Figure 3.9.3. Effects of subicular stimulation on gRSC local field activity. a) Example z-scored voltage traces from a superficial gRSC channel in response to sine wave stimulation of dorsal subiculum (bottom) and the average response from a superficial (blue) and a deep (red) channel (n = 2 sessions from one animal). b) Two example gRSC ripples (top, blue traces) induced by subicular stimulation (bottom, black traces). c) Wavelet spectrograms from superficial (bottom) and deep sites of gRSC centered around iHFOs induced in the subiculum (n = 6 sessions from 4 animals, 1,472 stimulations). Scale bar, 25 ms; same color bar; Y-axis, frequency. d) Cross-correlation between subicular stimulation and identified gRSC ripple events (n = 7 sessions from 4 animals 1,672 sine wave stimulations and 3,718 gRSC ripples)

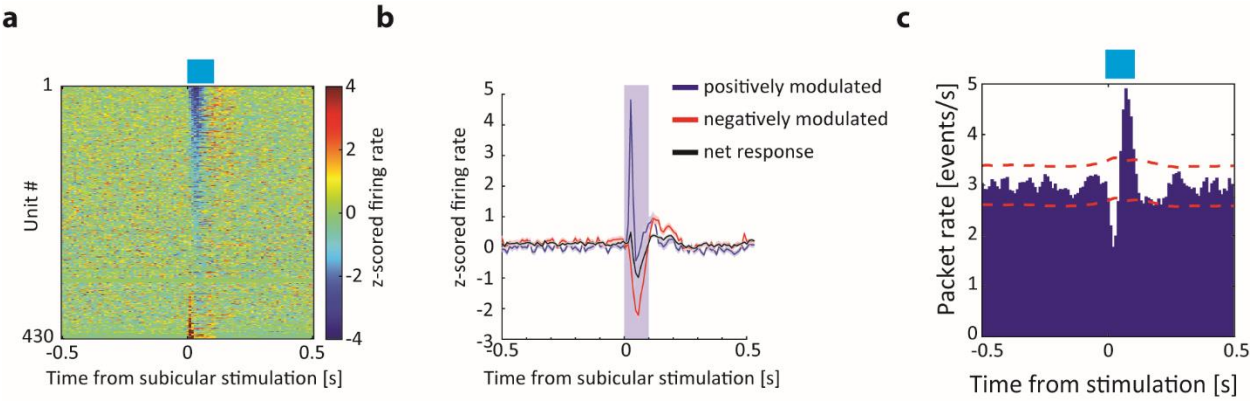

Figure 3.9.4. Effects of subicular stimulation on gRSC unit activity. a) z-score normalized PETHs of gRSC units in response to 100 ms optogenetic square pulse stimulation of VGlut2^{+} cells in subiculum. b) Average of z-score normalized responses of units in gRSC which were positively (blue) and negatively (red) modulated by light stimulation, as well as net response (grey) (n = 15 sessions from 4 animals). c) Cross-correlation of subicular VGlut2^{+} opto-stimulation with gRSC packets (n = 13 sessions from 4 animals 5,284 stimulations and 82,589 packets).

Finally, to directly test the contribution of VGlut2$^+$ subicular cells on gRSC activity, we simultaneously recorded from the CA1 and gRSC in VGlut2-Cre animals (n = 5) injected with an inhibitory optogenetic construct (AAV1-DIO-Arch-EYFP) into the dorsal subiculum. Green light stimulation (5 s pulses) of VGlut2$^+$ terminals in the gRSC was contingent upon ripple detection in CA1, with a varying random delay to onset (mean delay 85.5 ± 0.8 ms). This protocol guaranteed that stimulation was delivered in brain states with high ripple occurrence rates (Fig. 3.9.5a). Inhibition of VGlut2 terminals in gRSC significantly reduced the occurrence of gRSC ripples (Fig. 3.9.5b), despite a moderate increase in CA1 SPW-R incidence, possibly caused by the bias introduced by the closed-loop protocol (Fig. 3.9.5c). Firing rates of individual gRSC units were also affected by inhibition of VGlut2$^+$ terminals with the majority of modulated units (54/123, 44%) decreasing their activity and a small fraction of neurons positively modulated (12/123, 10%; possibly by disinhibition), suggesting complex microcircuit effects (Fig. 3.9.6a). To test whether the coupling of gRSC units to SPW-Rs was affected by the Arch-induced suppression, we computed the standardized cross-covariance between CA1 and gRSC unit pairs (n = 391) obtained from a ± 250 ms window around all SPW-R events occurring either within or outside of the stimulation. Average cross-covariance showed a significant reduction during stimulation,

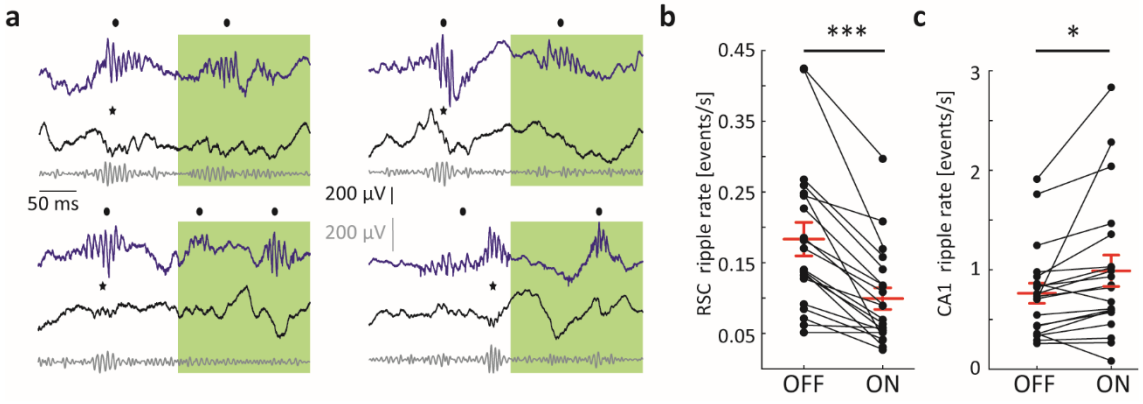

Figure 3.9.5. Inhibition of subicular VGlu2$^+$ fibers reduces the incidence of gRSC ripples. a) Example traces from a hippocampal channel (top, blue) and a superficial gRSC channel (middle, black), as well as the corresponding gRSC ripple-band filtered trace (bottom, grey) during and outside of green light illumination (shaded area) of subicular VGlut2$^+$ terminals in gRSC. Black dots, SPW-Rs detected in CA1; asterisk, ripples detected in gRSC. b) Optogenetic inhibition of subicular VGlut2$^+$ terminals decreased the rate of spontaneous gRSC ripples ($p = 0.0000885$, signed rank test; n = 20 sessions from 4 animals; 6,487 ripples during light-off and 1,068 ripples during light-on). c) CA1 SPW-R incidence is increased during stimulation of subicular VGlut2+ terminals in gRSC triggered on CA1 SPW-R detection (signed rank sum test, $p = 0.003$; n = 20 sessions from 4 animals; 28,220 ripples during light-off and 10,238 ripples during light-on).

suggesting a decrease in excitatory drive (Fig. 3.9.6b-c; p = 0.0000002, rank sum test). This finding was supported by a decreased modulation index for ripples occurring during illuminated epochs (Fig. 3.9.6d, p = 0.0001, z-statistics in shuffling analysis).

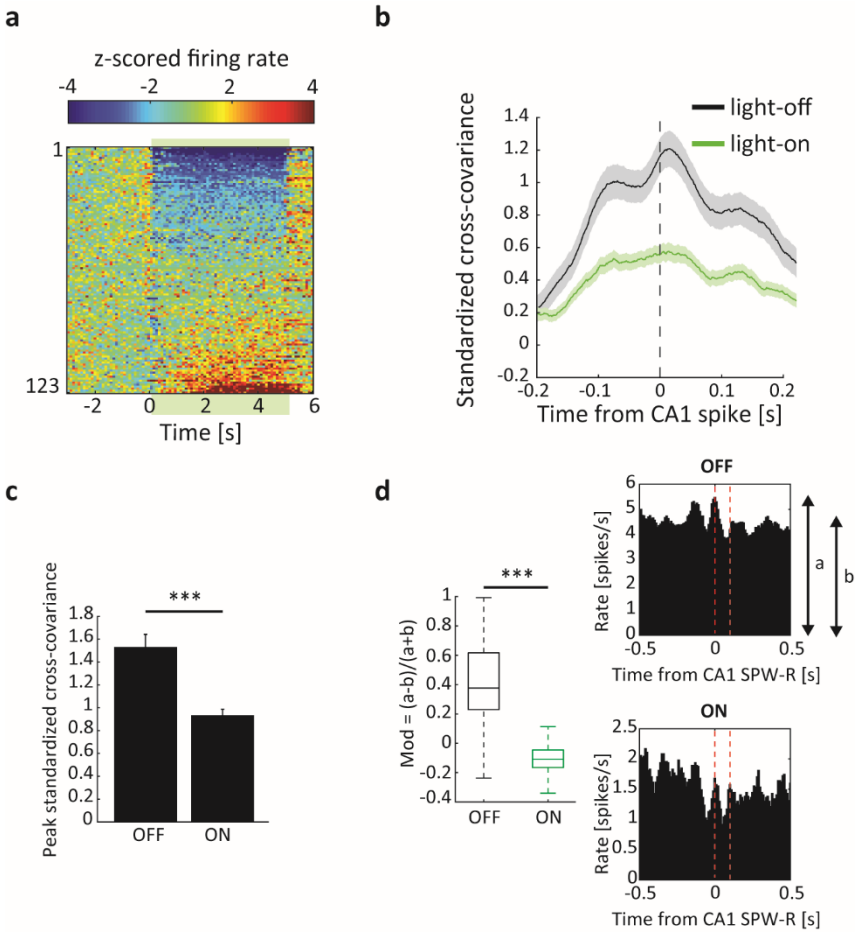

Figure 3.9.6. Inhibition of subicular VGlu2^{+} fibers reduces the coupling of gRSC units to SPW-Rs. a) Z-score normalized PETH of all recorded gRSC units. Shaded green area denotes time of stimulation. b) Standardized cross-covariance between CA1 and gRSC unit pairs (n = 391) from spikes occurring ± 250 ms around SPW-Rs either outside (black) or during (green) stimulation (n = 18 sessions from 5 animals). c) Peak standardized cross-covariance (mean ± s.e.m) between CA1 and gRSC unit pairs from spikes occurring ± 250 ms around CA1 SPW-Rs in either light-off or light-on periods (p = 0.0000002, rank sum test).d) Left: SPW-R modulation index (computed across all units which were significantly negatively modulated by Arch stimulation, n = 54), defined as the ratio between the peak of the SPW-R PETH between 0-100 ms after SPW-R onset ('a') and a baseline period between -500 and -300 ms before SPW-R onset ('b') is decreased for SPW-Rs occurring during light stimulation (p = 0.0001, z-statistics in shuffling analysis with 1000 shuffles). Right: PETH of an example unit for CA1 SPW-Rs occurring outside (top) or during (bottom) stimulation.

4 DISCUSSION

We outline a functional pathway that supports the propagation of SPW-R activity from the dorsal CA1 to the gRSC via the subiculum. This pathway is routed through a specific subpopulation of bursty VGlut2-expressing cells, which project to superficial layers of the gRSC. Single neuronal assemblies in gRSC reliably distinguished between different constellations of hippocampal unit activity during SPW-Rs. Spontaneously occurring SPW-Rs, optogenetic stimulation of pyramidal cells in the distal CA1 and subiculum, and optogenetic stimulation of VGlut2^{+} neurons in the subiculum all induced population spiking and two forms of patterns in the superficial gRSC: a negative wave and superimposed fast oscillation ('gRSC ripple'). In contrast, silencing VGlut2^{+} neurons disrupted the spread of hippocampal SPW-R activity to the gRSC. The coupling of hippocampal SPW-R and gRSC ripples was state-dependent and its occurrence was biased by ongoing cortical population patterns, associated with power increase in the 3-10 Hz band. These findings suggest that the gRSC is an important anatomical node for the dissemination of hippocampal messages to its wide neocortical partners during SPW-Rs.

4.1 Extension of the sharp-wave and ripple phenomena to the gRSC

Fast LFP oscillations typically arise in response to a strong excitatory drive in cortical networks (Buzsáki, 2015). In addition to the hippocampus, ripple oscillations have been described in the subicular complex, deep layers of the entorhinal cortex (Chrobak and Buzsáki, 1996), secondary motor cortex (Averkin et al., 2016), olfactory cortex (Manabe et al., 2011) and associational cortices (Axmacher et al., 2008; Khodagholy et al., 2017). In addition, extra-hippocampal ripples were also reported in subcortical structures, but those reports are scarcer and include the amygdala and the neighboring endopiriform nucleus (Ponomarenko et al., 2003), as well as faster oscillations in the lateral septum (Tingley and Buzsáki, 2019). Here, we expand this list of structures by reporting LFP ripple activity in superficial layers of the gRSC. A common hallmark of all cortical ripples described by the studies listed above, as well as by the present study, is their coupling to slower, large amplitude events. In the hippocampus, subicular complex and entorhinal cortex ripples are linked to a sharp wave (Chrobak and Buzsáki, 1996). Similarly, in

neocortical regions, ripples were observed locked to the trough of slow-waves (Grenier et al., 2001; Khodagholy et al., 2017) or spindle events (Averkin et al., 2016). Here, we report the coupling of gRSC ripples to large amplitude negative waves, shown as a sink by CSD analysis in the superficial layers, upon which the ripple was superimposed. This wave-ripple coupling is analogous to the SW-induced depolarization of the apical dendrites of CA1 pyramidal cells and the coupled ripple in the cell body layer. In support of this view, optogenetic excitation of cortical circuits gives rise to fast oscillations (100-200 Hz), reminiscent of the physiological SPW-Rs in the hippocampal CA1 area, even when induced in structures where ripples are not spontaneously observed such as layer V of S1 (Stark et al., 2014). Thus, it is likely that network interactions underlying ripples are brought about by transiently increased tonic drive of both excitatory cells and interneurons and their interactions in gRSC. This hypothesis is supported by the increased spiking of a large fraction of superficial gRSC neurons and interneurons in superficial layers. In summary, the sharp wave and ripple reflect two distinct but often coupled physiological events with homologous mechanisms in the hippocampus and gRSC.

4.2 Cortical ripples display a laminar profile

Similar to previous studies (Averkin et al., 2016; Khodagholy et al., 2017), we report here a strong localization of cortical ripples to superficial layers. In contrast, ripple activity in deep layers of the gRSC was less prevalent, and the engagement of deep pyramidal units in ripple events was weaker. A number of factors could contribute to the propensity of ripple activity in superficial layers. First, as our *in vivo* and *in vitro* analyses suggest, hippocampal output, which acts as one potential drive of gRSC ripples, is most strongly concentrated at superficial gRSC layers. Second, superficial gRSC pyramids strongly differ from their deep peers with respect to numerous intrinsic properties including their compact dendritic morphology, the lack of spike frequency accommodation, and importantly, their higher input resistance and lower rheobase, rendering those cells highly excitable (Table 3.7.1). Cellular intrinsic properties were previously suggested to contribute to subthreshold resonance and pacemaker properties in the gamma band (Gray and McCormick, 1996; Nuñez et al., 1992) and may play a role in the generation of ripple oscillations as well. Third, as recent work suggests (Sempere‐Ferràndez et al., 2019), superficial,

but not deep layers of the gRSC are governed by strong feed-forward inhibition, consistent with prevailing models of ripple emergence in the hippocampus (Ylinen et al., 1995). Lastly, the densely packed organization of the cell bodies in superficial gRSC layers, which highly resembles that of CA area, may contribute as well to the generation of LFP patterns (Buzsáki et al., 2012). In summary, multiple non-mutually exclusive factors favor the emergence of ripple oscillations in superficial gRSC layers. However, further work employing intracellular recordings from superficial pyramidal cells and interneurons in the gRSC as well as detailed circuit analysis is needed to determine the exact contribution of each of these factors.

4.3 Coupling between hippocampal SPW-Rs and gRSC ripples

A central question pertains to the relationship between gRSC and hippocampal ripples, with multiple alternative scenarios (illustrated in Fig. 4.3.1): (i) gRSC ripples could be directly driven by hippocampal ripples, (ii) gRSC ripples and hippocampal ripples could be triggered by a common third party or (iii) gRSC ripples could occur independently of the hippocampus.

In support of the first possibility, a substantial portion of gRSC ripples co-occurred with hippocampal SPW-Rs. Multiple lines of evidence suggest that the strong excitatory hippocampal outflow during SPW-R events is the source of excitation needed for gRSC ripples. First, gRSC ripples tended to follow CA1 SPW-R onset establishing temporal causality. Second, optogenetic induction of iHFO in the hippocampus often induced gRSC ripples. Third, the pattern of activity during hippocampal SPW-Rs could be differentiated by gRSC neurons. If the hippocampus is indeed the driving force behind gRSC ripples, then the question arises whether hippocampal SPW-Rs simply provide the necessary levels of tonic excitation necessary to induce local gRSC rippling or whether phasic hippocampal inputs during SPW-Rs entrain the phase of the oscillation downstream. Our data support a combination of both scenarios: we found a moderate phase coherence between hippocampal SPW-Rs and gRSC ripples and phase locking of multiple superficial pyramidal cells and interneurons to the remote CA1 ripples. However, phase locking of gRSC neurons to CA1 SPW-Rs was weaker compared to local ripples or the ripple phase-locked firing of CA1 neurons, possibly due to random variations added multisynaptically. It is therefore plausible that the majority of hippocampal ripples merely provide the gRSC with the sufficient

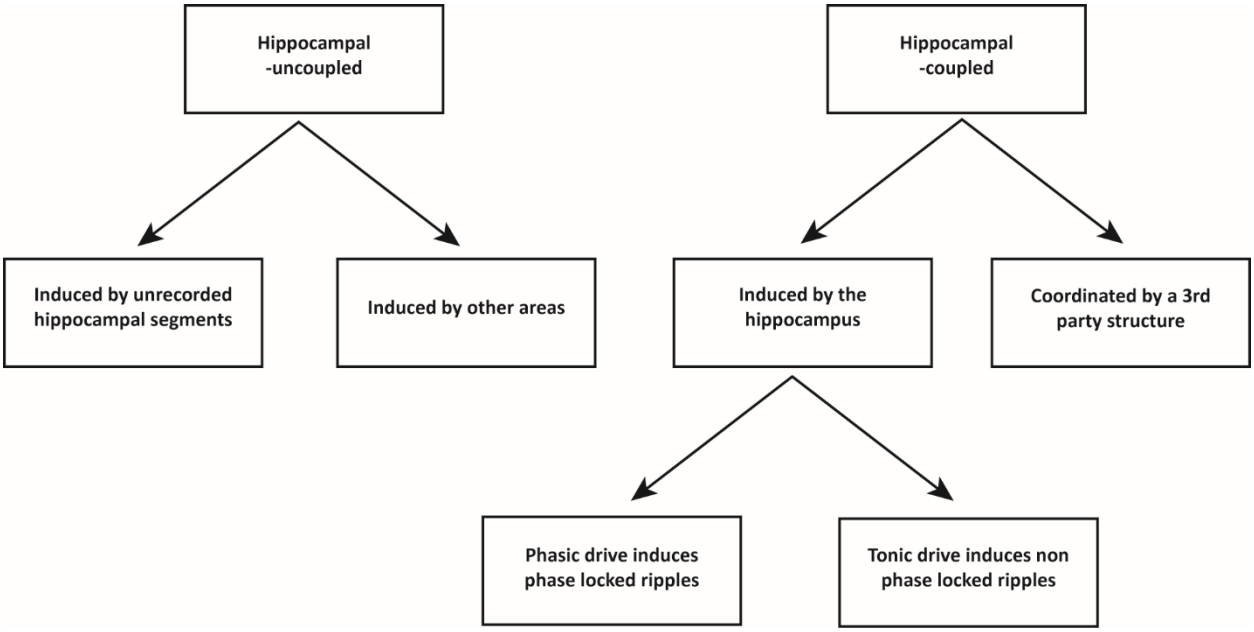

Figure 4.3.1. Schematic depiction of multiple possibilities that could explain the observed hippocampal-gRSC ripple coupling. Top: gRSC ripple oscillations were observed both in the presence and absence of hippocampal ripples. Middle: Hippocampal-coupled gRSC ripple could be induced either directly by the hippocampus or together with the hippocampus by a common upstream structure. Hippocampal-uncoupled gRSC ripples could be induced either by unrecorded hippocampal segments or by other areas. Bottom: gRSC ripples that are directly induced by the hippocampus could be phase coherent or non-coherent with hippocampal ripples.

excitatory drive needed to engage itself with local ripple activity while occasional strongly synchronized hippocampal SPW-R activity can actively propagate to the gRSC and bias the phase of local gRSC ripple oscillations.

Another alternative is that the timing of hippocampal and gRSC ripples is biased by the activity of yet another cortical or subcortical unrecorded structure. In support of this possibility, ripples in parietal cortex were strongly modulated by slow oscillations (Khodagholy et al., 2017), which are capable of temporally biasing the timing of hippocampal SPW-Rs within a window of 30 - 200 ms (Battaglia et al., 2004; Isomura et al., 2006; Mölle et al., 2006; Sirota et al., 2003), suggesting that both cortical and hippocampal ripples may be coordinated by cortical slow oscillations. Similarly, our findings here suggest that hippocampal SPW-Rs are coupled to ~6 Hz cortical activity packets, which in turn modulate local gRSC ripples.

Finally, a fraction of gRSC ripples were not associated with an increased hippocampal ripple-band power (Fig. 3.2.2e). These hippocampus-independent ripples were also associated with a negative wave in superficial layers. We cannot exclude that some of these events reflected

localized undetected SPW-R output from sites more posterior to our recording sites in dorsal CA1 and subiculum (Patel et al., 2013). Yet, the observation that gRSC ripples were often time-locked to 6-10 Hz oscillatory or intermittent events suggests that neocortical or thalamic excitatory inputs may drive local gRSC ripple independently of the hippocampus. In support of this idea, the anterior thalamus is known to provide dense axonal projections to superficial layers of the gRSC (Vélez-Fort et al., 2018), suggesting that a similarly concentrated drive may be provided by other areas as well.

In conclusion, we hypothesize that gRSC ripples emerge as long as superficial neurons experience sufficient level of excitatory drive, independent of the source of excitation. In light of this view, the reduction in gRSC ripple rate observed during optogenetic inhibition may, in addition to the suppression of SPW-R-associated inputs, be caused by reduced subicular inputs outside of SPW-Rs, which may lead to reduced excitability of superficial gRSC neurons and thereby a reduced likelihood of gRSC ripples, irrespective of the source of the afferent drive.

4.4 Diversity of hippocampal SPW-Rs

We found that hippocampal SPW-Rs could be classified into different clusters, and that individual neurons, both in the hippocampus and in the gRSC are preferentially activated by a subset of these clusters. Our t-SNE analysis and the observation that different SPW-R clusters occupy distinct subspaces of the dimensionality-reduced representations (Fig. 3.4.3), suggest that SPW-Rs patterns are not continuous but there exist discrete types of SPW-Rs that are correlated across regions. This observation is consistent with previous studies which have identified different SPW-R subtypes using different approaches than the one taken here: By analyzing the temporal alignment of the ripple and SW LFP signatures, Ramirez-Villegas and colleagues (2015) classified SPW-Rs into 4 discrete groups where the ripple peak either follows, precedes or occurs at the peak of the SW, or it lacks any clear SW component altogether. Importantly, spike-field coherence between hippocampal unit activity and LFP activity at different frequency bands revealed strong differences between different SPW-R clusters, suggesting different degrees of population synchrony. Moreover, distinct SPW-R subtypes elicited different blood oxygen level dependent (BOLD) signal responses in neocortical and subcortical regions, associated with up- or

down-regulation of metabolic activity (Ramirez-Villegas et al., 2015), suggesting that different SPW-R subtypes may convey different information. A similar approach was taken by another recent study, where SPW-R events were grouped into 18 classes according to their topological similarity in dimensionality-reduced space using a self-organizing maps algorithm (Valero et al., 2017). The authors reported that individual hippocampal units selectively participate in SPW-Rs of only few subtypes and found that this selectivity is impaired in epileptic rats. By classifying SPW-Rs based on the firing rate vectors of hippocampal units, instead of the LFP, our findings add further support to the heterogeneity of hippocampal SPW-Rs and the existence of discrete SPW-R subtypes. Furthermore, we demonstrate that this heterogeneity is extended to SPW-R responses downstream, suggesting that cortical neurons are differentially tuned to different hippocampal messages conveyed during SPW-Rs.

4.5 Strength of excitatory responses to hippocampal SPW-Rs changes as a function of synaptic path length

We found that SPW-R responses were stronger among superficial pyramidal cells compared to their deep pyramidal peers but weaker when compared to local gRSC interneurons. In contrast, SPW-R responses of CA1 and subiculum pyramids exceeded those of local hippocampal interneurons (Fig. 3.2.5). Thus, there exists a trend of a decreasing gain in SPW-R associated responses of pyramidal cells, as a function of synaptic distance from the hippocampus, paralleled by an increase in the responses of interneurons. Interestingly, a similar trend was reported along the CA1 - subiculum - medial EC axis, where SPW-R responses of excitatory cells decrease from deep layers (receiving direct hippocampal output) to superficial layers, whereas interneurons show the opposite trend (Chrobak and Buzsáki, 1994; Mizuseki et al., 2009). This effect was hypothesized to serve as a 'dampening' mechanism to prevent the reverberation of processed information from re-entering the hippocampal loop (Buzsáki, 2015). Consistent with this idea, direct back-projections from the gRSC to the subiculum exist and arise from deep layer pyramidal cells (Roy et al., 2017), where SPW-R evoked responses are relatively moderate. Nevertheless, it is not clear what impact gRSC activity might have on hippocampal SPW-Rs, as in contrast to inputs from the medial EC which enter the hippocampus via the perforant path and reach the CA3 area

in canonical projections, gRSC projections are sparse and target only the subiculum. Therefore, they may exert their influence either locally in the subiculum or spread to CA1 area via non-canonical pathways (Xu et al., 2016). Future studies manipulating cortical, rather than hippocampal activity, will be insightful in this regard.

4.6 Bursting pyramidal neurons in dorsal subiculum convey hippocampal SPW-R messages to gRSC

We demonstrate that individual cortical cells are tuned to specific combinations of hippocampal activity, and show that the majority of the SPW-R related hippocampal signals reaching the gRSC emerge from bursty cells in dorsal subiculum. While the exact content of the information conveyed by these neurons remains unknown, given the strong gradients in the degree of spatial activity and of VGlut2 expression along the proximal – distal axis of the dorsal subiculum (Cembrowski et al., 2018b; Kim et al., 2012) it is likely that the pathway reported here carries substantial spatial information from CA1. Consistently, a recent study has reported that a large portion of excitatory gRSC cells carries highly tuned spatial information (Mao et al., 2017). More recently it was further demonstrated that bilateral lesions to the hippocampus can impair this spatial activity (Mao et al., 2018), pinpointing it as the source of spatial information to the gRSC. Importantly, these studies found that the majority of gRSC place cells are located in superficial layers, which receive direct subicular inputs, as our data suggest. Thus, the fast and reliable transmission needed for accurate navigation in the environment could me mediated by the high fidelity of burst firing (Kepecs and Lisman, 2003; Lisman, 1997) which is likely to result from the supra-linear summation of burst-induced EPSPs downstream (Thomson, 2000). Importantly, burst firing could also account for the relatively high phase coherence observed between hippocampal and gRSC ripples. Moreover, due to their prolonged depolarizing effect downstream bursting subicular cells may efficiently activate NMDA receptors in the postsynaptic gRSC targets thereby boosting synaptic plasticity and stabilizing the spatial map downstream.

Intriguingly, a recent study employing high-resolution juxtacellular recordings from freely behaving rats *in vivo* found that subicular principal cells could be better classified as sparsely and dominantly bursting cells, based on their tendency to emit complex spike bursts (Simonnet and

Brecht, 2019). Notably, sparsely bursting cells carried higher spatial information as compared to dominantly bursting cells, which were less spatially tuned. However, in support of the higher fidelity of bursts as units of transmission, when isolated spikes and bursts were analyzed separately, burst firing provided sharper spatial tuning, resulting in more finely tuned rate maps. These findings raise the possibility that the bursty subicular neurons represent a heterogeneous population which can be further subdivided based on the extent of burstiness. This view is supported by the observation that, following the initial burst discharge, bursting cells emit isolated spikes to different degrees *in vitro* (cf. Fig. 3.6.1e and 3.7.5c). Alternatively, these findings may imply that burst firing in the intact brain is dynamic and may change depending on variations in inputs (Harris et al., 2001) or metabotropic receptor activation and neuromodulatory tone (Moore et al., 2009). In support of the latter view, CA1 pyramidal cells fire single spikes *in vitro* but can occasionally discharge bursts of action potential *in vivo* (Bittner et al., 2015; Harris et al., 2001). This could explain why Simonnet and Brecht (2019) were not able to reproduce previously established differences in burstiness along the proximo-distal axis of the subiculum seen *in vitro* (Cembrowski et al., 2018a; Greene and Totterdell, 1997; Kim and Spruston, 2012). Thus, complex dendritic mechanisms contributing to burst generation which are not present in the slice preparation are likely to exert strong effects *in vivo* (Larkum, 2013; Traub et al., 1994). In light of this illustrated difficulty in determining the unique characteristics which delineate the bursting cells subpopulation, our present data offer a useful feature for their identification based on physiological activity patterns, namely their recruitment by SPW-Rs (Fig. 3.8.2).

Finally, we present evidence that stimulation of VGlut2$^+$ subicular bursting cells is sufficient to phase-reset activity packets in the gRSC (Fig. 3.9.4), thereby influencing awake cortical population activity. These data implicate the subicular VGlut2$^+$ bursting cells as a boosting mechanism in hippocampal – cortical communication by means of maintaining cross-structural synchrony.

4.7 Potential role of other subicular cells in the context of SPW-Rs

In contrast to the strong subicular inputs from VGlut2$^+$ cells, inputs to the gRSC from VGlut2-immunonegative cells were weaker, targeted mostly L1 and deeper cortical layers and recruited

mostly inhibitory responses (Fig. 3.7.6). While these non-VGlut2$^+$ projections were only marginally addressed by this study, it is important to discuss their potential role in the propagation of ripple activity from the hippocampus to the gRSC. Subicular VGlut2-immunonegative fibers could arise from either VGlut1$^+$ pyramidal cells in the subiculum or from long-range interneurons in subiculum and CA1, which are known to project to the gRSC (Jinno et al., 2007; Miyashita and Rockland, 2007; Yamawaki et al., 2019b). The long-range GABAergic projections could explain the inhibitory responses following the activation of non-VGlut2$^+$ subicular fibers. However, caution is in order since, unlike in the case of Cre-switch experiments, neither TTX nor 4-AP were applied to test whether these inhibitory responses are conveyed monosynaptically, or whether they recruit local inhibition. Nevertheless, long-range interneurons are a potent powerful mechanism to efficiently mediate phase coupling between anatomically remote neuronal ensembles (Caputi et al., 2013), and could have contributed to the observed phase coherence between CA1 and gRSC ripples and the observed phase locking of superficial gRSC neurons to the remote CA1 ripples. However, the reported paucity of these long-range interneurons (Jinno et al., 2007; Miyashita and Rockland, 2007) is in contradiction to the moderate arborization of VGlut2-immunonegative fibers in layer I and V (Fig. 3.7.6a) and their actual contribution to cortical ripple rhythmogenesis remains to be further tested.

The fact that in our Cre-off experiments we observed excitatory responses in a subset of gRSC cells suggests that there must exist some glutamatergic non-VGlut2 projections into the gRSC as well. A previous study investigating the distribution of VGlut1 and VGlut2 in the forebrain reported the mutually exclusive expression pattern of those proteins in deep and superficial layers of the gRSC, respectively (Varoqui et al., 2002). Moreover, according to publicly available data from the Allen Brain Atlas repository (Experiment 286317619), VGlut1$^+$ projections to the gRSC are extremely sparse. It is noteworthy that, unlike VGlut2, VGlut1 does not show expression gradients in the subiculum (Allen Brain Atlas repository Experiment 704436317) and its presence in the distal subiculum suggests that it might be expressed in bursting pyramidal cells as well. It was previously reported that the majority of subicular cells projecting to the gRSC are of the bursting subtype. However, a small minority (<20%) of the projections stemmed from regularly firing cells (putatively VGlut2-immunonegative) in intermediate subiculum (Kim and Spruston,

2012). Since the firing probability of regularly firing subicular cells is strongly reduced during SPW-Rs (Böhm et al., 2015), inputs from these cells are unlikely to shape the SPW-R associated responses of gRSC neurons. However, their potential contribution during other brain states remains to be tested.

4.8 Embedding of hippocampal SPW-Rs in cortical rhythms

The brain-state dependence of hippocampal SPW-Rs has been well studied during sleep, where their occurrence was shown to be strongly confined to SWS (Buzsáki, 2015; Buzsáki et al., 1992). Correspondingly, the strength of hippocampal – cortical communication, reflecting the efficacy of information transfer between these structures is known to be enhanced during SWS as compared to REM sleep, an observation that is likely attributed to the selective occurrence of SPW-Rs during SWS (Wierzynski et al., 2009). In contrast, how hippocampal - cortical communication varies with brain-state changes in the awake resting state has been less clear. Our present data support previous considerations regarding the existence of three distinct cortical brain states in the awake state (Kay and Frank, 2019; McGinley et al., 2015b): a locomotive state characterized by a desynchronized LFP and high EMG activity, an immobile state with desynchronized LFP (previously identified by microdilations in pupil diameter; McGinley et al., 2015a) and a highly synchronized state

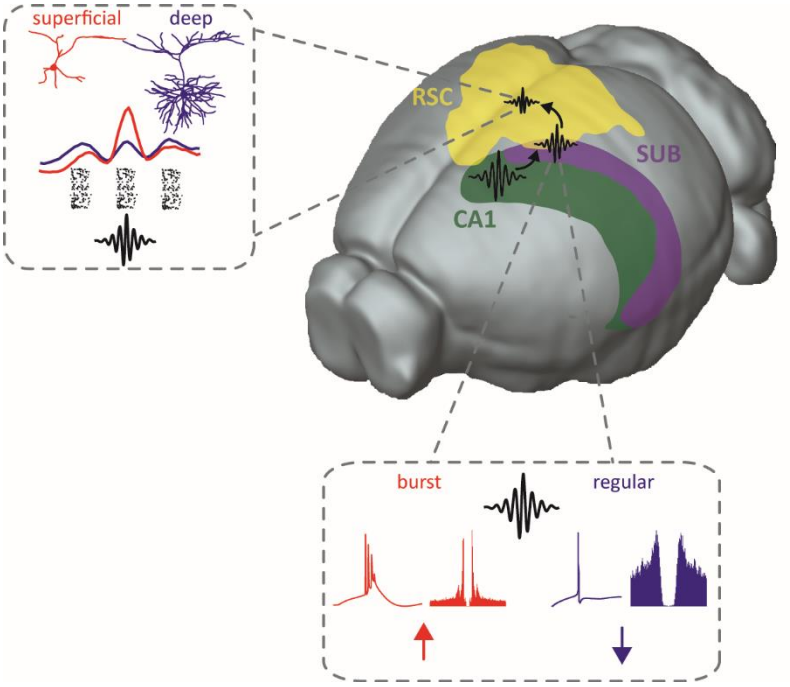

Figure 4.8.1. Illustration of the signal outflow from CA1 to gRSC. Ripples propagate from CA1 (green) via the subiculum (SUB, purple) to the gRSC (yellow). This is mediated by bursting subicular cells which are selectively activated during SPW-Rs (bottom box). Hippocampal SPW-Rs are coupled to cortical activity packets, which modulate cortical activity across both superficial and deep layers at around 6 Hz (top left). However, only the activity of superficial pyramidal cells is additionally modulated by hippocampal SPW-Rs.

characterized by large LFP fluctuations and strongly coordinated population bursts ('activity packets'). Importantly, our data present evidence that the occurrence of hippocampal SPW-Rs is strongly biased by the synchronized state, and that the efficacy of hippocampal – cortical communication is maximal during this state (Fig. 3.5.2).

Responses of gRSC neurons to SPW-Rs were multiphasic and exhibited a short latency peak surrounded by a pre-SPW-R and a delayed peak ~150 ms before and after SPW-R onset, respectively, suggesting that SPW-Rs are embedded within more complex cortical dynamics oscillating at around 6 Hz (Fig. 4.8.1). This cortical rhythm was associated with both increased gamma and multi-unit activity, primarily in deep layers (Fig. 3.5.1) (Alexander et al., 2018). A previous study found a correlation between low frequency (~30Hz) cortical gamma power and hippocampal SPW-Rs (Remondes and Wilson, 2015). Since the onset of an UP-state is associated with high gamma power (Watson et al., 2016), the known synchronization between hippocampal SPW-Rs and UP-states/cortical packets (Battaglia et al., 2004; Isomura et al., 2006; Sirota et al., 2003) may contribute to the coupling of hippocampal SPW-Rs and cortical gamma power.

While numerous studies have reported the coupling of hippocampal SPW-Rs to cortical rhythms such as slow-waves or spindles (Battaglia et al., 2004; Mölle et al., 2006; Peyrache et al., 2011; Siapas and Wilson, 1998; Sirota et al., 2003; Wierzynski et al., 2009), the precise contribution of hippocampal output has been difficult to disentangle in the absence of known monosynaptic connections in anatomically or molecularly defined cortical subpopulations. As a result, cortical activity that is temporally correlated with hippocampal SPW-Rs is often interpreted as being directly driven by the hippocampus, thereby neglecting the contribution of locally generated cortical currents (Fig. 4.8.1). Here, we report that deep gRSC pyramids show weak phase locking to hippocampal ripples and a lack of prominent short latency excitatory responses to subicular drive both *in vitro* (Fig. 3.7.3) and subicular or CA1 drive *in vivo* (Fig.3.2.5, Fig. 3.9.3), suggesting that these cells are more likely recruited by cortical packets rather than by the SPW-R themselves. In contrast, the additional SPW-R-locked activity seen mainly in superficial layers is suggestive of direct ripple associated currents. Consistent with this view, superficial gRSC pyramidal cells receive monosynaptic inputs from the subiculum and show rate and phase locking to CA1 SPW-Rs (Fig. 3.2.6). These findings suggest that while the hippocampal and cortical

networks are globally coupled, only certain populations of cortical neurons are tuned to hippocampal inputs, while others are engaged in other cortical dynamics.

Lastly, the observation that subicular stimulation interrupted cortical packet dynamics suggests that, similar to UP and DOWN states of SWS (or perhaps as an awake variant thereof), activity packets represent a metastable regime, and that any perturbations to it will result in a state transition as long as they are sufficiently strong (Gelinas et al., 2016; Levenstein et al., 2019; Maingret et al., 2016; Massimini et al., 2006).

4.9 Pathology of hippocampal-cortical communication

Understanding the hippocampal-cortical dialogue in the intact, healthy brain will likely contribute for understanding memory consolidation deficits associated with a wide range of diseases affecting memory. In one recent example, the accumulation of β-amyloid in medial prefrontal cortex was shown to strongly correlate with impairments in cortical slow-wave activity and with reduced hippocampal activation during memory retention, suggesting an impoverished hippocampal-cortical memory transformation (Mander et al., 2015). Similarly, the coordination between cortical slow waves with cortical spindles and hippocampal SPW-Rs was shown to be disrupted in an animal model of schizophrenia, which is associated with deficits in memory processing (Phillips et al., 2012). Perhaps even more relevant for the present study, in a recent study, a pathological form of hippocampal-cortical communication was shown to be manifested in epilepsy, where interictal epileptiform discharges suppressed ripple-spindle coupling and induced a cortical downstate (Gelinas et al., 2016). Here, we demonstrate that stimulation of bursting cells can result in a similar effect namely the temporary suppression of cortical activity reminiscent of a DOWN state (Fig. 3.9.4). Interestingly, the subiculum has been strongly implicated in temporal lobe epileptogenesis, where the ratio of subicular bursting to non-bursting cells was shown to be altered (Wellmer et al., 2002). In future experiments, it would be interesting to test the role of subicular bursting cells on hippocampal-cortical interactions in animal models of epilepsy.

4.10 Limitation of the current study

Despite the various insights offered by the current study a number of caveats and possible limitations shall be discussed in the following. First, for technical reasons, we chose to investigate the SPW-R phenomenon only under head-fixed, immobile conditions. In spite of the many advantages offered by these experimental settings, and the fact that SPW-Rs are readily observed under these conditions (Böhm et al., 2015), this is a non-ecological paradigm that is likely to affect brain-state changes. The prominence of synchronized activity and activity packets, which are highly reminiscent of UP and DOWN states observed during SWS, suggest that mice were in a drowsy state. Indeed, while there is abundant evidence for packet-like activity in head-fixed animals (Crochet and Petersen, 2006; Luczak et al., 2006, 2009, 2013; Petersen et al., 2003), these patterns have not been described in awake immobile freely behaving animals. We cannot exclude the possibility that, following long habituation, head-fixed mice occasionally display SWS as shown by a previous study (Seibt et al., 2017). However, in the absence of behavioral measures such as pupil dilation no exact distinction could be made here between quite awake, SWS or intermittent brain states. This limitation might explain a discrepancy with a recent study (Wang and Ikemoto, 2016) which reported strong SPW-R responses of cells in the anterior cingulate cortex, a structure neighboring the gRSC, in naturally sleeping animals, but not during awake SPW-Rs.

Another limitation pertains the interpretation of our optogenetic inhibition experiments. While still a widely used tool for light-controlled inhibition of axon terminals, it is important to acknowledge that synaptic silencing mediated by Arch seems to rely on its proton pumping activity and the subsequent extracellular acidification (El-gaby et al., 2016). If this is indeed the case, activation of this opsin is expected to result in unspecific effects. Moreover, sustained activation of Arch causes elevation of presynaptic Ca^{2+} levels which can result in the paradoxical increase of spontaneous neurotransmitter release (Mahn et al., 2016). Those constraints may explain why some neurons increased their firing rates during the illumination period (Fig. 3.9.6a) and shed doubts on whether the observed effect was exclusively mediated by the silencing of $VGlut2^{+}$ subicular fibers.

Finally, despite the clear evidence presented here regarding the existence of multiple SPW-R clusters and their correlates in the gRSC, we could not draw conclusions about their functional relevance in the absence of an appropriate behavioral readout. It is tempting to speculate that discrete SPW-R clusters convey different information about recent experiences (e.g. in the form of place cell activity), which engage unique gRSC ensembles, reflecting memory consolidation. Yet, testing this prediction will require the extraction of behavioral variables such as place cell sequences, which was not feasible in the present study.

4.11 Conclusions

Our findings demonstrate that, in addition to the hippocampal-entorhinal and hippocampal-prefrontal routes, the hippocampal-subicular-gRSC path is an alternative channel to broadcast hippocampal content to the neocortex. In addition, our findings suggest that the mechanisms of SPW-Rs in the hippocampus apply to the retrosplenial cortex as well: a synchronous, anatomically concentrated excitatory drive (reflected in a sharp wave) enables a state change and triggers high-frequency oscillations, supported by fast spiking GABAergic interneurons. It remains to be clarified how ripple-associated information routed to the gRSC differs in its content from spike information sent to other areas, and how the transformed spike pattern at each synapse contributes to memory. By elucidating a specific anatomical pathway linking hippocampal SPW-Rs to gRSC activity, involving a genetically defined subpopulation of bursting cells in the subiculum, we provide concrete targets for future studies addressing these questions.

4.12 Outlook

Although SPW-Rs were long assumed to reflect a phenomenon which is unique to the hippocampal network, accumulating evidence, including the present work, suggests that other cortical networks are also capable of spontaneous ripple generation (Averkin et al., 2016; Khodagholy et al., 2017). However, unlike the affluent evidence that unequivocally supports the role of hippocampal SPW-Rs in memory processing (Girardeau et al., 2009; Jadhav et al., 2012; Roux et al., 2017), the behavioral correlates of cortical ripples remain unknown. It is possible that, similar to hippocampal SPW-Rs, cortical ripples support the emergence of neuronal sequences,

which could give rise to cortical replay. However, while replay of awake sequences has been previously reported in a variety of cortical areas (Jadhav et al., 2016; Ji and Wilson, 2007; O'Neill et al., 2017; Ólafsdóttir et al., 2016; Rothschild et al., 2017), no study to date has linked cortical replay to high frequency LFP oscillations. Investigating this issue will require pairing high-density cortical recordings with a memory-dependent behavioral paradigm. Moreover, it is not clear whether the coupling seen between hippocampal and cortical ripples is of physiological and behavioral relevance or whether it reflects an epiphenomenal effect. A recent study has shown that the coupling of ripples in the hippocampus and posterior parietal cortex increased during sleep following the learning of a spatial task (Khodagholy et al., 2017). However, as cortical ripples were also shown to be strongly coupled to slow waves, which are themselves up-modulated following learning (Huber et al., 2004), this increased coupling may reflect an indirect effect. To convincingly demonstrate that the coupling between hippocampal and cortical ripples in itself contributes to memory processing, it would be necessary to design intervention experiments with a learning component, where the activity of one, but not the other, structure is manipulated.

Finally, we demonstrate here that superficial gRSC pyramidal neurons are strongly tuned to hippocampal signals. However, the contribution of these cells to cognitive functions remains elusive. This is partly because their downstream targets are largely unknown, rendering it difficult to assess their contribution to signal flow in the brain. Nevertheless, one could try to understand the function of these cells based on the inputs they receive, their intrinsic properties and their physiological correlates. Another prominent source of inputs to the superficial gRSC is the anterior thalamus, a major source of head-direction signals. A previous study has demonstrated that thalamic axons converge onto superficial layers of the gRSC in a remarkably similar pattern to that of subicular inputs described here (Vélez-Fort et al., 2018). In this context, the late spiking property of superficial gRSC cells, which is attributed to the expression of delayed rectifier potassium channels (Kurotani et al., 2013) was hypothesized to serve as an integrative mechanism where different inputs are compared during the delay period. According to this view, superficial pyramidal cells in the gRSC may serve as a coincidence detector that integrates spatial

inputs from the subiculum and head-direction inputs from the thalamus and produces an output only when these inputs are temporally coherent.

5 BIBLIOGRAPHY

Acharya, L., Aghajan, Z.M., Vuong, C., Moore, J.J., and Mehta, M.R. (2016). Causal Influence of Visual Cues on Hippocampal Directional Selectivity. Cell *164*, 197–207.

Aggleton, J.P., and Brown, M.W. (1999). Episodic memory, amnesia, and the hippocampal-anterior thalamic axis. Behav. Brain Sci. *22*, 425–444.

Aggleton, J.P., and Christiansen, K. (2015). The subiculum: The heart of the extended hippocampal system. In Progress in Brain Research, (Elsevier B.V.), pp. 65–82.

Alexander, A.S., and Nitz, D.A. (2015). Retrosplenial cortex maps the conjunction of internal and external spaces. Nat. Neurosci. *18*, 1143–1151.

Alexander, A.S., Rangel, L.M., Tingley, D., and Nitz, D.A. (2018). Neurophysiological signatures of temporal coordination between retrosplenial cortex and the hippocampal formation. Behav. Neurosci. *132*, 453–468.

Alvarez, P., and Squire, L.R. (1994). Memory consolidation and the medial temporal lobe: a simple network model. Proc. Natl. Acad. Sci. *91*, 7041–7045.

Antony, J.W., Schönauer, M., Staresina, B.P., and Cairney, S.A. (2019). Sleep Spindles and Memory Reprocessing. Trends Neurosci. *42*, 1–3.

Averkin, R.G., Szemenyei, V., Bordé, S., and Tamás, G. (2016). Identified Cellular Correlates of Neocortical Ripple and High-Gamma Oscillations during Spindles of Natural Sleep. Neuron *92*, 916–928.

Axmacher, N., Elger, C.E., and Fell, J. (2008). Ripples in the medial temporal lobe are relevant for human memory consolidation. Brain *131*, 1806–1817.

Battaglia, F.P., Sutherland, G.R., and McNaughton, B.L. (2004). Hippocampal sharp wave bursts coincide with neocortical “up-state ” transitions. Learn. Mem. *11*, 697–704.

Behr, J., Wozny, C., Fidzinski, P., and Schmitz, D. (2009). Synaptic plasticity in the subiculum. Prog. Neurobiol. *89*, 334–342.

Belluscio, M.A., Mizuseki, K., Schmidt, R., Kempter, R., and Buzsáki, G. (2012). Cross-frequency phase-phase coupling between theta and gamma oscillations in the hippocampus. J. Neurosci. *32*, 423–435.

Bir, S.C., Ambekar, S., Kukreja, S., and Nanda, A. (2015). Julius Caesar Arantius (Giulio Cesare Aranzi, 1530-1589) and the hippocampus of the human brain: History behind the discovery. J. Neurosurg. *122*, 971–975.

Bittner, K.C., Grienberger, C., Vaidya, S.P., Milstein, A.D., Macklin, J.J., Suh, J., Tonegawa, S., and Magee, J.C. (2015). Conjunctive input processing drives feature selectivity in hippocampal CA1 neurons. Nat. Neurosci. *18*, 1133–1142.

Boccara, C.N., Sargolini, F., Thoresen, V.H., Solstad, T., Witter, M.P., Moser, E.I., and Moser, M.-B. (2010). Grid cells in pre- and parasubiculum. Nat. Neurosci. *13*, 987–994.

Böhm, C., Peng, Y., Maier, N., Winterer, J., Poulet, J.F., Geiger, J.R.P., and Schmitz, D. (2015). Functional Diversity of Subicular Principal Cells during Hippocampal Ripples. J. Neurosci. *35*, 13608–13618.

Bokil, H., Andrews, P., Kulkarni, J.E., Mehta, S., and Mitra, P.P. (2010). Chronux: A platform for analyzing neural signals. J. Neurosci. Methods *192*, 146–151.

Brandon, M.P., Koenig, J., Leutgeb, J.K., and Leutgeb, S. (2014). New and Distinct Hippocampal Place Codes Are Generated in a New Environment during Septal Inactivation. Neuron *82*, 789–796.

Brunel, N., and Wang, X.J. (2003). What determines the frequency of fast network oscillations with irregular neural discharges? I. Synaptic dynamics and excitation-inhibition balance. J. Neurophysiol. *90*, 415–430.

Buzsáki, G. (1989). Two-stage model of memory trace formation: a role for “noisy” brain states. Neuroscience *31*, 551–570.

Buzsáki, G. (1996). The Hippocampo-Neocortical Dialogue. Cereb. Cortex *6*, 81–92.

Buzsáki, G. (2002). Theta Oscillations in the Hippocampus. Neuron *33*, 325–340.

Buzsáki, G. (2006). Rhythms of the Brain (Oxford University Press).

Buzsáki, G. (2010). Neural Syntax: Cell Assemblies, Synapsembles, and Readers. Neuron *68*, 362–385.

Buzsáki, G. (2015). Hippocampal sharp wave-ripple: A cognitive biomarker for episodic memory and planning. Hippocampus *25*, 1073–1188.

Buzsáki, G., and Moser, E.I. (2013). Memory, navigation and theta rhythm in the hippocampal-entorhinal system. Nat. Neurosci. *16*, 130–138.

Buzsáki, G., and Tingley, D. (2018). Space and Time: The Hippocampus as a Sequence Generator. Trends Cogn. Sci. *22*, 853–869.

Buzsáki, G., and Wang, X.-J. (2012). Mechanisms of Gamma Oscillations. Annu. Rev. Neurosci. *35*, 203–225.

Buzsáki, G., Wise, K., Hetke, J., Horvath, Z., and Urioste, R. (1992). High-frequency network oscillation in the hippocampus. Science (80-.). *256*, 1025–1027.

Buzsáki, G., Anastassiou, C.A., and Koch, C. (2012). The origin of extracellular fields and currents — EEG , ECoG , LFP and spikes. Nat. Rev. Neurosci. *13*, 407–420.

Caputi, A., Melzer, S., Michael, M., and Monyer, H. (2013). The long and short of GABAergic neurons. Curr. Opin. Neurobiol. *23*, 179–186.

Cembrowski, M.S., and Spruston, N. (2019). Heterogeneity within classical cell types is the rule: lessons from hippocampal pyramidal neurons. Nat. Rev. Neurosci. *20*, 193–204.

Cembrowski, M.S., Bachman, J.L., Wang, L., Sugino, K., Shields, B.C., and Spruston, N. (2016). Spatial Gene-Expression Gradients Underlie Prominent Heterogeneity of CA1 Pyramidal Neurons. Neuron *89*, 351–368.

Cembrowski, M.S., Phillips, M.G., DiLisio, S.F., Shields, B.C., Winnubst, J., Chandrashekar, J., Bas, E., and Spruston, N. (2018a). Dissociable Structural and Functional Hippocampal Outputs via Distinct Subiculum Cell Classes. Cell *173*, 1280-1292.e18.

Cembrowski, M.S., Wang, L., Lemire, A.L., Copeland, M., DiLisio, S.F., Clements, J., and Spruston, N. (2018b). The subiculum is a patchwork of discrete subregions. Elife *7*, 1–21.

Chen, L.L., Lin, L.-H., Green, E.J., Barnes, C.A., and McNaughton, B.L. (1994). Head-direction cells in the rat posterior cortex. Exp. Brain Res. *101*, 8–23.

Cho, J., and Sharp, P.E. (2001). Head direction, place, and movement correlates for cells in the rat retrosplenial cortex. Behav. Neurosci. *115*, 3–25.

Chrobak, J.J., and Buzsáki, G. (1994). Selective activation of deep layer (V-VI) retrohippocampal cortical neurons during hippocampal sharp waves in the behaving rat. J. Neurosci. *14*, 6160–6170.

Chrobak, J.J., and Buzsáki, G. (1996). High-Frequency Oscillations in the Output Networks Axis of the Freely Behaving of the Rat. J. Neurosci. *76*, 3056–3066.

Cohen, M.X. (2014). Analyzing neural time series data (MIT Press).

Colgin, L.L. (2016). Rhythms of the hippocampal network. Nat. Rev. Neurosci. *17*, 239–249.

Colgin, L.L., Denninger, T., Fyhn, M., Hafting, T., Bonnevie, T., Jensen, O., Moser, M.-B., and Moser, E.I. (2009). Frequency of gamma oscillations routes flow of information in the hippocampus. Nature *462*, 353–357.

Corkin, S. (1965). Tactually-guided maze learning in man: Effects of unilateral cortical excisions and bilateral hippocampal lesions. Neuropsychologia *3*, 339–351.

Cowansage, K.K., Shuman, T., Dillingham, B.C., Chang, A., Golshani, P., and Mayford, M. (2014). Direct Reactivation of a Coherent Neocortical Memory of Context. Neuron *84*, 432–441.

Crochet, S., and Petersen, C.C.H. (2006). Correlating whisker behavior with membrane potential in barrel cortex of awake mice. Nat. Neurosci. *9*, 608–610.

Czajkowski, R., Jayaprakash, B., Wiltgen, B., Rogerson, T., Guzman-Karlsson, M.C., Barth, A.L., Trachtenberg, J.T., and Silva, A.J. (2014). Encoding and storage of spatial information in the retrosplenial cortex. Proc. Natl. Acad. Sci. U. S. A. *111*, 8661–8666.

Danielson, N.B., Zaremba, J.D., Kaifosh, P., Bowler, J., Ladow, M., and Losonczy, A. (2016).

Sublayer-specific coding dynamics during spatial navigation and learning in hippocampal area CA1. Neuron *91*, 1–14.

Davidson, T.J., Kloosterman, F., and Wilson, M.A. (2009). Hippocampal Replay of Extended Experience. Neuron *63*, 497–507.

Diba, K., and Buzsáki, G. (2007). Forward and reverse hippocampal place-cell sequences during ripples. Nat. Neurosci. *10*, 1241–1242.

Diekelmann, S., and Born, J. (2010). The memory function of sleep. Nat. Rev. Neurosci. *11*, 114–126.

Draguhn, A., Traub, R.D., Schmitz, D., and Jefferys, J.G.R. (1998). Electrical coupling underlies high-frequency oscillations in the hippocampus in vitro. Nature *394*, 189–192.

Ego-Stengel, V., and Wilson, M.A. (2010). Disruption of ripple-associated hippocampal activity during rest impairs spatial learning in the rat. Hippocampus *20*, 1–10.

Eichenbaum, H., Dudchenko, P., Wood, E., Shapiro, M., and Tanila, H. (1999). The hippocampus, memory, and place cells: Is it spatial memory or a memory space? Neuron *23*, 209–226.

El-gaby, M., Zhang, Y., Wolf, K., Schwiening, C.J., Paulsen, O., Shipton, O.A., El-gaby, M., Zhang, Y., Wolf, K., Schwiening, C.J., et al. (2016). Archaerhodopsin Selectively and Reversibly Silences Synaptic Transmission through Altered pH Resource. Cell Rep. *16*, 2259–2268.

English, D.F., Peyrache, A., Stark, E., Roux, L., Vallentin, D., Long, M.A., and Buzsáki, G. (2014). Excitation and Inhibition Compete to Control Spiking during Hippocampal Ripples: Intracellular Study in Behaving Mice. J. Neurosci. *34*, 16509–16517.

English, D.F., McKenzie, S., Evans, T., Kim, K., Yoon, E., and Buzsáki, G. (2017). Pyramidal Cell-Interneuron Circuit Architecture and Dynamics in Hippocampal Networks. Neuron *96*, 505–520.

Fanselow, M.S., and Dong, H.W. (2010). Are the Dorsal and Ventral Hippocampus Functionally Distinct Structures? Neuron *65*, 7–19.

Fernández-Ruiz, A., Oliva, A., Maurer, A.P., Nagy, G.A., Berényi, A., and Buzsáki, G. (2017).

Entorhinal-CA3 Dual-Input Control of Spike Timing in the Hippocampus by Theta-Gamma Coupling. Neuron *93*, 1213–1226.

Frankland, P.W., and Bontempi, B. (2005). The organization of recent and remote memories. Nat. Rev. Neurosci. *6*, 119–130.

Freund, T.F., and Buzsáki, G. (1996). Interneurons of the Hippocampus. Hippocampus *6*, 347–470.

Fries, P. (2015). Rhythms for Cognition: Communication through Coherence. Neuron *88*, 220–235.

Gelinas, J.N., Khodagholy, D., Thesen, T., Devinsky, O., and Buzsáki, G. (2016). Interictal epileptiform discharges induce hippocampal-cortical coupling in temporal lobe epilepsy. Nat. Med. *22*, 641–648.

Girardeau, G., Benchenane, K., Wiener, S.I., Buzsáki, G., and Zugaro, M.B. (2009). Selective suppression of hippocampal ripples impairs spatial memory. Nat. Neurosci. *12*, 1222–1223.

Girardeau, G., Inema, I., and Buzsáki, G. (2017). Reactivations of emotional memory in the hippocampus-amygdala system during sleep. Nat. Neurosci. *20*, 1634–1642.

Góis, Z.H.T.D., and Tort, A.B.L. (2018). Characterizing Speed Cells in the Rat Hippocampus. Cell Rep. *25*, 1872-1884.e4.

Graves, A.R., Moore, S.J., Bloss, E.B., Mensh, B.D., Kath, W.L., and Spruston, N. (2012). Hippocampal Pyramidal Neurons Comprise Two Distinct Cell Types that Are Countermodulated by Metabotropic Receptors. Neuron *76*, 776–789.

Gray, C.M., and McCormick, D.A. (1996). Chattering cells: Superficial pyramidal neurons contirbuting to the generation of synchronous oscillations in the visual cortex. Science (80-.). *274*, 109–113.

Green, J.D., and Arduini, A.A. (1954). Hippocampal electrical activity in arousal. J. Neurophysiol. *17*, 533–557.

Greene, J.R.T., and Totterdell, S. (1997). Morphology and distribution of electrophysiologically defined classes of pyramidal and nonpyramidal neurons in rat ventral subiculum in vitro. J. Comp.

Neurol. *380*, 395–408.

Grenier, F., Timofeev, I., and Steriade, M. (2001). Focal Synchronization of Ripples (80 – 200 Hz) in Neocortex and Their Neuronal Correlates. J. Neurophysiol. 1884–1898.

Van Groen, T., and Wyss, J.M. (1990). Extrinsic projections from area CA1 of the rat hippocampus: Olfactory, cortical, subcortical, and bilateral hippocampal formation projections. J. Comp. Neurol. *302*, 515–528.

Van Groen, T., and Wyss, J.M. (2003). Connections of the Retrosplenial Granular b Cortex in the Rat. J. Comp. Neurol. *463*, 249–263.

Hafting, T., Fyhn, M., Molden, S., Moser, M.-B., and Moser, E.I. (2005). Microstructure of a spatial map in the entorhinal cortex. Nature *436*, 801–806.

Hanslmayr, S., Staresina, B.P., and Bowman, H. (2016). Oscillations and Episodic Memory: Addressing the Synchronization/Desynchronization Conundrum. Trends Neurosci. *39*, 16–25.

Hargreaves, E., Rao, G., Lee, I., and Knierim, J. (2005). Major Dissociation Between Medial and Lateral Entorhinal Input to Dorsal Hippocampus. Science (80-.). *308*, 1792–1794.

Harris, K.D. (2005). Neural signatures of cell assembly organization. Nat. Rev. Neurosci. *6*, 399–407.

Harris, K.D., and Thiele, A. (2011). Cortical state and attention. Nat. Rev. Neurosci. *12*, 509–523.

Harris, K.D., Hirase, H., Leinekugel, X., Henze, D.A., and Buzsáki, G. (2001). Temporal interaction between single spikes and complex spike bursts in hippocampal pyramidal cells. Neuron *32*, 141–149.

Harris, K.D., Csicsvari, J., Hirase, H., Dragoi, G., and Buzsáki, G. (2003). Organization of cell assemblies in the hippocampus. Nature *424*, 552–556.

Hasselmo, M.E. (2007). Arc length coding by interference of theta frequency oscillations may underlie context-dependent hippocampal unit data and episodic memory function. Learn. Mem. *14*, 782–794.

Hazan, L., Zugaro, M., and Buzsáki, G. (2006). Klusters, NeuroScope, NDManager: A free software suite for neurophysiological data processing and visualization. J. Neurosci. Methods *155*, 207–216.

Hebb, D.O. (1949). The organization of behavior (John Wiley & Sons, Ltd).

Holzbecher, A., and Kempter, R. (2018). Interneuronal gap junctions increase synchrony and robustness of hippocampal ripple oscillations. Eur. J. Neurosci. *48*, 3446–3465.

Honda, Y., and Ishizuka, N. (2015). Topographic distribution of cortical projection cells in the rat subiculum. Neurosci. Res. *92*, 1–20.

Huber, R., Ghilardi, M.F., Massimini, M., and Tononi, G. (2004). Local sleep and learning. Nature *430*, 78–81.

Hulse, B.K., Lubenov, E. V., and Siapas, A.G. (2017). Brain State Dependence of Hippocampal Subthreshold Activity in Awake Mice. Cell Rep. *18*, 136–147.

Isomura, Y., Sirota, A., Özen, S., Montgomery, S., Mizuseki, K., Henze, D.A., and Buzsáki, G. (2006). Integration and Segregation of Activity in Entorhinal-Hippocampal Subregions by Neocortical Slow Oscillations. Neuron *52*, 871–882.

Ito, H.T., and Schuman, E.M. (2012). Functional division of hippocampal area CA1 via modulatory gating of entorhinal cortical inputs. Hippocampus *22*, 372–387.

Jacob, P.Y., Casali, G., Spieser, L., Page, H., Overington, D., and Jeffery, K. (2017). An independent, landmark-dominated head-direction signal in dysgranular retrosplenial cortex. Nat. Neurosci. *20*, 173–175.

Jadhav, S.P., Kemere, C., German, P.W., and Frank, L.M. (2012). Awake Hippocampal Sharp-Wave Ripples Support Spatial Memory. Science (80-.). *336*, 1454–1458.

Jadhav, S.P.P., Rothschild, G., Roumis, D.K.K., and Frank, L.M.M. (2016). Coordinated Excitation and Inhibition of Prefrontal Ensembles during Awake Hippocampal Sharp-Wave Ripple Events. Neuron *90*, 113–127.

Ji, D., and Wilson, M.A. (2007). Coordinated memory replay in the visual cortex and hippocampus during sleep. Nat. Neurosci. *10*, 100–107.

Jinno, S., Klausberger, T., Marton, L.F., Dalezios, Y., Roberts, J.D.B., Fuentealba, P., Bushong, E.A., Henze, D., Buzsáki, G., and Somogyi, P. (2007). Neuronal diversity in GABAergic long-range projections from the hippocampus. J. Neurosci. *27*, 8790–8804.

Johnston, and Wu (1995). Foundations of cellular neurophysiology (MIT Press).

Joo, H.R., and Frank, L.M. (2018). The hippocampal sharp wave – ripple in memory retrieval for immediate use and consolidation. Nat. Neurosci. *19*, 744–757.

Jung, M.W., and McNaughton, B.L. (1993). Spatial selectivity of unit activity in the hippocampal granular layer. Hippocampus *3*, 165–182.

Jung, H.Y., Staff, N.P., and Spruston, N. (2001). Action potential bursting in subicular pyramidal neurons is driven by a calcium tail current. J. Neurosci. *21*, 3312–3321.

Kay, K., and Frank, L.M. (2019). Three brain states in the hippocampus and cortex. Hippocampus *29*, 184–238.

Keene, C.S., and Bucci, D.J. (2008). Neurotoxic lesions of retrosplenial cortex disrupt signaled and unsignaled contextual fear conditioning. Behav. Neurosci. *122*, 1070–1077.

Kepecs, A., and Lisman, J. (2003). Information encoding and computation with spikes and bursts. Netw. Comput. Neural Syst. *14*, 103–118.

Khodagholy, D., Gelinas, J.N., and Buzsáki, G. (2017). Learning-enhanced coupling between ripple oscillations in association cortices and hippocampus. Science (80-.). *358*, 369–372.

Kim, Y., and Spruston, N. (2012). Target-specific output patterns are predicted by the distribution of regular-spiking and bursting pyramidal neurons in the subiculum. Hippocampus *22*, 693–706.

Kim, S.M., Ganguli, S., and Frank, L.M. (2012). Spatial Information Outflow from the Hippocampal Circuit: Distributed Spatial Coding and Phase Precession in the Subiculum. J. Neurosci. *32*, 11539–11558.

Klausberger, T., Magill, P.J., Márton, L.F., Roberts, J.D.B., Cobden, P.M., Buzsáki, G., and Somogyi, P. (2003). Brain-state- and cell-type-specific firing of hippocampal interneurons in vivo. Nature *421*, 844–848.

Kohara, K., Pignatelli, M., Rivest, A.J., Jung, H.-Y., Kitamura, T., Suh, J., Frank, D., Kajikawa, K., Mise, N., Obata, Y., et al. (2014). Cell type-specific genetic and optogenetic tools reveal hippocampal CA2 circuits. Nat. Neurosci. *17*, 269–279.

Korte, M., and Schmitz, D. (2016). Cellular and System Biology of Memory: Timing, Molecules, and Beyond. Physiol. Rev. *96*, 647–693.

Kropff, E., Carmichael, J.E., Moser, M.-B., and Moser, E.I. (2015). Speed cells in the medial entorhinal cortex. Nature *523*, 419–424.

Kumaran, D., Hassabis, D., and McClelland, J.L. (2016). What Learning Systems do Intelligent Agents Need? Complementary Learning Systems Theory Updated. Trends Cogn. Sci. *20*, 512–534.

Kurotani, T., Miyashita, T., Wintzer, M., Konishi, T., Sakai, K., Ichinohe, N., and Rockland, K.S. (2013). Pyramidal neurons in the superficial layers of rat retrosplenial cortex exhibit a late-spiking firing property. Brain Struct. Funct. *218*, 239–254.

Larkum, M. (2013). A cellular mechanism for cortical associations: An organizing principle for the cerebral cortex. Trends Neurosci. *36*, 141–151.

Latchoumane, C.F. V., Ngo, H.V. V., Born, J., and Shin, H.S. (2017). Thalamic Spindles Promote Memory Formation during Sleep through Triple Phase-Locking of Cortical, Thalamic, and Hippocampal Rhythms. Neuron *95*, 424-435.e6.

Lavenex, P.B., Amaral, D.G., and Lavenex, P. (2006). Hippocampal lesion prevents spatial relational learning in adult macaque monkeys. J. Neurosci. *26*, 4546–4558.

Lee, A.K., and Wilson, M.A. (2002). Memory of Sequential Experience in the Hippocampus during Slow Wave Sleep. Neuron *36*, 1183–1194.

Levenstein, D., Buzsáki, G., and Rinzel, J. (2019). NREM sleep in the rodent neocortex and hippocampus reflects excitable dynamics. Nat. Commun. *10*, 1–12.

Lever, C., Burton, S., Jeewajee, A., O'Keefe, J., and Burgess, N. (2009). Boundary vector cells in the subiculum of the hippocampal formation. J. Neurosci. *29*, 9771–9777.

Lisman, J.E. (1997). Bursts as a unit of neural information: Making unreliable synapses reliable. Trends Neurosci. *20*, 38–43.

Logothetis, N.K., Eschenko, O., Murayama, Y., Augath, M., Steudel, T., Evrard, H.C., Besserve, M., and Oeltermann, A. (2012). Hippocampal-cortical interaction during periods of subcortical silence. Nature *491*, 547–553.

Luczak, A., Bartho, P., Harris, K.D., Marguet, S.L., and Buzsáki, G. (2006). Sequential structure of neocortical spontaneous activity in vivo. Proc. Natl. Acad. Sci. *104*, 347–352.

Luczak, A., Barthó, P., and Harris, K.D. (2009). Spontaneous Events Outline the Realm of Possible Sensory Responses in Neocortical Populations. Neuron *62*, 413–425.

Luczak, A., Bartho, P., and Harris, K.D. (2013). Gating of Sensory Input by Spontaneous Cortical Activity. J. Neurosci. *33*, 1684–1695.

van der Maaten, L., and Hinton, G. (2008). Visualizing Data using t-SNE Laurens. J. Mach. Learn. Res. *9*, 2579–2605.

MacDonald, C.J., Lepage, K.Q., Eden, U.T., and Eichenbaum, H. (2011). Hippocampal "time cells" bridge the gap in memory for discontiguous events. Neuron *71*, 737–749.

Magee, J.C., and Johnston, D. (1997). A synaptically controlled, associative signal for Hebbian plasticity in hippocampal neurons. Science *275*, 209–213.

Mahn, M., Prigge, M., Ron, S., Levy, R., and Yizhar, O. (2016). Biophysical constraints of optogenetic inhibition at presynaptic terminals. Nat. Neurosci. *19*, 554–556.

Maingret, N., Girardeau, G., Todorova, R., Goutierre, M., and Zugaro, M. (2016). Hippocampo-cortical coupling mediates memory consolidation during sleep. Nat. Neurosci. *19*, 959–964.

Malik, R., Dougherty, K.A., Parikh, K., Byrne, C., and Johnston, D. (2016). Mapping the electrophysiological and morphological properties of CA1 pyramidal neurons along the

longitudinal hippocampal axis. Hippocampus *26*, 341–361.

Manabe, H., Kusumoto-yoshida, I., Ota, M., and Mori, K. (2011). Olfactory Cortex Generates Synchronized Top-Down Inputs to the Olfactory Bulb during Slow-Wave Sleep. J. Neurosci. *31*, 8123–8133.

Mander, B.A., Marks, S.M., Vogel, J.W., Rao, V., Lu, B., Saletin, J.M., Ancoli-Israel, S., Jagust, W.J., and Walker, M.P. (2015). β-amyloid disrupts human NREM slow waves and related hippocampus-dependent memory consolidation. Nat. Neurosci. *18*, 1051–1057.

Mankin, E.A., Diehl, G.W., Leutgeb, S., Leutgeb, J.K., Mankin, E.A., Diehl, G.W., Sparks, F.T., Leutgeb, S., and Leutgeb, J.K. (2015). Hippocampal CA2 Activity Patterns Change over Time to a Larger Extent than between Spatial Contexts. Neuron *85*, 190–201.

Mao, D., Kandler, S., McNaughton, B.L., and Bonin, V. (2017). Sparse orthogonal population representation of spatial context in the retrosplenial cortex. Nat. Commun. *8*, 1–12.

Mao, D., Neumann, A.R., Sun, J., Bonin, V., Mohajerani, M.H., and McNaughton, B.L. (2018). Hippocampus-dependent emergence of spatial sequence coding in retrosplenial cortex. Proc. Natl. Acad. Sci. *115*, 8015–8018.

Markram, H., Lübke, J., Frotscher, M., and Sakmann, B. (1997). Regulation of synaptic efficacy by coincidence of postsynaptic APs and EPSPs. Science *275*, 213–215.

Marr, D. (1971). Simple Memory: A Theory for Archicortex. Philos. Trans. R. Soc. B Biol. Sci. *262*, 23–81.

Marshall, L., and Born, J. (2007). The contribution of sleep to hippocampus-dependent memory consolidation. Trends Cogn. Sci. *11*, 442–450.

Marshall, L., Helgadóttir, H., Mölle, M., and Born, J. (2006). Boosting slow oscillations during sleep potentiates memory. Nature *444*, 610–613.

Massimini, M., Ferrarelli, F., Esser, S.K., Riedner, B.A., Reto, H., Murphy, M., Peterson, M.J., and Tononi, G. (2006). Triggering sleep slow waves by transcranial magnetic stimulation. Proc. Natl. Acad. Sci. *104*, 8496–8501.

McClelland, J.L., McNaughton, B.L., and O'Reilly, R.C. (1995). Why there are complementary learning systems in the hippocampus and neocortex: Insights from the successes and failures of connectionist models of learning and memory. Psychol. Rev. *102*, 419–457.

McGinley, M.J., David, S. V., and McCormick, D.A. (2015a). Cortical Membrane Potential Signature of Optimal States for Sensory Signal Detection. Neuron *87*, 179–192.

McGinley, M.J., Vinck, M., Reimer, J., Batista-Brito, R., Zagha, E., Cadwell, C.R., Tolias, A.S., Cardin, J.A., and McCormick, D.A. (2015b). Waking State: Rapid Variations Modulate Neural and Behavioral Responses. Neuron *87*, 1143–1161.

Memmesheimer, R.M. (2010). Quantitative prediction of intermittent high-frequency oscillations in neural networks with supralinear dendritic interactions. Proc. Natl. Acad. Sci. U. S. A. *107*, 11092–11097.

Milczarek, M.M., Vann, S.D., and Sengpiel, F. (2018). Spatial Memory Engram in the Mouse Retrosplenial Cortex. Curr. Biol. *28*, 1–6.

Miyashita, T., and Rockland, K.S. (2007). GABAergic projections from the hippocampus to the retrosplenial cortex in the rat. Eur. J. Neurosci. *26*, 1193–1204.

Mizumori, S.J.Y., Perez, G.M., Alvarado, M.C., Barnes, C.A., and McNaughton, B.L. (1990). Reversible inactivation of the medial septum differentially affects two forms of learning in rats. Brain Res. *528*, 12–20.

Mizuseki, K., Sirota, A., Pastalkova, E., and Buzsáki, G. (2009). Theta Oscillations Provide Temporal Windows for Local Circuit Computation in the Entorhinal-Hippocampal Loop. Neuron *64*, 267–280.

Mizuseki, K., Diba, K., Pastalkova, E., and Buzsáki, G. (2011). Hippocampal CA1 pyramidal cells form functionally distinct sublayers. Nat. Neurosci. *14*, 1174–1181.

Mölle, M., Yeshenko, O., Marshall, L., Sara, S.J., and Born, J. (2006). Hippocampal Sharp Wave-Ripples Linked to Slow Oscillations in Rat Slow-Wave Sleep. J. Neurophysiol. *96*, 62–70.

Moore, S.J., Cooper, D.C., and Spruston, N. (2009). Plasticity of Burst Firing Induced by Synergistic

Activation of Metabotropic Glutamate and Acetylcholine Receptors. Neuron *61*, 287–300.

Morris, R.G.M., Garrud, P., Rawlins, J.N.P., and O'Keefe, J. (1982). Place navigation impaired in rats with hippocampal lesions. Nature *297*, 681–683.

Morris, R.G.M., Schenk, F., Tweedie, F., and Jarrard, L.E. (1990). Ibotenate Lesions of Hippocampus and/or Subiculum: Dissociating Components of Allocentric Spatial Learning. Eur. J. Neurosci. *2*, 1016–1028.

Naber, P.A., and Witter, M.P. (1998). Subicular efferents are organized mostly as parallel projections: A double-labeling, retrograde-tracing study in the rat. J. Comp. Neurol. *393*, 284–297.

Nadel, L., and Moscovitch, M. (1997). Memory consolidation, retrograde amnesia and the hippocampal complex. Curr. Opin. Neurobiol. *7*, 217–227.

Nairne, J.S., Thompson, S.R., and Pandeirada, J.N.S. (2007). Adaptive memory: Survival processing enhances retention. J. Exp. Psychol. Learn. Mem. Cogn. *33*, 263–273.

Nakashiba, T., Buhl, D.L., McHugh, T.J., and Tonegawa, S. (2009). Hippocampal CA3 Output Is Crucial for Ripple-Associated Reactivation and Consolidation of Memory. Neuron *62*, 781–787.

Nicolelis, M.A., Baccala, L.A., Lin, R.C.S., and Chaplin, J.K. (1995). Sensorimotor Encoding by Synchronous Neural Ensemble Activity at Multiple Levels of the Somatosensory System. Science (80-.). *268*, 1353–1358.

de Nó, R.L. (1934). Studies on the structure of the cerebral cortex. J. Psychol. Neurol. *46*, 113–177.

Norimoto, H., Makino, K., Gao, M., Shikano, Y., Okamoto, K., Ishikawa, T., Sasaki, T., Hioki, H., Fujisawa, S., and Ikegaya, Y. (2018). Hippocampal ripples down-regulate synapses - supplementary info. Science (80-.). *1527*, 1–8.

Nuñez, A., Amzica, F., and Steriade, M. (1992). Voltage-dependent fast (20-40 Hz) oscillations in long-axoned neocortical neurons. Neuroscience *51*, 7–10.

Nyhus, E., and Curran, T. (2010). Functional role of gamma and theta oscillations in episodic memory. Neurosci. Biobehav. Rev. *34*, 1023–1035.

O'Keefe, J., and Dostrovsky, J. (1971). The hippocampus as a spatial map. Preliminary evidence from unit activity in the freely-moving rat. Brain Res. *34*, 171–175.

O'Keefe, J., and Nadel, L. (1978). The hippocampus as a cognitive map (Oxford University Press).

O'Mara, S.M. (2006). Controlling hippocampal output: The central role of subiculum in hippocampal information processing. Behav. Brain Res. *174*, 304–312.

O'Neill, J., Boccara, C.N., Stella, F., Schoenenberger, P., and Csicsvari, J. (2017). Superficial layers of the medial entorhinal cortex replay independently of the hippocampus. Science (80-.). *188*, 184–188.

Ólafsdóttir, H.F., Carpenter, F., and Barry, C. (2016). Coordinated grid and place cell replay during rest. Nat. Neurosci. *19*, 1–6.

Pachitariu, M., Steinmetz, N., Kadir, S., Carandini, M., and Harris, K.D. (2016). Kilosort : realtime spike-sorting for extracellular electrophysiology with hundreds of channels. BioRxiv.

Pais, I., Hormuzdi, S.G., Monyer, H., Traub, R.D., Wood, I.C., Buhl, E.H., Whittington, M.A., and LeBeau, F.E.N. (2003). Sharp Wave-Like Activity in the Hippocampus In Vitro in Mice Lacking the Gap Junction Protein Connexin 36. J. Neurophysiol. *89*, 2046–2054.

Pan, W.X., and McNaughton, N. (2002). The role of the medial supramammillary nucleus in the control of hippocampal theta activity and behaviour in rats. Eur. J. Neurosci. *16*, 1797–1809.

Pastalkova, E., Itskov, V., Amarasingham, A., and Buzsáki, G. (2008). Internally generated cell assembly sequences in the rat hippocampus. Science *321*, 1322–1327.

Patel, J., Schomburg, E.W., Bere, A., and Fujisawa, S. (2013). Local Generation and Propagation of Ripples along the Septotemporal Axis of the Hippocampus. J. Neurosci. *33*, 17029–17041.

Pelkey, K.A., Chittajallu, R., Craig, M.T., Tricoire, L., Wester, J.C., and McBain, C.J. (2017). Hippocampal GABAergic Inhibitory Interneurons. Physiol. Rev. *97*, 1619–1747.

Petersen, C.C.H., Hahn, T.T.G., Mehta, M., Grinvald, A., Sakmann, B., Grinvald, A., and Mehta, M. (2003). Interaction of sensory responses with spontaneous depolarization in layer 2/3 barrel cortex. Proc. Natl. Acad. Sci. *100*, 13638–13643.

Petsche, H., Stumpf, C., and Gogolak, G. (1962). The significance of the rabbit's septum as a relay station between the midbrain and the hippocampus I. The control of hippocampus arousal activity by the septum cells. Electroencephalogr. Clin. Neurophysiol. *14*, 202–211.

Pettersen, K.H., Devor, A., Ulbert, I., Dale, A.M., and Einevoll, G.T. (2006). Current-source density estimation based on inversion of electrostatic forward solution: Effects of finite extent of neuronal activity and conductivity discontinuities. J. Neurosci. Methods *154*, 116–133.

Peyrache, A., Khamassi, M., Benchenane, K., Wiener, S.I., and Battaglia, F.P. (2009). Replay of rule-learning related neural patterns in the prefrontal cortex during sleep. Nat. Neurosci. *12*, 919–926.

Peyrache, A., Battaglia, F.P., and Destexhe, A. (2011). Inhibition recruitment in prefrontal cortex during sleep spindles and gating of hippocampal inputs. Proc. Natl. Acad. Sci. *108*, 17207–17212.

Phillips, K.G., Bartsch, U., McCarthy, A.P., Edgar, D.M., Tricklebank, M.D., Wafford, K.A., and Jones, M.W. (2012). Decoupling of Sleep-Dependent Cortical and Hippocampal Interactions in a Neurodevelopmental Model of Schizophrenia. Neuron *76*, 526–533.

Ponomarenko, A.A., Korotkova, T.M., and Haas, H.L. (2003). High frequency (200 Hz) oscillations and firing patterns in the basolateral amygdala and dorsal endopiriform nucleus of the behaving rat. Behav. Brain Res. *141*, 123–129.

Rajasethupathy, P., Sankaran, S., Marshel, J.H., Kim, C.K., Ferenczi, E., Lee, S.Y., Berndt, A., Ramakrishnan, C., Jaffe, A., Lo, M., et al. (2015). Projections from neocortex mediate top-down control of memory retrieval. Nature *526*, 653–659.

Ramirez-Villegas, J.F., Logothetis, N.K., and Besserve, M. (2015). Diversity of sharp-wave–ripple LFP signatures reveals differentiated brain-wide dynamical events. Proc. Natl. Acad. Sci. *112*, E6379–E6387.

Remondes, M., and Wilson, M.A. (2015). Slow-γ Rhythms Coordinate Cingulate Cortical Responses to Hippocampal Sharp-Wave Ripples during Wakefulness. Cell Rep. *13*, 1327–1335.

Robinson, T.E., Kramis, R.C., and Vanderwolf, C.H. (1977). Two types of cerebral activation during active sleep: relations to behavior. Brain Res. *124*, 544–549.

Rothschild, G., Eban, E., and Frank, L.M. (2017). A cortical-hippocampal-cortical loop of information processing during memory consolidation. Nat. Neurosci. *20*, 251–259.

Roux, L., Hu, B., Eichler, R., Stark, E., and Buzsáki, G. (2017). Sharp wave ripples during learning stabilize the hippocampal spatial map. Nat. Neurosci. *20*, 845–853.

Roy, D.S., Kitamura, T., Okuyama, T., Obata, Y., Roy, D.S., Kitamura, T., Okuyama, T., Ogawa, S.K., Sun, C., and Obata, Y. (2017). Distinct Neural Circuits for the Formation and Retrieval of Episodic Memories Article Distinct Neural Circuits for the Formation and Retrieval of Episodic Memories. Cell 1–13.

Sadowski, J.H.L.P., Jones, M.W., and Mellor, J.R. (2016). Sharp-Wave Ripples Orchestrate the Induction of Synaptic Plasticity during Reactivation of Place Cell Firing Patterns in the Hippocampus. Cell Rep. *14*, 1916–1929.

Sagar, H.J., Cohen, N.J., Corkin, S., and Growdon, J.H. (1985). Dissociations Among Processes in Remote Memory. Ann. N. Y. Acad. Sci. *444*, 533–535.

Sanchez-Vives, M. V., and McCormick, D.A. (2000). Cellular and network mechanisms of rhythmic recurrent activity in neocortex. Nat. Neurosci. *3*, 1027–1034.

Sargolini, F., Fyhn, M., Hafting, T., Mcnaughton, B.L., Witter, M.P., Moser, M.-B., and Moser, E.I. (2006). Conjunctive Representation of Position, Direction, and Velocity in Entorhinal Cortex. Science (80-.). *312*, 758–762.

Schlingloff, D., Kali, S., Freund, T.F., Hajos, N., and Gulyas, A.I. (2014). Mechanisms of Sharp Wave Initiation and Ripple Generation. J. Neurosci. *34*, 11385–11398.

Schmitz, D., Schuchmann, S., Fisahn, A., Draguhn, A., Buhl, E.H., Petrasch-Parwez, E., Dermietzel, R., Heinemann, U., and Traub, R.D. (2001). Axo-axonal coupling: A novel mechanism for ultrafast

neuronal communication. Neuron *31*, 831–840.

Schomburg, E.W., Fernández-Ruiz, A., Mizuseki, K., Berényi, A., Anastassiou, C.A., Koch, C., and Buzsáki, G. (2014). Theta Phase Segregation of Input-Specific Gamma Patterns in Entorhinal-Hippocampal Networks. Neuron *84*, 470–485.

Scoville, W.B., and Milner, B. (1957). Loss of recent memory after bilateral hippocampal lesions. J. Neurol. Neurosurg. Psychiatry *20*, 11–21.

Seibt, J., Richard, C.J., Sigl-Glöckner, J., Takahashi, N., Kaplan, D.I., Doron, G., De Limoges, D., Bocklisch, C., and Larkum, M.E. (2017). Cortical dendritic activity correlates with spindle-rich oscillations during sleep in rodents. Nat. Commun. *8*, 1–13.

Sempere‐Ferràndez, A., Salvador, M., and Barrientos, E.G. (2019). Synaptic mechanisms underlying the intense firing of neocortical layer 5B pyramidal neurons in response to cortico-cortical inputs. Brain Struct. Funct. *224*, 1403–1416.

Senzai, Y., Fernandez-Ruiz, A., and Buzsáki, G. (2019). Layer-Specific Physiological Features and Interlaminar Interactions in the Primary Visual Cortex of the Mouse. Neuron *101*, 500-513.e5.

Sharp, P.E., and Green, C. (1994). Spatial correlates of firing patterns of single cells in the subiculum of the freely moving rat. J. Neurosci. *14*, 2339–2356.

Siapas, A.G., and Wilson, M.A. (1998). Coordinated Interactions between Hippocampal Ripples and Cortical Spindles during Slow-Wave Sleep. Neuron *21*, 1123–1128.

Siapas, A.G., Lubenov, E. V., and Wilson, M.A. (2005). Prefrontal phase locking to hippocampal theta oscillations. Neuron *46*, 141–151.

Simonnet, J., and Brecht, M. (2019). Burst firing and spatial coding in subicular principal cells. J. Neurosci. *39*, 3651–3662.

Sirota, A., Csicsvari, J., Buhl, D., and Buzsáki, G. (2003). Communication between neocortex and hippocampus during sleep in rodents. Proc. Natl. Acad. Sci. *100*, 2065–2069.

Skaggs, W.E., McNaughton, B.L., Wilson, M.A., and Barnes, C.A. (1996). Theta phase precession

in hippocampal neuronal populations and the compression of temporal sequences. Hippocampus *6*, 149–172.

Solstad, T., Boccara, C.N., Kropff, E., Moser, M.-B., and Moser, E.I. (2008). Representation of geometric borders in the entorhinal cortex. Science *322*, 1865–1868.

Somogyi, P., and Klausberger, T. (2005). Defined types of cortical interneurone structure space and spike timing in the hippocampus. J. Physiol. *562*, 9–26.

Spruston, N., and Johnston, D. (1992). Perforated patch-clamp analysis of the passive membrane properties of three classes of hippocampal neurons. J. Neurophysiol. *67*, 508–529.

Squire, L.R., and Alvarez, P. (1995). Retrograde amnesia and memory consolidation: a neurobiological perspective. Curr. Opin. Neurobiol. *5*, 169–177.

Staff, N.P., Jung, H.Y., Thiagarajan, T., Yao, M., and Spruston, N. (2000). Resting and active properties of pyramidal neurons in subiculum and CA1 of rat hippocampus. J. Neurophysiol. *84*, 2398–2408.

Stark, E., and Abeles, M. (2009). Unbiased estimation of precise temporal correlations between spike trains. J. Neurosci. Methods *179*, 90–100.

Stark, E., Roux, L., Eichler, R., Senzai, Y., Royer, S., and Buzsáki, G. (2014). Pyramidal cell-interneuron interactions underlie hippocampal ripple oscillations. Neuron *83*, 467–480.

Steriade, M., Mccormick, D.A., and Sejnowski, T.J. (1993). Thalamocortical Oscillations in the Sleeping and Aroused Brain. Science (80-.). *262*, 679–685.

Steward, O. (1976). Topographic organization of the projections from the entorhinal area to the hippocampal formation of the rat. J. Comp. Neurol. *167*, 285–314.

van Strien, N.M., Cappaert, N.L.M., and Witter, M.P. (2009). The anatomy of memory: an interactive overview of the parahippocampal-hippocampal network. Nat. Rev. Neurosci. *10*, 272–282.

Sugar, J., Witter, M.P., van Strien, N.M., and Cappaert, N.L.M. (2011). The retrosplenial cortex:

intrinsic connectivity and connections with the (para)hippocampal region in the rat. An interactive connectome. Front. Neuroinform. *5*, 7.

Sun, Y., Nguyen, A.Q., Nguyen, J.P., Le, L., Saur, D., Choi, J., Callaway, E.M., and Xu, X. (2014). Cell-type-specific circuit connectivity of hippocampal CA1 revealed through cre-dependent rabies tracing. Cell Rep. *7*, 269–280.

Sun, Y., Jin, S., Lin, X., Chen, L., Qiao, X., Jiang, L., Johnston, K.G., Golshani, P., Nie, Q., Holmes, T.C., et al. (2019). CA1-Projecting Subiculum Neurons Facilitate Object-Place Learning. Nat. Neurosci.

Swanson, L.W., and Cowan, W.M. (1977). An Autoradiographic Study of the Organization of the Efferent Connections of the Hippocampal Formation in the Rat. J. Comp. Neurol. *172*, 49–84.

Takeuchi, S., Murai, R., Shimazu, H., Isomura, Y., Mima, T., and Tsujimoto, T. (2016). Spatiotemporal Organization and Cross-Frequency Coupling of Sleep Spindles in Primate Cerebral Cortex. Sleep *39*, 1719–1735.

Taube, J.S. (2007). The Head Direction Signal: Origins and Sensory-Motor Integration. Annu. Rev. Neurosci. *30*, 181–207.

Taube, J.S., Muller, R.U., and Ranck, J.B. (1990). Head-direction cells recorded from the postsubiculum in freely moving rats. I. Description and quantitative analysis. J. Neurosci. *10*, 420–435.

Taxidis, J., Coombes, S., Mason, R., and Owen, M.R. (2012). Modeling sharp wave-ripple complexes through a CA3-CA1 network model with chemical synapses. Hippocampus *22*, 995–1017.

Tervo, D.G.R., Hwang, B.Y., Viswanathan, S., Gaj, T., Lavzin, M., Ritola, K.D., Lindo, S., Michael, S., Kuleshova, E., Ojala, D., et al. (2016). A Designer AAV Variant Permits Efficient Retrograde Access to Projection Neurons. Neuron *92*, 372–382.

Teyler, T.J., and DiScenna, P. (1986). The hippocampal memory indexing theory. Behav. Neurosci. *100*, 147–154.

Thomson, A.M. (2000). Facilitation, augmentation and potentiation at central synapses. Trends Neurosci. *23*, 305–312.

Timofeev, I., Grenier, F., and Steriade, M. (2001). Disfacilitation and active inhibition in the neocortex during the natural sleep-wake cycle: An intracellular study. Proc. Natl. Acad. Sci. *98*, 1924–1929.

Tingley, D., and Buzsáki, G. (2019). Routing of Hippocampal Ripples to Subcortical Structures via the Lateral Septum. Neuron 1–12.

Tolman, E.C. (1948). Cognitive maps in rats and men. Psychol. Rev. *55*, 189–208.

Tononi, G., and Cirelli, C. (2003). Sleep and synaptic homeostasis: A hypothesis. Brain Res. Bull. *62*, 143–150.

Tort, A.B.L., Kramer, M.A., Thorn, C., Gibson, D.J., Kubota, Y., Graybiel, A.M., and Kopell, N.J. (2008). Dynamic cross-frequency couplings of local field potential oscillations in rat striatum and hippocampus during performance of a T-maze task. Proc. Natl. Acad. Sci. U. S. A. *105*, 20517–20522.

Traub, R.D., and Bibbig, A. (2000). A model of high-frequency ripples in the hippocampus based on synaptic coupling plus axon-axon gap junctions between pyramidal neurons. J. Neurosci. *20*, 2086–2093.

Traub, R.D., Jefferys, J.G.R., Miles, R., Whittington, M.A., and Tóth, K. (1994). A branching dendritic model of a rodent CA3 pyramidal neurone. J. Physiol. *481*, 79–95.

Treves, A., and Rolls, E.T. (1994). Computational analysis of the role of the hippocampus in memory. Hippocampus *4*, 374–391.

Tulving, E. (1972). Episodic and semantic memory. In Organaization of Memory, (New York: Academic Press), pp. 381–402.

Valero, M., Cid, E., Averkin, R.G., Aguilar, J., Sanchez-Aguilera, A., Viney, T.J., Gomez-Dominguez, D., Bellistri, E., and de la Prida, L.M. (2015). Determinants of different deep and superficial CA1 pyramidal cell dynamics during sharp-wave ripples. Nat. Neurosci. *18*, 1281–1290.

Valero, M., Averkin, R.G., Fernandez-Lamo, I., Aguilar, J., Lopez-Pigozzi, D., Brotons-Mas, J.R., Cid, E., Tamas, G., and Menendez de la Prida, L. (2017). Mechanisms for Selective Single-Cell Reactivation during Offline Sharp-Wave Ripples and Their Distortion by Fast Ripples. Neuron *94*, 1234–1247.

Vanderwolf, C.H. (1969). Hippocampal electrical activity and voluntary movement in the rat. Electroencephalogr. Clin. Neurophysiol. *26*, 407–418.

Vanderwolf, C.H. (1971). Limbic-diencephalic mechanisms of voluntary movement. Psychol. Rev. *78*, 83–113.

Vann, S.D., Aggleton, J.P., and Maguire, E.A. (2009). What does the retrosplenial cortex do? Nat. Rev. Neurosci. *10*, 792–802.

Varoqui, H., Schäfer, M.K.H., Zhu, H., Weihe, E., and Erickson, J.D. (2002). Identification of the differentiation-associated Na+/PI transporter as a novel vesicular glutamate transporter expressed in a distinct set of glutamatergic synapses. J. Neurosci. *22*, 142–155.

Vélez-Fort, M., Bracey, E.F., Keshavarzi, S., Rousseau, C. V., Cossell, L., Lenzi, S.C., Strom, M., and Margrie, T.W. (2018). A Circuit for Integration of Head- and Visual-Motion Signals in Layer 6 of Mouse Primary Visual Cortex. Neuron *98*, 179–191.

Vertes, R.P., Hoover, W.B., and Viana Di Prisco, G. (2004). Theta rhythm of the hippocampus: subcortical control and functional significance. Behav. Cogn. Neurosci. Rev. *3*, 173–200.

De Vivo, L., Bellesi, M., Marshall, W., Bushong, E.A., Ellisman, M.H., Tononi, G., and Cirelli, C. (2017). Ultrastructural evidence for synaptic scaling across the wake/sleep cycle. Science (80-.). *355*, 507–510.

Vladimirov, N., and Sourjik, V. (2009). Chemotaxis: How bacteria use memory. Biol. Chem. *390*, 1097–1104.

Wang, D. V., and Ikemoto, S. (2016). Coordinated Interaction between Hippocampal Sharp-Wave Ripples and Anterior Cingulate Unit Activity. J. Neurosci. *36*, 10663–10672.

Wang, Y., Romani, S., Lustig, B., Leonardo, A., and Pastalkova, E. (2015). Theta sequences are

essential for internally generated hippocampal firing fields. Nat. Neurosci. *18*, 282–288.

Watson, B.O., Levenstein, D., Greene, J.P., Gelinas, J.N., and Buzsáki, G. (2016). Network Homeostasis and State Dynamics of Neocortical Sleep. Neuron *90*, 839–852.

Wellmer, J., Su, H., Beck, H., and Yaari, Y. (2002). Long-lasting modification of intrinsic discharge properties in subicular neurons following status epilepticus. Eur. J. Neurosci. *16*, 259–266.

Wierzynski, C.M., Lubenov, E. V, Gu, M., and Siapas, A.G. (2009). Article State-Dependent Spike-Timing Relationships between Hippocampal and Prefrontal Circuits during Sleep. Neuron *61*, 587–596.

Wilber, A.A., Skelin, I., Wu, W., and McNaughton, B.L. (2017). Laminar Organization of Encoding and Memory Reactivation in the Parietal Cortex. Neuron *95*, 1406-1419.e5.

Winocur, G. (1990). Anterograde and retrograde amnesia in rats with dorsal hippocampal or dorsomedial thalamic lesions. Behav. Brain Res. *38*, 145–154.

Winocur, G., McDonald, R.M., and Moscovitch, M. (2001). Anterograde and retrograde amnesia in rats with large hippocampal lesions. Hippocampus *11*, 18–26.

Winson, J. (1978). Loss of hippocampal theta rhythm results in spatial memory deficit in the rat. Science *201*, 160–163.

Wozny, C., Maier, N., Schmitz, D., and Behr, J. (2008). Two different forms of long-term potentiation at CA1-subiculum synapses. J. Physiol. *586*, 2725–2734.

Wozny, C., Beed, P., Nitzan, N., Pössnecker, Y., and Schmitz, D. (2018). VGLUT2 functions as a differential marker for hippocampal output neurons. Front. Cell. Neurosci. *44*, 1–7.

Wyss, J.M., and Van Groen, T. (1992). Connections Between the Retrosplenial Cortex and the Hippocampal Formation in the Rat : A Review. Hippocampus *2*, 1–12.

Xu, X., Sun, Y., Holmes, T.C., and López, A.J. (2016). Noncanonical connections between the subiculum and hippocampal CA1. J. Comp. Neurol. *524*, 3666–3673.

Yamawaki, N., Corcoran, K.A., Guedea, A.L., Shepherd, G.M.G., and Radulovic, J. (2019a).

Differential Contributions of Glutamatergic Hippocampal→Retrosplenial Cortical Projections to the Formation and Persistence of Context Memories. Cereb. Cortex *29*, 2728–2736.

Yamawaki, N., Li, X., Lambot, L., Ren, L.Y., Radulovic, J., and Shepherd, G.M. (2019b). Long-range inhibitory intersection of a retrosplenial thalamocortical circuit by apical tuft-targeting CA1 neurons. Nat. Neurosci. *22*, 618–626.

Ylinen, A., Bragin, A., Nádasdy, Z., Jandó, G., Szabó, I., Sik, A., and Buzsáki, G. (1995). Sharp wave-associated high-frequency oscillation (200 Hz) in the intact hippocampus: network and intracellular mechanisms. J. Neurosci. *15*, 30–46.

6 APPENDIX

6.1 List of abbreviations

ACC	Anterior Cingulate Cortex
ACG	Autocorrelogram
AMPA	α-amino-3-hydroxy-5-methyl-4-isoxazolepropionic acid
CA	Cornu Ammonis
CSD	Current Source Density
ChR	Channelrhodopsin
DG	Dentate Gyrus
EC	Entorhinal Cortex
EMG	Electromyogram
EPSP	Excitatory Postsynaptic Potential
GABA	Gamma Aminobutyric Acid
ICA	Independent Component Analysis
iHFO	induced High Frequency Oscillation
IPSP	Inhibitory Postsynaptic Potential
LFP	Local Field Potential
LTP	Long Term Potentiation
MUA	Multi Unit Activity
NMDA	N-methyl-D-aspartate
PETH	Peri Event Time Histogram

RSC	Retrosplenial Cortex
SPW-R	Sharp Wave Ripple
SW	Sharp Wave
SWS	Slow Wave Sleep
t-SNE	t-distributed Stochastic Neighbor Embedding
VGlut	Vesicular Glutamate Transporter

6.2 Statement of contributions

All experiments in this thesis, with the exception of data presented in chapter 3.6, were conceived and designed by my thesis supervisor, Prof. Dietmar Schmitz and myself. In addition, experiments in chapters 3.3-3.5 are the result of a collaboration with Dr. Sam McKenzie and Prof. György Buzsáki from the New York University, who jointly contributed to their experimental design. All data presented was acquired by me (sections 3.3-3.5 jointly with Dr. Sam McKenzie), with the help of colleagues specified below. All data analysis, with the exception of the data presented in chapter 3.4 was performed by me.

Detailed contributions of other people to the data presented in this work include:

Dr. Christian Wozny (Strathclyde Institute of Pharmacy and Biomedical Sciences, United Kingdom) conceived, designed, performed and analyzed the experiments presented in chapter 3.6. My contribution to those experiments was the data collection and analysis of 15 subicular cells.

Dr. Prateep Beed (AG Schmitz, Neuroscience Research Center, Charité, Berlin) performed patch clamp experiments used to generate figures 3.6.1 and 3.7.2 – 3.7.5.

Silvia Oldani (AG Schmitz, Neuroscience Research Center, Charité, Berlin) performed patch clamp experiments used to generate figure 3.7.6.

Dr. Daniel English (School of Neuroscience, College of Science, Virginia Tech, USA) implanted the CaMKII-Cre::Ai32 mice used in chapters 3.3-3.5 and help with data collection from those subjects.

Dr. Sam McKenzie (Neuroscience Institute and Department of Neurology, New York University, USA) collected data from CaMKII-Cre::Ai32 mice used in chapters 3.3-3.5 and analyzed data of those sections.

Prof. György Buzsáki (Neuroscience Institute and Department of Neurology, New York University, USA) guided the analysis of the data presented throughout.

6.3 List of publications

Wozny C, Beed P, Nitzan N, Pössnecker J, Rost BR, Schmitz D (2018) VGlut2 functions as a differential marker for hippocampal output neurons. Front. Cell. Neurosci. 12:337.

McKenzie S, Nitzan N, English DF (2019) Mechanisms of neural organization and rhythmogenesis during hippocampal and cortical ripples. Phil. Trans. R. Soc. B, accepted manuscript.

6.4 Erklärung an Eides statt

Ich, Noam Nitzan versichere an Eides statt durch meine eigenhändige Unterschrift, dass ich die vorgelegte Dissertation mit dem Thema: „Propagation of hippocampal ripples to the neocortex by way of a subiculum retrosplenial pathway“ selbstständig und ohne nicht offengelegte Hilfe Dritter verfasst und keine anderen als die angegebenen Quellen und Hilfsmittel genutzt habe.

Die Bedeutung dieser eidesstattlichen Versicherung und die strafrechtlichen Folgen einer unwahren eidesstattlichen Versicherung (§156,161 des Strafgesetzbuches) sind mir bekannt und bewusst.

Berlin, den 30 Januar 2020